

ELECTRICAL POTENTIALS IN BONE INDUCED BY MECHANICAL LOADING

CHARACTERISTICS OF THE STRESS-GENERATED ELECTRICAL POTENTIALS IN BONE  
INDUCED BY MECHANICAL LOADING

By LAURA PRAVATO, B.ENG.

A Thesis Submitted to the School of Graduate Studies in Partial Fulfilment of the  
Requirements for the Degree of Master of Applied Science

McMaster University © Copyright by Laura Pravato, August 2018

MASTER OF APPLIED SCIENCE (2018) McMaster University

School of Biomedical Engineering, Hamilton, Ontario

TITLE: Characteristics of the Stress-Generated Electrical Potentials in Bone Induced by Mechanical Loading

AUTHOR: Laura Pravato, B.Eng. (McMaster University)

SUPERVISOR: Gregory R. Wohl, Ph. D., P.Eng.

NUMBER OF PAGES: xiv, 140

## **Lay Abstract**

Mechanical deformation of bone produces electrical signals known as stress-generated potentials (SGPs). In this study, I mechanically tested wet beams of bone to assess how the SGPs were affected by hydration levels, load magnitudes, and deformation rates. Dry bone samples did not produce any acceptable SGP signals. The SGPs from wet bone, however, produced repeatable signals that decayed following deformation.

With a step load input, the decaying SGP signal fit a two-term exponential equation ( $V(t) = Ae^{t/\tau_1} + Ce^{t/\tau_2}$ ). The first term, made up of the A-coefficient and  $\tau_1$ , was found to be dependent on deformation rate whereas the second term, containing the C-coefficient and  $\tau_2$ , was dependent on load magnitude. The two coefficients, the A and C-coefficient, together determine the maximum voltage the SGP can reach. The result of this work showed that SGPs in bone are dependent on tissue hydration and vary with load magnitude and deformation rate.

## Abstract

Since the discovery of stress-generated potentials (SGPs) in bone by Fukada and Yasuda in 1957, researchers have tried to understand their origin and function in the maintenance of bone. There have been a variety of methods attempting to quantify these SGPs in both wet and dry bone. In this study, I prepared both dry and wet beams of cortical bovine bone and subjected them to mechanical deformation in cantilever bending. Mechanical testing was performed to explore how the magnitude of the SGPs was affected by hydration levels, strain, and pressure gradients associated with various load magnitudes and deformation rates. Signals that were collected from the dry bone samples were attributed to motion artifact resulting from the movement of the materials testing machine and load cell. The SGPs from wet bone, on the other hand, consistently produced exponentially decaying signals following deformation that were maintained throughout held deformation and produced an SGP of opposite magnitude upon release of deformation.

The exponentially decaying SGP signal produced after application of a step load to wet bone samples was determined to fit a two-term exponential equation ( $V(t) = Ae^{t/\tau_1} + Ce^{t/\tau_2}$ ). The first term, made up of the A-coefficient and  $\tau_1$ , was found to be dependent on deformation rate whereas the second term, containing the C-coefficient and  $\tau_2$ , was dependent on load magnitude. The sum of the two coefficients determine the maximum voltage the SGP can reach.

Additionally, samples were left to air dry for one hour and tested intermittently throughout that time period. SGP signals diminished significantly over the hour, therefore, it has been concluded that the majority of the SGP signal is due to streaming potentials caused by ionic fluid movement within the bone upon deformation.

## **Acknowledgements**

I cannot thank Dr. Wohl enough for his support of this project throughout the past three years. His ability to keep me focused on the scope of the project so that I didn't drown in the vast information base that is Google Scholar helped me be much more productive and *much* less stressed out. I am extremely grateful for not only his guidance but also his humor...and dad jokes.

I'd also like to thank Dr. de Bruin and Tyler Ackland for all the equipment they provided and for their help troubleshooting the electronics. A big thank you to Dr. Luciano Minuzzi for bestowing all his R knowledge upon me. I wouldn't have been able to finish my thesis without it.

To everyone, both past and present, who worked with me in the biomechanics lab: thanks for all the shenanigans and sass. A special thank you to Elyse Rier for taking on the grueling task that was curve fitting!

# Table of Contents

|   |      |
|---|------|
| Lay Abstract .....  | iii  |
| Abstract .....  | iv   |
| Acknowledgements.....   | v    |
| Table of Contents .....   | vi   |
| List of Figures.....  | ix   |
| List of Tables.....   | xii  |
| List of Abbreviations and Symbols .....                               | xiii |
| Declaration of Academic Achievement.....                              | xiv  |
| 1 Background.....   | 1    |
| 1.1 Introduction.....   | 1    |
| 1.2 Piezoelectricity and Electrical Potentials in Dry Bone.....       | 3    |
| 1.3 Exploring the Sources of Piezoelectricity in Bone .....           | 5    |
| 1.3.1 Collagen Piezoelectricity .....                                 | 6    |
| 1.3.2 Potential Differences and Bone Deposition.....                  | 7    |
| 1.3.4 Streaming Potentials .....                                      | 8    |
| 1.3.5 Shear Stress and SGPs.....                                      | 9    |
| 1.4 The Importance of Time on SGPs .....                              | 11   |
| 1.5 Research Objectives .....   | 16   |
| 2 Materials and Methods .....   | 18   |
| 2.1 Sample Preparation.....   | 18   |
| 2.2 Electrical Circuitry and Data Acquisition .....                   | 20   |
| 2.2.1 Bioinstrumentation Circuit for Stress-Generated Potentials..... | 20   |
| 2.2.2 Charge Amplifier Circuit for Piezoelectricity.....              | 24   |
| 2.3 Mechanical Testing .....  | 25   |
| 2.4 Dry vs. Wet Tests.....  | 26   |
| 2.4.1 Sample Preparation.....   | 26   |
| 2.4.2 Test Procedure .....  | 27   |
| 2.5 Charge Amplifier Test .....                                       | 28   |
| 2.5.1 Sample Preparation.....   | 28   |
| 2.5.2 Test Procedure .....  | 29   |
| 2.6 Evaporation Tests.....  | 30   |

|   |    |
|---|----|
| 2.6.1 Sample Preparation.....   | 30 |
| 2.6.2 Test Procedure .....  | 31 |
| 2.7 Unified Sample Preparation Tests.....                               | 32 |
| 2.7.1 Sample Preparation.....   | 32 |
| 2.7.2 Test Procedure .....  | 32 |
| 2.8 Drying Experiments.....   | 34 |
| 2.8.1 Sample Preparation.....   | 34 |
| 2.8.2 Test Procedures.....  | 36 |
| 2.9 Force Magnitude and Deformation Rate Tests .....                    | 39 |
| 2.9.1 Background.....   | 39 |
| 2.9.2 Recreating the Steinberg Tests.....                               | 41 |
| 2.9.3 Sample Prep.....  | 42 |
| 2.9.4 Test Procedure .....  | 42 |
| 2.10 Analysis Methods .....   | 44 |
| 2.10.1 Data Processing.....   | 46 |
| 2.10.2 Values of Interest .....   | 46 |
| 2.10.3 Curve Analysis – Fitting the Two-Term Decaying Exponential ..... | 49 |
| 2.10.4 RC Circuits and Stress Relaxation .....                          | 53 |
| 3 Results.....  | 55 |
| 3.1 Dry vs. Wet Tests.....  | 55 |
| 3.2 Charge Amplifier Tests.....   | 56 |
| 3.3 Evaporation Tests.....  | 57 |
| 3.4 Unified Sample Preparation Tests.....                               | 58 |
| 3.5 Drying Tests .....  | 63 |
| 3.5.1 Force Variations .....  | 63 |
| 3.5.2 Results from Statistical Analysis .....                           | 66 |
| 3.1.6 Force Magnitude and Rate Tests.....                               | 75 |
| 4 Discussion .....  | 85 |
| 4.1 Effect of Dehydration.....  | 85 |
| 4.1.1 Dry vs Wet .....  | 86 |
| 4.1.2 Charge Amplifier Tests.....                                       | 89 |
| 4.1.3 Evaporation Tests.....  | 91 |
| 4.1.4 Drying Experiments.....   | 91 |



|  |     |
|--|-----|
| 4.1.6 Overall.....                                       | 94  |
| 4.2 Effect of Sample Thickness .....                     | 96  |
| 4.2.1 Unified Sample Preparation Test.....               | 96  |
| 4.2 Effect of Varying Load and Displacement Rate .....   | 100 |
| 4.2.1 Force and Rate Tests.....                          | 100 |
| 4.2.2 Related Work.....                                  | 104 |
| 5 Conclusion .....                                       | 110 |
| 5.1 Future Work .....                                    | 111 |
| References.....  | 112 |
| APPENDICES.....  | 116 |
| Appendix 1.....  | 116 |
| 1.1 Sample Info.....                                     | 116 |
| Appendix 2.....  | 119 |
| 2.1 SGP Circuit Info.....                                | 119 |
| 2.2 Charge Amplifier Circuit Info .....                  | 122 |
| Appendix 3.....  | 123 |
| 3.1 Strain and Force Amplifier .....                     | 123 |
| Appendix 4.....  | 124 |
| 4.1 Admet Evaluation .....                               | 124 |
| 4.2 Force Calibration Results .....                      | 125 |
| Appendix 5.....  | 126 |
| 5.1 LabVIEW Program for Data Acquisition .....           | 126 |
| Appendix 6.....  | 130 |
| 6.1 Images of Similar SGPs from Other Papers.....        | 130 |
| 6.2 Summary of Signals Collected from Other Papers ..... | 136 |
| Appendix 7.....  | 137 |
| 7.1 MATLAB Code.....                                     | 137 |

## List of Figures

|             |   |    |
|-------------|---|----|
| Figure 1.1  | Direct and converse piezoelectric effects in dry bone as reported by Fukada in 1957.....                            | 3  |
| Figure 1.2  | Dependence of piezoelectric constants on direction of applied load.....   | 10 |
| Figure 1.3  | SGPs from wet bone reported by Bassett and Becker in 1962.....  | 12 |
| Figure 1.4  | SGPs from wet bone reported by Steinberg et al. in 1973.....  | 13 |
| Figure 1.5  | SGP response to a step load and the time constants to describe the decay as reported by Pollack et al. in 1984..... | 14 |
| Figure 1.6  | Dependence of SGP decay time on fluid viscosity as reported by Gross and Williams in 1982.....                      | 15 |
| Figure 2.1  | Average dimensions of the beams of cortical bone and location of strain gauge, applied load, and clamping.....      | 19 |
| Figure 2.2  | Actual photo of a sample with electrodes applied and ready for testing.....   | 19 |
| Figure 2.3  | Block diagram of bioinstrumentation amplifier used for stress-generated potential collection.....                   | 21 |
| Figure 2.4  | Positive and negative voltage limits of SGP circuit.....  | 22 |
| Figure 2.5  | Example of motion artifact collected in electrode leads from load cell movement.....                                | 23 |
| Figure 2.6  | Schematic of charge amplifier circuit.....  | 24 |
| Figure 2.7  | Schematic of cantilever bending.....  | 25 |
| Figure 2.8  | Plot demonstrating how plastic wrap helped keep samples more hydrated and improved SGP signal.....                  | 36 |
| Figure 2.9  | Plot showing stabilization of baseline through application of ten cycles of a pre-load.....                         | 37 |
| Figure 2.10 | Plot of SGP vs. load for zero second held displacement as reported by Steinberg in 1973.....                        | 40 |
| Figure 2.11 | Plot of SGP vs. load for thirty second held displacement as reported by Steinberg in 1973.....                      | 40 |
| Figure 2.12 | Relationship between SGP and load/displacement rate as reported by Steinberg in 1973.....                           | 41 |
| Figure 2.13 | Examples of bad tests which produced inadequate SGP signals.....  | 44 |
| Figure 2.14 | Diagram showing how data was processed for curve isolation.....   | 48 |
| Figure 2.15 | Isolated cycle showing a typical SGP, strain and force signal.....  | 48 |
| Figure 2.16 | How the two-term exponential curve is fit to the data.....  | 49 |
| Figure 2.17 | Plots explaining the values of interest .....   | 49 |
| Figure 2.18 | Plots explaining what the values in the two-term exponential equation represent.....                                | 52 |
| Figure 2.19 | Schematic and time response of a typical RC circuit.....  | 53 |
| Figure 3.1  | Comparison of signals collected from a wet and desiccated sample in the wet vs. dry tests.....                      | 55 |

|             |   |     |
|-------------|---|-----|
| Figure 3.2  | Comparison of signals collected from a wet and ethanol dried sample in the charge amplifier tests.....      | 56  |
| Figure 3.3  | Comparison of signals collected from a wet and air-dried sample in the evaporation tests.....               | 57  |
| Figure 3.4  | Max SGP vs. thickness.....  | 59  |
| Figure 3.5  | Max SGP vs. max strain.....   | 60  |
| Figure 3.6  | SGP tau 1 vs. strain tau 1.....   | 61  |
| Figure 3.7  | SGP tau 2 vs. strain tau 2.....   | 62  |
| Figure 3.8  | Boxplots showing variation of force between the three drying tests.....                                     | 65  |
| Figure 3.9  | Boxplots showing overshoot in force for higher deformation rates.....                                       | 65  |
| Figure 3.10 | Boxplots showing mean max SGP – Drying Tests.....   | 68  |
| Figure 3.11 | Boxplots showing mean delta SGP – Drying Tests.....   | 69  |
| Figure 3.12 | Boxplots showing ratio of mean max SGP – Drying Tests.....  | 70  |
| Figure 3.13 | Boxplots showing ratio of delta SGP – Drying Tests.....   | 70  |
| Figure 3.14 | Boxplots showing SGP Tau 1 – Drying Tests.....  | 71  |
| Figure 3.15 | Boxplots showing SGP Tau 2 – Drying Tests.....  | 72  |
| Figure 3.16 | Boxplots showing SGP A-coefficient – Drying Tests.....  | 73  |
| Figure 3.17 | Boxplots showing SGP C-coefficient – Drying Tests.....  | 74  |
| Figure 3.18 | Boxplots showing mean max force – Force and Rate Tests.....   | 77  |
| Figure 3.19 | Boxplots showing mean max strain – Force and Rate Tests.....  | 78  |
| Figure 3.20 | Boxplots showing mean max SGP – Force and Rate Tests.....   | 79  |
| Figure 3.21 | Boxplots showing mean delta SGP – Force and Rate Tests.....   | 80  |
| Figure 3.22 | Boxplots showing SGP Tau 1 – Force and Rate Tests.....  | 81  |
| Figure 3.23 | Boxplots showing SGP Tau 2 – Force and Rate Tests.....  | 82  |
| Figure 3.24 | Boxplots showing SGP A-coefficient – Force and Rate Tests.....  | 83  |
| Figure 3.25 | Boxplots showing SGP C-coefficient – Force and Rate Tests.....  | 84  |
| Figure 4.1  | Plot showing relationship between water content and resistance of bone as reported by Eriksson in 1974..... | 87  |
| Figure 4.2  | Response of dry bone to a step load as reported by Hou in 2011.....   | 88  |
| Figure 4.3  | Amplified signal from charge amplifier tests.....   | 90  |
| Figure 4.4  | Schematic demonstrating effect of sample thickness on strain for equal forces.....                          | 97  |
| Figure 4.5  | Plots showing tau 2 values for SGP and Strain – Preliminary Tests.....                                      | 99  |
| Figure 4.6  | Boxplots of mean max SGP and delta SGP – Force and Rate Tests.....  | 102 |
| Figure 4.7  | Plots showing the effects of individual values in the two-term exponential curves.....                      | 103 |
| Figure 4.8  | Plots of the relationship between SGP and load/deformation in wet bone as reported by Cochran in 1968.....  | 106 |
| Figure 4.9  | Plots of SGPs produced by different deformation rates as reported by Cochran in 1968.....                   | 107 |

Figure 4.10 Plots of the relationship between SGP and load/strain rate in wet bone as reported by Gross and Williams in 1982.....108

## List of Tables

|            |  |     |
|------------|--|-----|
| Table 2.1  | Dry vs. Wet Test Groups.....   | 26  |
| Table 2.2  | Dry vs. Wet Test Information.....  | 27  |
| Table 2.3  | Charge Amplifier Test Information.....   | 29  |
| Table 2.4  | Evaporation Test Sample Information.....                                       | 30  |
| Table 2.5  | Evaporation Test Information.....  | 31  |
| Table 2.6  | Unified Sample Preparation Test Information.....                               | 33  |
| Table 2.7  | Drying Test Sample Information.....  | 34  |
| Table 2.8  | Pre-Load Test Information.....   | 37  |
| Table 2.9  | Drying Test Information for Long and Short Duration Tests.....                 | 38  |
| Table 2.10 | Force and Rate Test Information.....   | 43  |
| Table 2.11 | Variations of Test Order for the Force and Rate Tests.....                     | 43  |
| Table 2.12 | Descriptions of Values Collected from Tests.....                               | 50  |
| Table 2.13 | What the Values in Equation 3.1 Represent.....                                 | 51  |
| Table 3.1  | Avg. Thicknesses of All Samples vs. Samples with Thicknesses < 3.15 mm.....    | 58  |
| Table 3.2  | T-Test Results Comparing Max SGP Between All Three Drying Tests.....           | 68  |
| Table 3.3  | T-Test Results Comparing Delta SGP Between All Three Drying Tests.....         | 69  |
| Table 3.4  | T-Test Results Comparing SGP Tau 1 Between All Three Drying Tests.....         | 71  |
| Table 3.5  | T-Test Results Comparing SGP Tau 2 Between All Three Drying Tests.....         | 72  |
| Table 3.6  | T-Test Results Comparing SGP A-coefficient Between All Three Drying Tests..... | 73  |
| Table 3.7  | T-Test Results Comparing SGP C-coefficient Between All Three Drying Tests..... | 74  |
| Table 4.1  | Summary of Results Obtained from Curve Values - Force and Rate Tests.....      | 102 |

## List of Abbreviations and Symbols

|                  |                                 |
|------------------|---------------------------------|
| %                | per cent                        |
| SGP(s)           | stress-generated potential(s)   |
| •                | degrees                         |
| >                | greater than                    |
| <                | less than                       |
| HA               | hydroxyapatite                  |
| mm               | millimeters                     |
| $\tau$           | time constant, tau value        |
| °C               | degrees Celsius                 |
| V                | volts/voltage                   |
| $\pm$            | plus or minus                   |
| Hz               | hertz                           |
| $f_c$            | cut-off frequency               |
| $V_{cc}$         | voltage supplied to the circuit |
| G                | gain                            |
| C                | capacitance/capacitor           |
| R                | resistance/resistor             |
| DC               | direct current                  |
| N                | newtons                         |
| $\mu\epsilon$    | micro-strain                    |
| min              | minute                          |
| ANOVA            | analysis of variance            |
| LTI              | linear time-invariant           |
| $V_o$            | initial voltage                 |
| mV               | millivolts                      |
| mg               | milligram                       |
| H <sub>2</sub> O | chemical name for water         |
| max              | maximum                         |
| std              | standard deviation              |

## **Declaration of Academic Achievement**

I, Laura Pravato performed all preliminary research, sample preparation, electrical set up, mechanical testing of bones, and statistical analysis presented in this thesis and am solely responsible for the content. My supervisor, Dr. Gregory Wohl, provided expertise in mechanics, supervised and guided in this work. My co-supervisor, Dr Hubert de Bruin, provided guidance for the electrical instrumentation set up. Elyse Rier aided in curve fitting the data in MATLAB.

# **1 Background**

## **1.1 Introduction**

Bone is a complex material that constantly rebuilds itself to adapt to its environment. The activation process behind bone remodeling is not well understood and can be initiated by a variety of stimuli such as hormonal signals, mechanical loading, or damage (Buckwalter, Glimcher, Cooper, & Recker, 1995; Duncan & Turner, 1995; Robling, Castillo, & Turner, 2006). In general, bone adaptation is believed to depend primarily on mechanical stimuli as bone tends to reinforce itself in the parts where forces are irregular (Currey, 1968; Robling et al., 2006). For example, it has been shown that the bones in tennis players' dominant arms are thicker and denser than their non-dominant arms (Jones, Preist, Hayes, Tichenor, & Nagel, 1977).

Osteocytes are the main cells that regulate bone remodeling. These fully-matured bone cells are mechanotransducers that produce biochemical signals in response to mechanical deformation. These biochemical signals then trigger the production of osteoblasts, which are then recruited to the particular sites where new bone deposition is needed (Duncan & Turner, 1995; Robling et al., 2006). Osteocytes and other bone-lining cells, make up about 95% of all bone cells and are imbedded within the lacuno-canalicular network (Buckwalter et al., 1995; Duncan & Turner, 1995; Robling et al., 2006). The canaliculi are filled with extracellular fluid and house the cellular processes that allow osteocytes to connect to each other via gap junctions. These connections allow for intercellular signalling, nutrient transfer, and the removal of wastes (Buckwalter et al., 1995; Burger & Klein-Nulend, 1999; Marks Jr & Popoff, 1988).



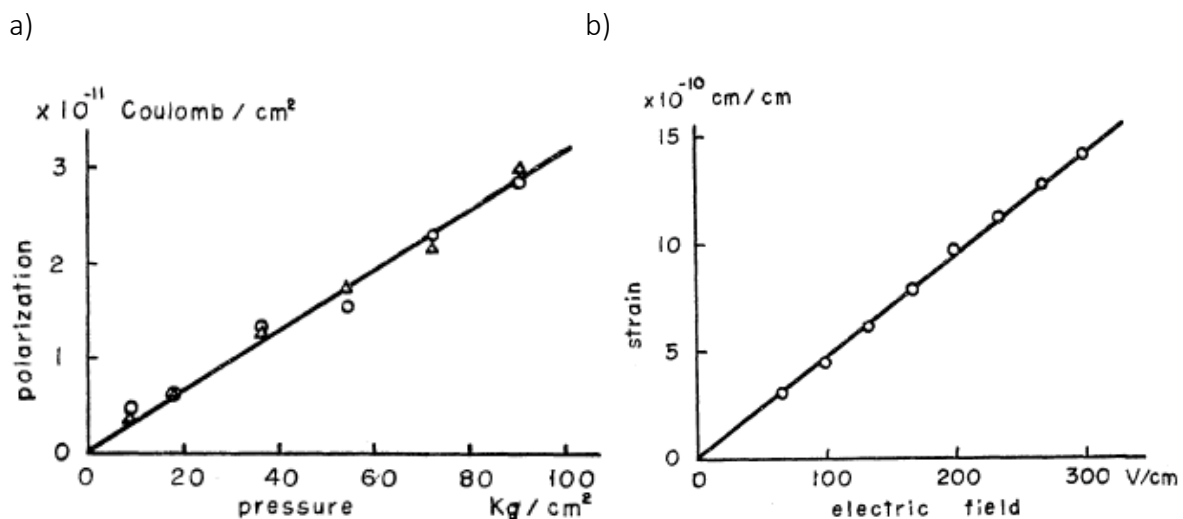
The process by which osteocytes are able to transduce a mechanical signal into a biochemical one is not entirely understood as a variety of changes occur within the bone during deformation – particularly, interstitial fluid movement causes shear stress on the cell membranes, changes the extracellular pressure and produces stress-generated electrical potentials (Iller & Papapoulos, 2013). Although it is likely a combination of all these occurrences that result in an overall change in bone architecture, each of these changes have been studied in an attempt to determine the impact on overall bone homeostasis both *in vivo* and *in vitro*.

Although it is generally accepted that biochemical signals are produced in response to mechanical deformation, the relationship between stress-generated electrical potentials and cellular signaling is less clear. Some studies have reported that electrical stimulation of bone leads to osteogenesis (Mcleod & Clinton, 1992) and helps accelerate bone healing (Bassett, Pawluk, & Pilla, 1974). At this point, it is unclear if/how osteocytes respond to electrical stimulation, but it has been reported that osteoblasts and osteoclasts clearly migrated in response to an electrical field. Specifically, osteoclasts migrated towards to positive electrode and osteoblasts to the negative electrode (Ferrier, Ross, Kanehisa, & Aubin, 1986). On a similar note, a common theme in mechanical loading experiments show that bone surfaces under compression produced negative electrical potentials and bone surfaces under tension produce positive potentials (Bassett & Becker, 1962; Cochran, Pawluk, & Bassett, 1967; Eriksson, 1974; E. Fukada, 1968; Gross & Williams, 1982; Isaacson & Bloebaum, 2010; Steinberg, Wert, Korostoff, & Black, 1973). Since bone is deposited in areas of compression and reabsorbed in areas of tension, this discovery adds validation to the proposal that there is an electrical component to bone remodeling (Currey, 1968; Robling et al., 2006).

Although it has been well-demonstrated that strain leads to the activation of the bone remodeling process, and that there would be high amount of strain in areas under compression, there is also evidence showing that extracellular fluid movement within the bone also triggers remodeling (Robling et al., 2006). Studies have shown that shear stress on the osteocytes and their cellular processes caused by fluid movement has led to activation (Burger & Klein-Nulend, 1999), but there is also a possibility that osteocytes respond to the electrical potentials produced by loads that induce fluid movement within the bone.

## 1.2 Piezoelectricity and Electrical Potentials in Dry Bone

Bone remodeling is believed to be initiated predominantly by mechanical loading which, in turn, has been shown to produce stress-generated potentials (SGPs). In 1957, Fukada and Yasuda reported linear relationships (Fig. 1.1a-b) between mechanical deformation of dry bone causing electrical polarization, and mechanical strain produced by subjecting bone to an electric field (Eiichi Fukada & Yasuda, 1957).



Figures 1.1a-b: Figure 1a shows the direct piezoelectric effect of dry bone. Figure 1b shows the converse piezoelectric effect of dry bone. Both are linear relationships (Eiichi Fukada & Yasuda, 1957).

Since this discovery, numerous researchers have explored the electrical properties of bone and have tried to determine whether or not it is a true piezoelectric material. Classically, a material is piezoelectric if it produces an electric charge when subjected to mechanical stress, and if a charge is applied to the material it deforms mechanically (Jacob, More, Kalia, & Kapusetti, 2018; McElhaney, 1967). All piezoelectric crystals are anisotropic and must be asymmetric (lack a center of symmetry) in order to produce charge (Jacob et al., 2018; Shamos & Lavine, 1964). Some known natural piezoelectric crystals are quartz, tourmaline, and sucrose. Biological tissues such as bone tendon and cartilage have demonstrated piezoelectric properties. There are also man-made piezoelectric crystals and ceramics such as langasite and PZT, which is commonly found in ultrasound transducers (Jacob et al., 2018).

Piezoelectricity has been measured in anisotropic crystals by experimentally determining the “d-coefficient” matrix (shown below) that relates polarization in a material to applied stress:

$$(d_{ij}) = \begin{bmatrix} d_{11} & d_{12} & d_{13} & d_{14} & d_{15} & d_{16} \\ d_{21} & d_{22} & d_{23} & d_{24} & d_{25} & d_{26} \\ d_{31} & d_{32} & d_{33} & d_{34} & d_{35} & d_{36} \end{bmatrix}$$

Fukada and Yusada determined that SGPs in bone and tendon were only produced when subjected to shear stress, and modified the matrix accordingly:

$$(d_{ij}) = \begin{bmatrix} 0 & 0 & 0 & d_{14} & 0 & 0 \\ 0 & 0 & 0 & 0 & -d_{14} & 0 \\ 0 & 0 & 0 & 0 & 0 & 0 \end{bmatrix}$$

This holds true for a z-axis that is angled 10° with respect to the bone long axis. This matrix is similar to two other biological piezoelectric materials, wood and ramie (Eiichi Fukada & Yasuda, 1957). Piezoelectricity of both bone and collagen have been classified using these d-coefficients. SGPs have been found to be directly proportional to the material's d-coefficients as shown in equation 1.1 (Ahn & Grodzinsky, 2009).

$$V = \frac{d_{ijk}L}{\epsilon} B e^{-\frac{\sigma t}{\epsilon}}$$

**Equation 1.1:** Equation showing how SGPs ( $V$ ) are proportional to the d-coefficient. In this case the d-coefficient ( $d_{ijk}$ ) is a third rank piezoelectric tensor.  $L$  is sample thickness,  $\epsilon$  is the dielectric constant of permittivity,  $\sigma$  is the solution conductivity,  $B$  is load and  $t$  is time.

### 1.3 Exploring the Sources of Piezoelectricity in Bone

Bone is made up of an extensive extracellular matrix that is, by weight, approximately 10% water, 20% collagen fibers and 65% crystalized mineral salts (calcium phosphate, calcium hydroxide, hydroxyapatite, calcium carbonate, magnesium, fluoride, potassium and sulfate) (Buckwalter et al., 1995). Collagen is what provides bone's elasticity, while minerals account for bone's hardness. Oddly enough, the inorganic mineral/crystal part of bone is not the main source of the piezoelectric effect and is believed to have little effect, if any, on the SGPs of bone (Guzelsu & Walsh, 1990; Marino, Becker, & Soderholm, 1971). Hydroxyapatite (HA) crystals are not believed to be piezoelectric because they are centrosymmetric (Anderson & Eriksson, 1968).

Both the direct and converse piezoelectric effect can be beneficial biologically. Research has suggested that electric and magnetic fields can help heal nonunion fractures (Bassett et al., 1974; Isaacson & Bloebaum, 2010), while other studies explored the possibility that subjecting bones to vibrations (> 30Hz, < 1MPa) could help increase bone density (Chen, Liu, You, & Simmons, 2010).

These applications can be useful in many clinical settings, such as maintaining bone density in bedridden patients (Buckwalter et al., 1995; Cowin & Hegedus, 1976) or in astronauts in zero-gravity situations (Duncan & Turner, 1995; Ehrlich & Lanyon, 2002; Robling et al., 2006).

Proving bone is a piezoelectric material in the classic sense has proven to be much more difficult. There have been many different approaches to evaluating the piezoelectricity of bone such as considering the polarizability of HA (Hiratai, Nakamura, & Yamashita, 2014; Nakamura, Hiratai, & Yamashita, 2012), dielectric properties of bone (Johnson, Chakkalakal, Harper, & Katz, 1980; Saha & Williams, 1992), and classification using piezoelectric constants as for a known piezoelectric material (E. Fukada, 1968; Marino & Becker, 1974; Williams & Breger, 1975). Since bone is an anisotropic material it is difficult to classify its signals based off piezoelectric or dielectric constants because they tend to change with orientation (Anderson & Eriksson, 1970; Johnson et al., 1980; McElhaney, 1967). Due to the high amount of variation in both function and type of bone, classifiers such as d-coefficients produce inconclusive results on a microscopic scale (Marino et al., 1971). Therefore, researchers have attempted to classify the SGPs produced by bone on a larger, macroscopic scale.

### **1.3.1 Collagen Piezoelectricity**

In bone, collagen fibers are highly oriented along bone's long axis and have HA crystals embedded among them. Tendon is made up of densely packed collagen fibers that are aligned along the tendon's long axis (Anderson & Eriksson, 1968). Research involving tendon has found dry collagen to be a strongly piezoelectric material (Anderson & Eriksson, 1968; Eiichi Fukada & Yasuda, 1957). Collagen's piezoelectric effect seems to be highly dependent on its hydration level since deformation of fully hydrated collagen does not produce any sort of piezoelectric effect (Johnson

et al., 1980; Marino & Becker, 1974). Collagen is asymmetric, and therefore is piezoelectric, but it is possible that collagen becomes a more symmetrical material as it becomes more hydrated (Anderson & Eriksson, 1968). Upon further research, Anderson determined that SGPs from dry bone were due to collagen since the piezoelectric constants were similar to those found in pure, dry collagen (Anderson & Eriksson, 1970).

Since bone is 10% water *in vivo*, it is reasonable to assume that collagen in bone should be reasonably hydrated. Though, it has been hypothesized that the HA crystals could help keep water molecules away from the collagen and therefore prevent the collagen from becoming fully hydrated (Marzec, Kubisz, & Jaroszyk, 1996). This relationship between the two main components of bone's extracellular matrix may cause a piezoelectric effect due to the collagen fibers being partially dehydrated by the embedded minerals (Ahn & Grodzinsky, 2009; Anderson & Eriksson, 1970; Noris-Suárez et al., 2007).

### **1.3.2 Potential Differences and Bone Deposition**

There is much research demonstrating the effect of SGPs on bone deposition. As mentioned in Section 1.1, a common theme throughout multiple experiments show that bone surfaces under compression become negatively charged and bone surfaces under tension become positively charged (Bassett & Becker, 1962; Cochran et al., 1967; Eriksson, 1974; E. Fukada, 1968; Gross & Williams, 1982; Isaacson & Bloebaum, 2010; Steinberg et al., 1973). A study by Johnson showed that this only held true in wet bone, whereas in dry bone the charges were independent of stress (Johnson et al., 1980). This supports McElhaney's findings that the polarity of SGPs varied, seemingly randomly, with orientation in a dry whole femur (McElhaney, 1967). These results make

sense due to bone's high level of anisotropy and the variability of piezoelectric coefficients throughout the bone structure.

Other research conducted on misaligned fractures found that bone is deposited on the concave side of bone and is resorbed on the convex side, allowing for the bone to straighten over time (Currey, 1968; Fernández, García-Aznar, & Martínez, 2012). It has been reported that osteoblasts, the cells that form new bone, gather in negatively charged areas (Isaacson & Bloebaum, 2010). In 2007, Noris-Suarez found high levels of HA crystal deposition on the concave side of a demineralized bone that was subjected to a steady flow of simulated body fluid for four weeks (Noris-Suárez et al., 2007). This study suggested that highly saturated collagen produced enough piezoelectric charge to recruit osteoblasts to deposit mineralized bone at its concave surfaces. This also contradicts the claim that hydrated collagen loses its piezoelectric properties. It is possible that the mineral deposition is simply due to the shear stress and/or streaming potentials caused by the simulated body fluid on the surface cells of the collagen and has no correlation to collagen orientation.

#### 1.3.4 Streaming Potentials

In bone, streaming potentials are caused by collective ionic fluid movement where the majority of ions in the fluid are negatively charged due to a collection of positively charged ions which remain close to the negatively charged surface of the bone (Duncan & Turner, 1995). The magnitude of

$$V = \frac{\zeta \epsilon \Delta P}{\sigma \eta}$$

**Equation 1.2:** The streaming potential is proportional to the zeta potential ( $\zeta$ ), the dielectric permittivity ( $\epsilon$ ) and the pressure gradient ( $\Delta P$ ). It is inversely proportional to viscosity ( $\eta$ ) and conductivity ( $\sigma$ ) of the solution/liquid that is being displaced.

the streaming potential depends on the pH, viscosity, NaCl concentration, conductivity of the fluid and the type of molecules within it (equation 1.2). The work done by Pienkowski confirms that streaming potentials are the primary source of SGPs in wet bone by demonstrating the dependence of the signal on the fluid's physical properties (Pienkowski & Pollack, 1983).

It is possible to completely remove streaming potentials by finding a pH that corresponds to the isoelectric point of a solution. This pH value results in a streaming potential of zero magnitude by causing the ion concentration to be in equilibrium (Anderson & Eriksson, 1970). Upon reaching the isoelectric point of tendon, Anderson was able to measure solely the piezoelectric effect of the collagen fibers. They found no SGPs produced by the wet tendon. This led to the conclusion that streaming potentials were the sole source of piezoelectricity in wet tendon.

The Zeta potential is the difference between the charge of particles on a surface and the charge of the ionic fluid flows to produce a streaming potential (Eriksson, 1974). Zeta potentials have a direct effect on the magnitude of the streaming potential in the bone. In 1988, Otter determined that streaming potential SGPs in both de-collagenated and demineralized bone were smaller than those found in whole bone but acknowledged that it is possible that changes in the bone geometry could have caused this effect. This study also determined that the Zeta potential in demineralized bone was almost the same as in whole bone, whereas the Zeta potential in de-collagenated bone was much smaller (Otter, Goheen, & Williams, 1988).

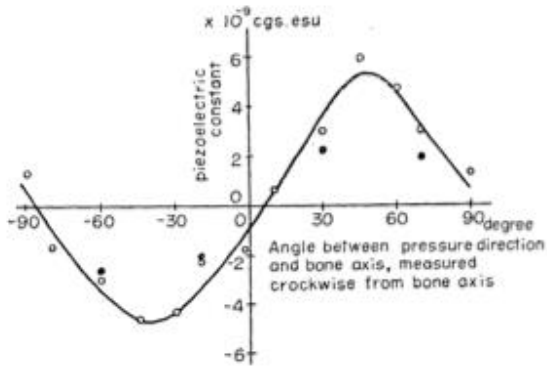
### **1.3.5 Shear Stress and SGPs**

It has been discussed that osteocytes trigger bone remodeling when subjected to shear stress by the movement of fluid past their cellular processes (Burger & Klein-Nulend, 1999). This hypothesis



has been challenged by other authors who believe that fluid movement alone does not give the osteocytes information on what kind of stress the bone is being subjected to (shear, bending,

a)



b)

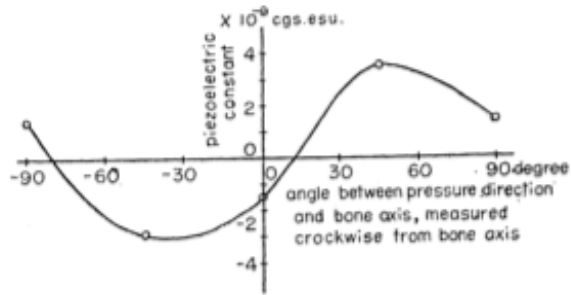


**Figure 1.2a-b:** Dependence of piezoelectric constants of bovine femur (7a) and human femur (7b) on the angle between direction of applied load and long axis of the bone (Eiichi Fukada & Yasuda, 1957).

tension, compression etc.). Bone remodels based on the stresses it experiences and it has been suggested that collagen fibers can relay to osteocytes the kinds of stresses they are experiencing (Ahn & Grodzinsky, 2009; Duncan & Turner, 1995). Fukada found that dry bone produced the maximum piezoelectric effect when the loads were applied at a  $45^\circ$  shear force on the longitudinal collagen fibers along the bone axis (Fig. 1.2a-b) (Eiichi Fukada & Yasuda, 1957). This was attributed to the collagen fibers slipping past each other at this orientation and possibly changing the electric properties of collagen (Hou, Fu, & Qin, 2011). Since the collagen is what experiences the highest amount of stress during deformation, compared the mineral components, it would also explain why bone only remodels when subjected to irregular loads such as shear stress and bending (Gjelsvik, 1973).

## **1.4 The Importance of Time on SGPs**

While many papers reported d-coefficients or dielectric constants of dry bone, few papers showed actual time-domain plots of SGPs in response to bone loading. The electrical response to applied loads with respect to time can reveal valuable information about the relationship between the electrical and mechanical properties of bone. Only two papers (Bassett & Becker, 1962; Steinberg et al., 1973) reported SGP signals from wet bone that showed time response curves with identifiable traits including 1) a clear exponential decay following the application of a load/displacement, 2) a steady-state SGP maintained throughout that held load/displacement and 3) a negative voltage produced upon the release of that load. The data reported by Bassett and Steinberg can be seen in (Fig. 1.3 – 1.4).

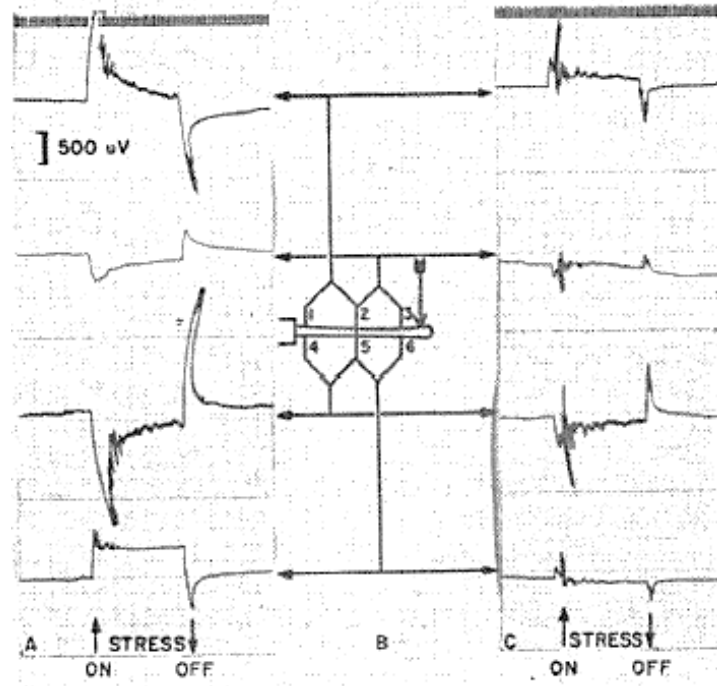


**Figure 1.3:** In 1962 Bassett and Becker attributed signals in bone solely to collagen piezoelectricity. They were not aware of streaming potentials produced in wet bone at this time (it was proposed by Anderson in 1968). The electrode placements are shown in (B). 30g of stress was applied in (A) and 15g in (C). Both have the same gain implying that increased loads increase the magnitude of the SGPs. A small steady state potential is seen during the held load (Bassett & Becker, 1962).

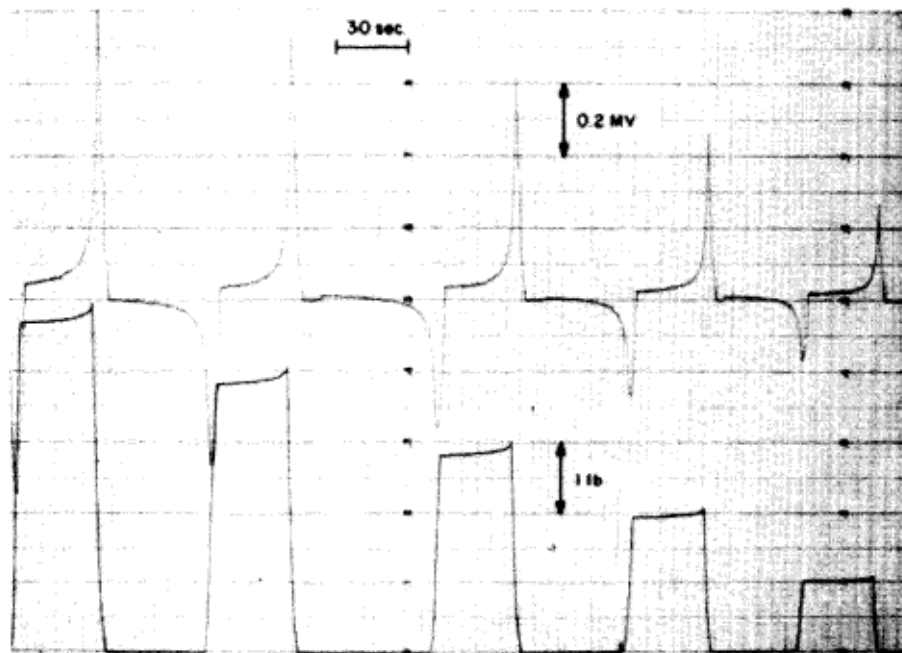


**Figure 1.4:** In 1973 Steinberg performed tests on whole (wet) rat femurs and determined the relationship between SGPs and types of loading. The top signal is the SGP and the bottom signal is the deformation. The amount of deformation was increased each time (increasing from left to right) and it is clear that the SGP amplitude increased with the deformation. Each deformation was held for 30 seconds. After almost a decade it is clear that these plots are much cleaner than the ones from Bassett's study (Fig. 1.3) (Steinberg et al., 1973).

Although qualitative assessment of these signals can provide some insight on the electromechanical properties of bone, the quantitative characteristics of these SGP signals were not examined by these authors. For example, they noted the effect increasing loads had on SGPs but did not investigate what the shape of these signals indicated, particularly the rate of decay following the applied load. Three other groups investigated how the time-dependence of SGPs reveal information, not only about the properties of the bone, but also the fluid within it (Gross & Williams, 1982; Hou et al., 2011; Pienkowski & Pollack, 1983). Most notably, Pienkowski and Pollack examined the effects of solution conductivity and viscosity on the time constants ( $\tau$ ) they identified from their SGP curves (Pienkowski & Pollack, 1983).

Pienkowski and Pollack observed that they would need two different time constants to describe the relaxation times of their SGP curves. Due to technical limitations they were unable to confidently determine the tau values associated with the decaying exponentials they found in their curves. They stated the time constants as  $\tau_{fast}$  and  $\tau_{slow}$ .  $\tau_{fast}$  characterized the inverse of the slope of the SGP curve from 0 – 0.031 seconds after the load was applied and  $\tau_{slow}$  characterized the inverse of the slope of the curve from 0.31 seconds after the load was applied until the signal decayed to zero (Fig. 1.5). They found that  $\tau_{fast}$  increased with increasing fluid viscosity within the bone.

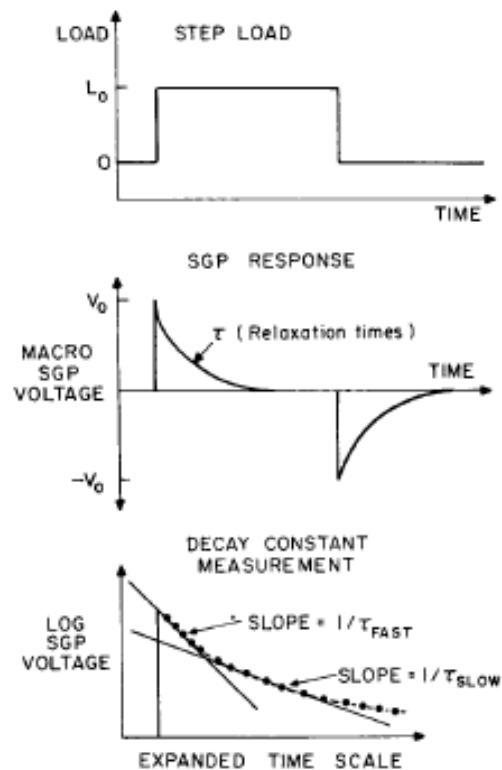


**Figure 1.5:** The SGP response (middle) to a step load (top) and the method for determining the time constants associated with the exponential decay of the SGP curve (bottom) (Pollack et al., 1984).

On a similar note, Gross and Williams also found larger time constants proportional to increasing viscosity for various fluid viscosities (Fig. 1.6). In this study they were measuring the effect of different ionic concentrations and fluid viscosities on the streaming potentials in wet bone (Gross & Williams, 1982).

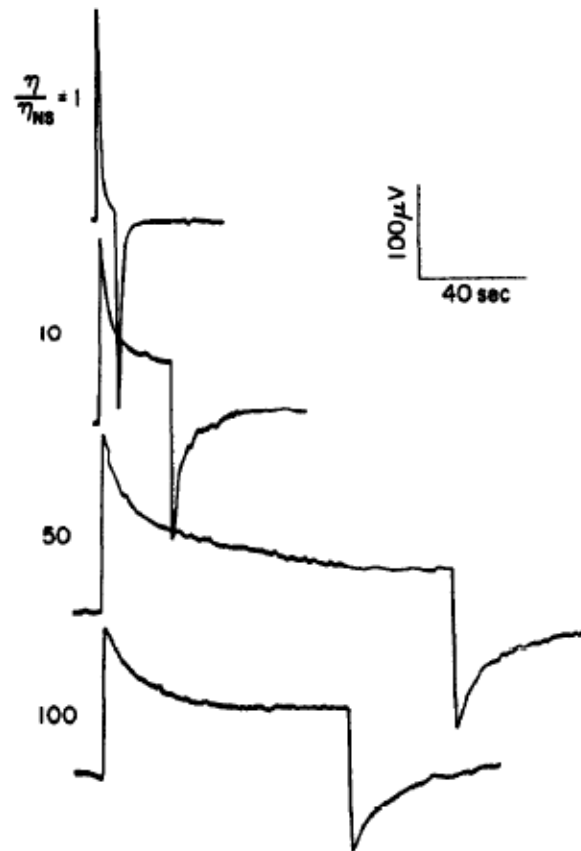


**Figure 1.6:** The dependence of viscosity on the time it takes the SGP to decay. Deformation rate was constant for each curve but the time between loading and unloading varies (Gross & Williams, 1982).

There is other work that reported similar SGP signals with decaying exponential curves in both wet and dry bone (Bassett & Becker, 1962; Cochran, Pawluk, & Bassett, 1968; Gross & Williams, 1982; Hou et al., 2011; Pienkowski & Pollack, 1983; Steinberg et al., 1973; Williams & Breger, 1975) (see Appendix 6). These signals varied in magnitude, shape (i.e. was there a steady-state voltage or did

they rapidly decay to zero?) and symmetry (i.e. are the positive and negative peaks of equal magnitude?). A summary of these papers and their measured voltage signals can be found in Appendix 6.

## **1.5 Research Objectives**

A variety of changes occur within the bone during loading – particularly, interstitial fluid movement causing shear stresses on the cell membranes within the matrix, changes in extracellular pressure, and production of stress-generated electrical potentials (Iller & Papapoulos, 2013). Although it is likely the combination of all these occurrences that result in an overall change in bone architecture, each of these changes have been studied in an attempt to determine their contribution to overall bone homeostasis both *in vivo* and *in vitro*.

The electrical component to bone remodeling is much less understood compared to the mechanical components. Through our studies, we hope to gain a better understanding of the role SGPs play in bone remodeling. Since bone is sensitive to strain magnitude, strain rate, and dynamic loading (Currey, 1968; Frost, 1992), the relationship between the SGPs and mechanical strains will be directly analyzed with reference to time. Specifically, how the load magnitude and strain rate relate to the magnitude and gradual decay of these SGPs.

By understanding the role these electrical potentials play in bone remodeling, future researchers can apply that knowledge to develop therapies using electrical stimulation for patients experiencing a decrease in bone strength as a result of osteopenia or osteoporosis.

In this work, I explored the effects of drying, increased load magnitudes and increased deformation rates on the SGPs produced by streaming potentials<sup>1</sup> in beams of wet cortical bone. To measure the electrical charge response in the time domain, I fit two-term exponential curves to the SGPs. The parameters from these curves, including gain and time constants, were used to characterize the decaying exponential in the SGP signal in response to mechanical loading.

---

<sup>1</sup> From this point on, SGP will refer to those produced by streaming potentials rather than by piezoelectric charge unless stated otherwise.



## **2 Materials and Methods**

### **2.1 Sample Preparation**

The use of animal tissues was approved by the Animal Research Ethics Board at McMaster University in accordance with the guidelines of the Canadian Council for Animal Care. Frozen bovine femurs (purchased from the grocer) were cut into rectangular beams (50mm x 20mm x 3mm) (Fig. 2.1a). These samples were all cut so that the long axis of the sample was parallel to the long axis of the bone. The bones were initially cut using a band saw (Skil 9 Inch Benchtop Band Saw) to isolate the diaphysis and subsequently to cut the diaphysis into smaller segments. From those segments, the beams were cut using a low-speed diamond wafer saw (Beuhler Isomet). Samples were cut in this manner based off previous work that cut beams of similar dimensions (Cochran et al., 1968; Hou et al., 2011; Williams & Breger, 1975).

A total of 26 samples were originally cut but, due to exclusions, only 21 samples were used during testing. Reasons for exclusion included samples being too thin or damage, such as fracture. Samples were all given a number for identification. The sample number was written on the bottom right corner of the sample using permanent marker and sealed using nail polish to ensure the saline solution would not fade the number (Fig. 2.2). The samples were wrapped in saline-soaked (NaCl 0.9% Irrigation, Baxter Corporation, Mississauga Ontario) paper towel before being stored in the freezer at -20 °C.

Uniaxial strain gauges (FLA-2-11-3LJC, Tokyo Sokki Kenkyujo Co., Ltd.) were applied to all samples before testing. The location of the strain gauge was on the top of the sample, approximately 30 mm from the bottom of the sample (Fig. 2.1b). The strain gauge application procedure was as

follows: dry the surface of the sample, dehydrate the location of strain gauge placement using ethanol/acetone, apply the strain gauge using super glue, once dry, apply nail polish fully covering the strain gauge, and secure the strain gauge wires with either nail polish or super glue.

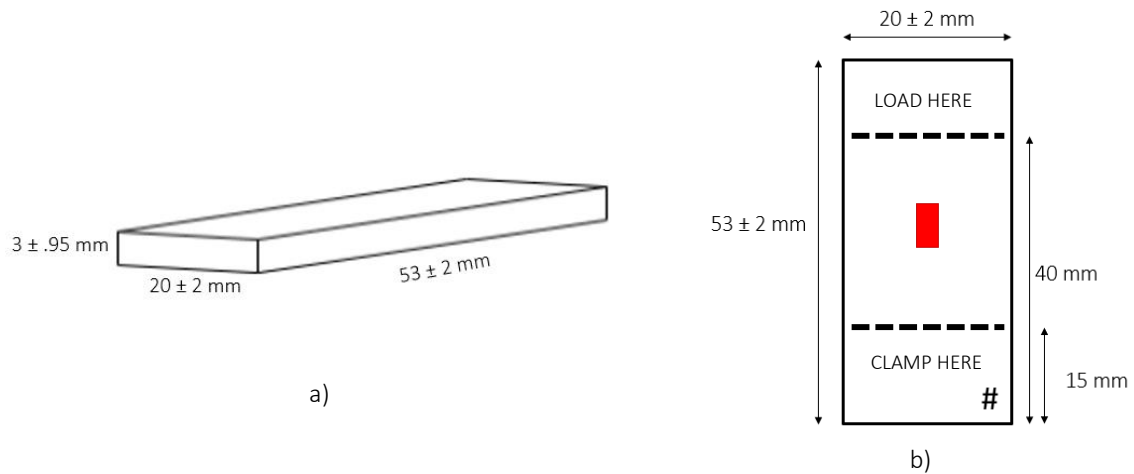


**Figure 2.1a:** Average dimensions of the beams of cortical bone.

**Figure 2.1b:** Schematic of sample showing location of strain gauge, sample identification number and the location where the samples were clamped and where the loads were applied.

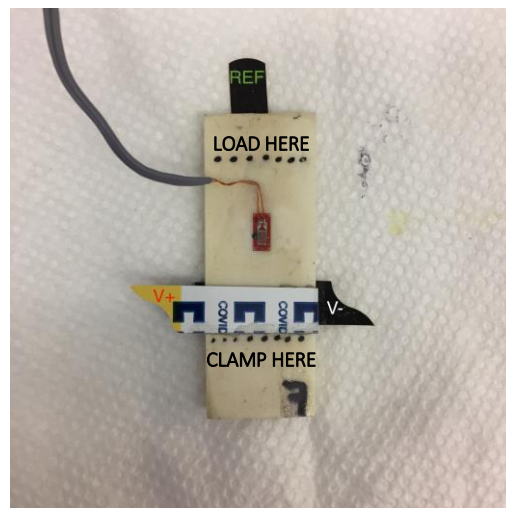


**Figure 2.2:** Photo of sample 7 showing location of strain gauge, sample identification number, the location where the samples were clamped, where the loads were applied as well as how the electrodes strips were applied. The top electrode was always V+, the bottom electrode was always V- and the electrode at the end of the sample was always V<sub>ref</sub>.

## **2.2 Electrical Circuitry and Data Acquisition**

### **2.2.1 Bioinstrumentation Circuit for Stress-Generated Potentials**

SGPs were collected using sticky tab electrodes (COVIDIEN, Kendall 550 Diagnostic Tab Electrodes). One electrode was used per sample by cutting it into three strips: one electrode strip was placed at the end of the bone to collect the reference potential, and two strips were placed on opposing sides of the bone 15 mm from the bottom of the sample (Fig. 2.2). The electrodes were not placed on top of the strain gauge because 1) we did not want the strain gauges to come off or break when the sticky electrodes were removed and 2) there was leakage of the SGP through the strain gauge leads which diminished the magnitude of the signal being collected by the electrodes.

Before signal acquisition into the computer, the SGP signal was preprocessed by a custom analog bioinstrumentation amplifier<sup>2</sup>. There were four stages to the bioinstrumentation amplifier (Fig. 2.3). The first stage was the instrumentation amplifier (LT1920, input impedance 200 G $\Omega$ ), which removed any common-mode signals measured between the electrodes and amplified the signal by a gain of 100. The second stage was a non-inverting amplifier (TLC2274), which had a gain of 2, resulting in a total gain of 200. The third stage was a fourth-order Chebyshev low pass filter with a cut-off frequency ( $f_c$ ) of 6 Hz. The fourth stage was an inverting DC offset circuit. On occasion, the SGP voltage baseline was too large and saturated the amplifier, so adding a DC offset allowed for the collection of any signals that went beyond the circuit voltage limitations.

---

<sup>2</sup> The bioinstrumentation amplifier circuit will be referred to as the SGP circuit from now on.

The SGP, strain and force signals (see section 2.3, Mechanical Testing) were input to a National Instruments DAQ (National Instruments USB-6009) and then into a LabVIEW (2014) program (see program details in Appendix 5). The data was sampled continuously at 100 Hz. Before saving the data to a file, all signals were digitally filtered in LabVIEW, by a 5th order low-pass Butterworth infinite-impulse response filter with a cut-off frequency of 5 Hz.

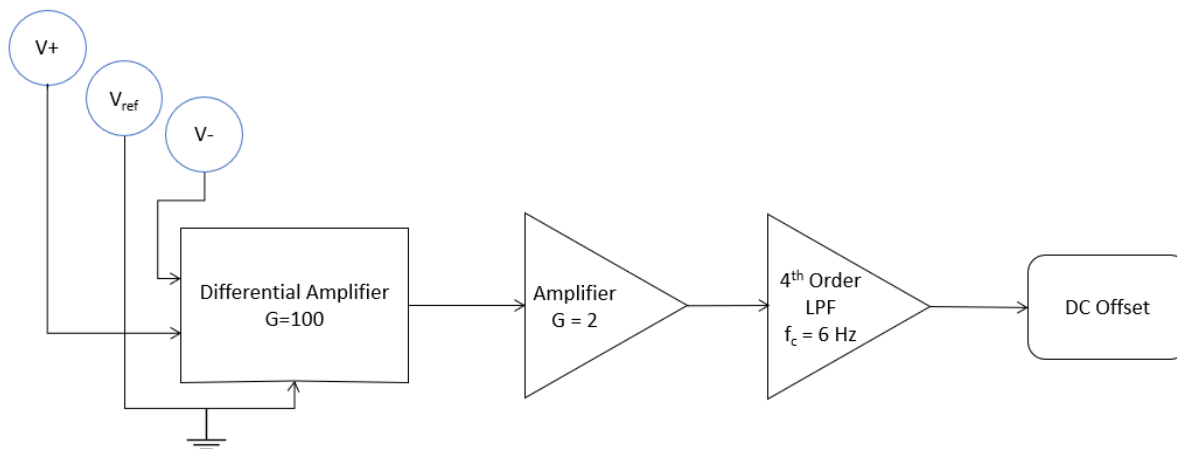


**Figure 2.3:** Block schematic of bioinstrumentation circuit for SGP filtering and amplification. Circuit details as well as the calculations can be found in Appendix 2.

## Troubleshooting

To reduce ambient noise in the lab, a custom Faraday cage was placed under the mechanical testing system and completely encased the bone sample and SGP circuit. The Faraday cage was made from a cardboard box wrapped in heavy-duty aluminum foil that was grounded to common ground. This helped reduce the noise produced when people would move around the lab but, if anyone touched the cage, the SGP circuit would still pick up a noisy signal. This was avoided by making sure the cage was not touched during testing.

During initial testing, some SGPs were saturating the amplification circuit. This was eventually discovered to be caused by too much signal amplification (at this point the gain was 1,100). Oddly, the saturation boundaries of the circuit were approximately -5.6V and +2.8V, resulting in a range of 8.4 V (Fig. 2.4). Since these are not symmetrical voltage boundaries, since most circuits operate on a symmetrical  $\pm V_{cc}$ , it is likely the correct zero baseline is around -1.8V. After the gain was reduced from  $G = 1,100$  to  $G = 200$ , samples were tested and signals were collected.

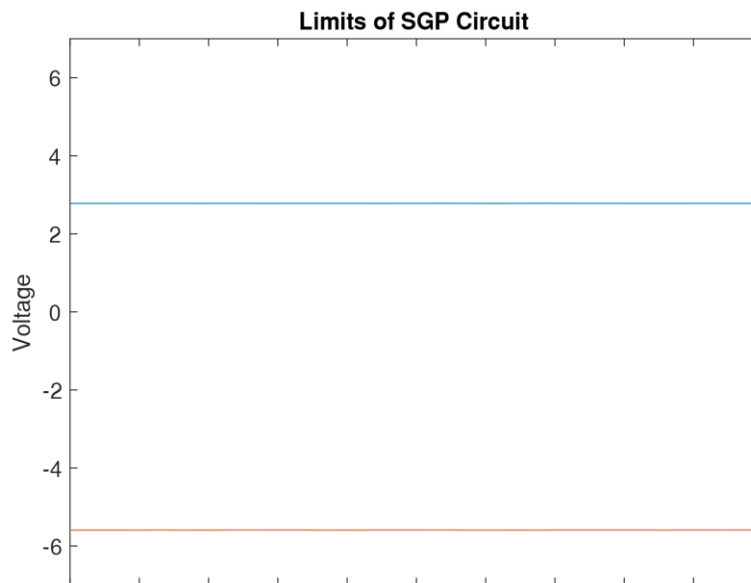


**Figure 2.4:** Plot shows positive and negative voltage limits of the SGP circuit at +2.8V (blue) and -5.6V (orange).

Another source of noise was due to movement of the load cell and load cell wires as the sample was being mechanically loaded. Since these components were inside the Faraday cage, this was an unavoidable source of error. The motion of the load cell wires could be the cause of capacitive coupling motion artifact collected in the electrode leads as seen in figure 2.5.

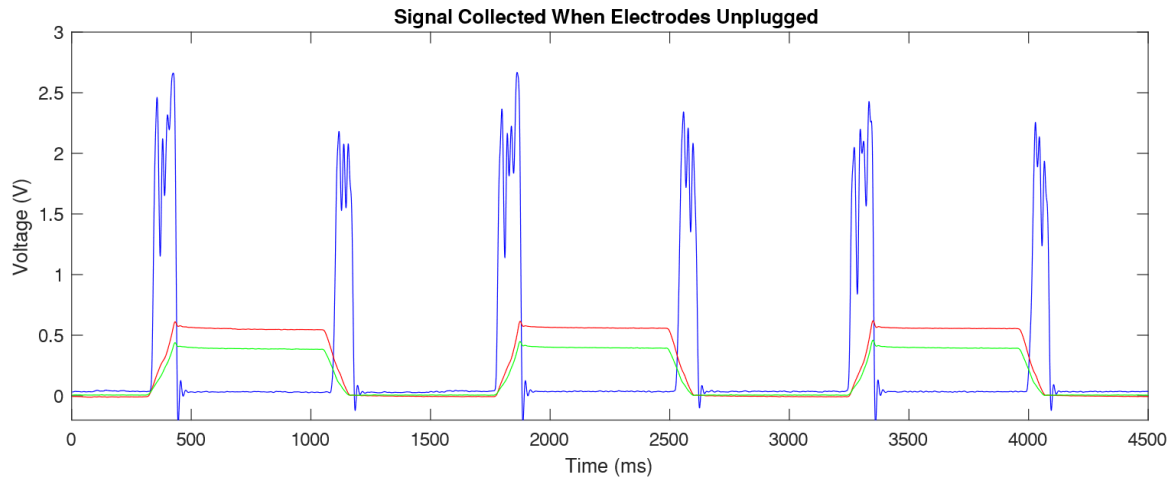


**Figure 2.5:** Capacitive coupling – motion artifact during loading/unloading (indicated by strain (red) and force (green) signals) caused by load cell movement collected by electrode leads (blue). Electrode leads were not attached to electrodes during this test so that no SGPs were collected.

### 2.2.2 Charge Amplifier Circuit for Piezoelectricity

For one experiment we used a charge amplifier (rather than a voltage amplifier) in an attempt to measure piezoelectric charge within a dry bone sample. A charge amplifier allowed us to collect any piezoelectric charge produced upon mechanical deformation and convert it into a voltage. The charge is collected at the negative input and charges up the capacitor C (Fig. 2.6). The resistor R “bleeds” charge from the capacitor to stop it from reaching saturation as well as creating a path for DC bias (Karki, 2000).

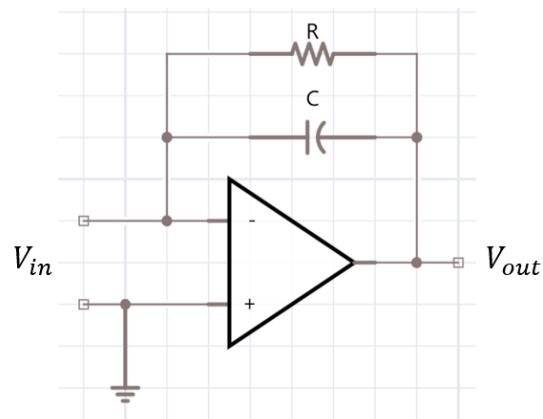


**Figure 2.6:** Schematic of charge amplifier circuit. Circuit details as well as the calculations can be found in Appendix 2.

## 2.3 Mechanical Testing

Mechanical deformation was performed by a material testing machine (eXpert 5601, Admet, Norwood, MA). A second 25lb load cell (SML-25, Interface) was placed in parallel to the Admet load cell to capture load data externally and to keep it synchronized with the SGP and strain data. The load and strain data were amplified by Vishay signal-conditioning amplifiers (amplifier details in Appendix 3). All samples were subjected to mechanical deformation by cantilever bending (Fig. 2.7) to create as much deformation as possible (compared to four point etc.). The samples were held in place by a clamp up to 15 mm from the base of the sample (Fig. 2.1b) and the load was applied at 40 mm from the base. These boundaries were drawn onto each sample (Fig. 2.1b and 2.2) to ensure that the loads were consistently applied at the correct location. Testing parameters varied by design with each experiment (see sections 2.4-2.9). The samples were shielded from the metal clamp using electrical tape at all contact points.

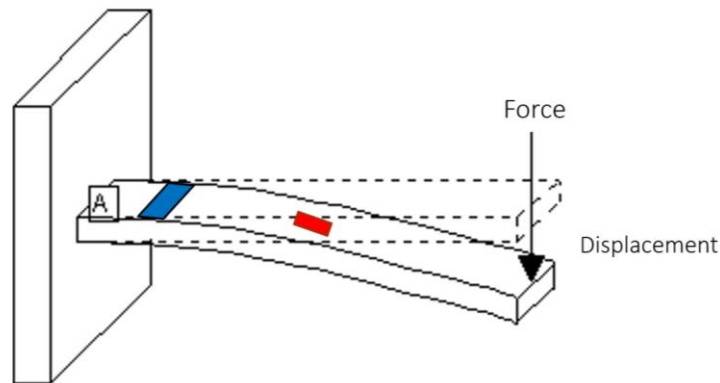


**Figure 2.7:** Schematic showing the process behind cantilever bending. Samples were displaced until a target force was reached (Whitney, 1999).

All tests were performed in a similar manner. After the samples were clamped into place, the sample was deformed to a target load. Then the displacement was held for six seconds allowing the sample to relax under the load.



## 2.4 Dry vs. Wet Tests

### 2.4.1 Sample Preparation

For these tests, a total of  $n = 17$  additional samples were originally created but three were excluded from testing resulting in only  $n = 14$  samples. This sample group was called the S16 group because they were created in the summer of 2016. The S16 group of 14 samples was then divided into two groups: dry and wet. Groups were created based off similar sample thicknesses (see Table 2.1) The 'wet' group was made up of  $n = 7$  samples that were kept hydrated by wrapping them in saline-soaked paper towel and stored at  $-20\text{ }^{\circ}\text{C}$ . The other  $n = 7$  samples were desiccated at  $33\text{ }^{\circ}\text{C}$  in an oven (Barnstead Thermolyne) for four days until dehydrated then stored at  $-20\text{ }^{\circ}\text{C}$  but without being wrapped in the saline-soaked paper towel. To monitor water loss during desiccation, the samples were weighed (Mettler Toledo AL54  $\pm 0.1\text{ mg}$ ) every 24 hours. Dehydration was said to be reached once the weight of the samples was unchanged. The wet and dry samples were then subjected to mechanical testing to determine if there was a difference in SGPs.

**Table 2.1:** Dry vs. Wet Test Groups

| Pair # | Sample # |     | Thickness (mm) |
|--------|----------|-----|----------------|
|        | Wet      | Dry |                |
| 1      | 1        | 2   | 3.2            |
| 2      | 3        | 10  | 3.1            |
| 3      | 4        | 8   | 2.8            |
| 4      | 6        | 17  | 3.0/2.9        |
| 5      | 7        | 11  | 4.1/4.0        |
| 6      | 9        | 13  | 2.8/2.6        |
| 7      | 15       | 16  | 2.7            |

### 2.4.2 Test Procedure

Wet samples were cyclically loaded to a peak strain of  $750 \mu\epsilon \pm 50 \mu\epsilon$  and dry samples were cyclically loaded to  $650 \mu\epsilon \pm 50 \mu\epsilon$ . Each sample was loaded for five cycles. Each cycle included a  $100 \frac{mm}{min}$  load ramp, a held displacement for six seconds, and then unloaded at  $100 \frac{mm}{min}$  (Table 2.2). The main purpose of this test was to identify any differences in shape and magnitude of SGPs produced by the wet versus the dry samples.

**Table 2.2:** Dry vs. Wet Test Information

| <i>Test Number</i> | <i>Displacement Rate</i> | <i>Target Strain (<math>\mu\epsilon</math>)</i> | <i>Time Held (seconds)</i> |
|--------------------|--------------------------|---|----------------------------|
| 1                  | $100 \frac{mm}{min}$     | 750 (wet)<br>650 (dry)                          | 6                          |

## **2.5 Charge Amplifier Test**

This is the only experiment in which we used a charge amplifier (rather than a voltage amplifier in the case of the SGP circuit) to try and measure piezoelectric charge within a thoroughly dry bone sample. Instead of using the SGP circuit to collect a voltage from the dry bone, a charge amplifier collected any piezoelectric charges produced upon mechanical deformation and then converted it into a voltage for measurement.

### **2.5.1 Sample Preparation**

Sample 12 was excluded from regular testing because it was much thinner than the other samples (see Appendix 1) and was therefore used for the charge amplifier testing. This sample was subjected to ethanol drying. Ethanol drying is a procedure in which the sample is soaked in increasing percentages of ethanol solutions until the majority of water in the sample is replaced with ethanol. This procedure removes virtually all the water in the sample, both bound<sup>3</sup> and unbound, making it difficult to rehydrate the sample for regular testing (hence the reason why an excluded sample was selected). To perform the ethanol drying, the sample was soaked in a 70% ethanol solution for 48 hours, with the solution being refreshed every 24 hours. Then the sample was soaked in a 95% ethanol solution for 120 hours, with the solution replaced every 48 hours. Finally, the sample was soaked in a 100% ethanol solution for 168 hours after which the sample was removed from the solution and left to air dry for 48 hours. The intent of dehydrating the sample with ethanol was to measure only the piezoelectric change produced by the dry collagen

---

<sup>3</sup> Bound water refers to water which is bound to collagen molecules.

without subjecting sample proteins to heat (i.e. desiccating the samples like in the dry vs. wet tests).

### 2.5.2 Test Procedure

The sample was tested before and after ethanol drying, with the same test being performed both times. The voltage was collected using the charge amplifier circuit<sup>4</sup> as well as the strain as the force via the Vishay amplifier. The test information can be seen in Table 2.3. Each test was cycled three times.

**Table 2.3:** Charge Amplifier Test Information

| <i>Test Number</i> | <i>Displacement Rate (<math>\frac{mm}{min}</math>)</i> | <i>Target Force (N)</i> | <i>Time Held (seconds)</i> |
|--------------------|--|-------------------------|----------------------------|
| 1                  | 100  | 10                      | 6                          |
| 2                  | 100  | 15                      | 6                          |
| 3                  | 100  | 20                      | 6                          |

---

<sup>4</sup> This was the only experiment that used the charge amplifier. All other experiments used the SGP circuit.

## 2.6 Evaporation Tests

### 2.6.1 Sample Preparation

The assumption from the dry vs. wet tests was that the loss of SGP signal was due to the loss of unbound water in the sample. However, high temperatures can denature proteins (Hiratai et al., 2014; Marino, Becker, & Bachman, 1967; Noris-Suárez et al., 2007). The evaporation tests were performed on the samples before and after long-term air exposure to determine if dehydration caused by evaporation would affect the SGP signal.

To assess the effect of dehydration due to air exposure on SGP magnitude, five samples were left out to air dry. The samples selected for these tests (Table 2.4) were prepared by leaving them to sit out, at room temperature, for an extended period until the unbound water inside of them had the chance to evaporate. The samples were weighed throughout the drying period. Samples were weighed every 24 hours and were determined to be dehydrated once the weight of the sample was unchanged. We expected the mass to decrease as the unbound water evaporated, and for the SGP to be essentially nonexistent. This experiment allowed us to determine if the loss in mass associated with the evaporation of unbound water during the 48-72 hour drying period affects the SGP signal collected.

**Table 2.4:** Evaporation Test Sample Information

| <i>Sample #</i> | <i>Thickness (mm)</i> |
|-----------------|-----------------------|
| 7               | 4.11                  |
| 10              | 3.21                  |
| 11              | 3.94                  |
| 22              | 3.07                  |
| 23              | 2.54                  |

## 2.6.2 Test Procedure

The same test was performed on each sample initially, when it was still hydrated, and then again after it was dehydrated. The samples were loaded at  $100 \frac{mm}{min}$  to a target of 30N, and then immediately unloaded at  $100 \frac{mm}{min}$  (Table 2.5).

**Table 2.5:** Evaporation Test Information

| <i>Displacement Rate (<math>\frac{mm}{min}</math>)</i> | <i>Target Force (N)</i> | <i>Time Held (seconds)</i> |
|--|-------------------------|----------------------------|
| 100  | 30                      | 0                          |

## **2.7 Unified Sample Preparation Tests**

### **2.7.1 Sample Preparation**

In May 2017, a new group of samples (samples 18-26) were created for testing called the S17 group (n = 9). These samples were cut from a bovine femur in the same manner as the S16 samples (all sample info can be seen in Appendix 1). While S17 samples were being created, the (non-excluded) S16 samples were stored by soaking them in a saline solution in the fridge. This was in an attempt to rehydrate the previously 'dry' samples and to determine if soaking would be a better storage solution. After a few days, it was determined to not be a better alternative for storage in comparison to freezing for two main reasons: 1) the saline solution began to smell, indicating the samples were deteriorating and 2) the strain gauges began falling off the samples. Consequently, samples were stored the same way as before; wrapped in saline-soaked paper towel and stored in the freezer.

The samples undergoing testing were removed from the freezer and allowed to thaw for 20 minutes, then left to air dry for another five minutes. Before the electrodes were applied, the sample was wiped down to remove any condensation. After application, the electrodes were left to settle onto the bone sample for another five minutes.

### **2.7.2 Test Procedure**

After new (S17) samples were cut and prepared for testing, all samples (S16 and S17) were subject to testing. These tests were performed to 1) verify the SGP circuit was working properly, 2) see if acceptable signals were being obtained from each sample, 3) compare the signals collected from the S16 group to those collected the previous summer and 4) determine how SGP and strain depend on sample thickness. Although no difference was expected, it was possible that the

magnitude of strain may have changed due to some strain gauges needing replacement as well as the SGP magnitude due to S16 samples being soaked in saline.

Each test took less than ten minutes to complete. Each sample was tested at least three times. The test procedure can be seen in (Table 2.6). After testing was completed, the samples were wrapped in paper towel saturated with the saline solution and stored in the freezer until the next test was to take place.

**Table 2.6:** Preliminary Test Information

| <i>Displacement Rate (<math>\frac{mm}{min}</math>)</i> | <i>Target Force (N)</i> | <i>Time Held (seconds)</i> |
|--|-------------------------|----------------------------|
| 100  | 30                      | 6                          |



## 2.8 Drying Experiments

When preparing for the force and rate tests (section 2.9) it became evident that the samples were drying out over the hour that testing was taking place. To verify if the samples were drying out, and to attempt to counteract the drying, these experiments were put into place. The experiments were performed on six samples, two from each group<sup>5</sup> (Table 2.7).

A total of three different experiments were performed to analyze the effect of drying of the samples during testing. The first experiment involved testing a sample over a period of one hour to see how the SGP signal deteriorated as the unbound water in the sample evaporated (unwrapped long duration test). The next experiment was to repeat the same test, but to wrap the samples in plastic wrap to prevent the free water from evaporating during the hour of testing (wrapped long duration test). The third experiment was to wrap the samples but perform the tests at a much more rapid pace so that the total testing period was about 15 minutes rather than one hour (wrapped short duration test).

**Table 2.7:** Drying Test Sample Information

| <i>Sample #</i> | <i>Group</i> | <i>Thickness (mm)</i> |
|-----------------|--------------|-----------------------|
| 1               | S16 dry      | 3.15                  |
| 7               | S16 dry      | 4.11                  |
| 10              | S16 wet      | 3.21                  |
| 11              | S16 wet      | 3.94                  |
| 22              | S17          | 3.07                  |
| 23              | S17          | 2.54                  |

### 2.8.1 Sample Preparation

Samples were prepared the same way for all variations of the drying experiments. Samples were removed from the freezer and placed in the fridge (at 4 °C) for a minimum of 24 hours before

---

<sup>5</sup> Note that the dry samples from the S16 group were rehydrated prior to testing.

testing took place. This allowed for the samples to fully thaw and for the saline solution within the wrapping to sufficiently saturate the samples. Compared to previous attempts at maximizing hydration of the samples, this was found to be the best way to ensure the samples were as hydrated as possible before testing took place<sup>6</sup>.

Before beginning mechanical testing, the samples were removed from the fridge, unwrapped, dried with paper towel and allowed to sit at room temperature for approximately 15-20 minutes before being dried again with paper towel to remove any condensation. Then the electrodes were applied to the sample and the strain gauge was connected to the Vishay amplifier circuit.

To try and counteract the amount of drying, a group of tests were arranged where the samples were wrapped in plastic/cling wrap. A practice test was performed to analyze the affect of wrapping and can be seen in figure 2.8.

---

<sup>6</sup> A drawback of this sample preparation method was that the strain gauges would regularly fall off as the glue was not able to remain adhered to the saturated bone samples.

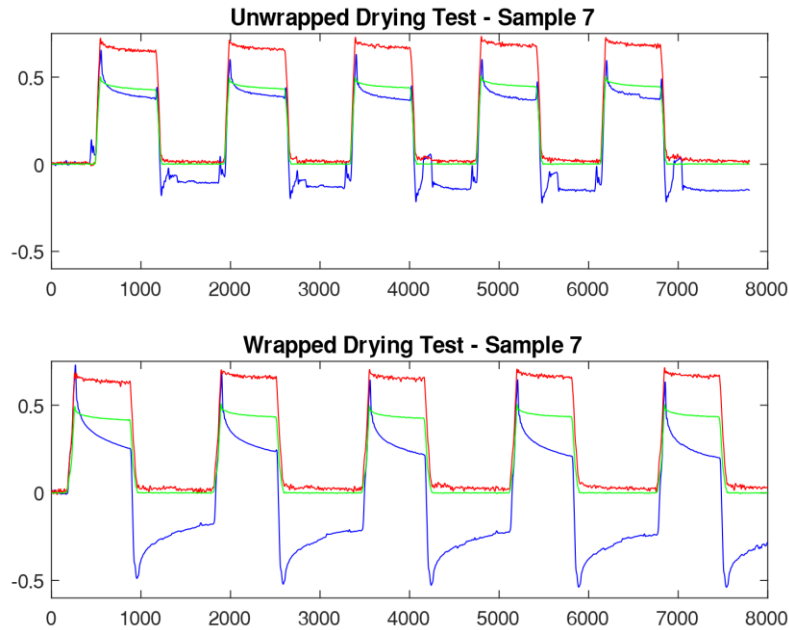


**Figure 2.8:** Example of how wrapping the sample in plastic wrap kept the sample more hydrated during testing. SGP (blue), strain (red) and force (green). Notice the difference in magnitude and clarity of the negative portion of the SGP (blue) in the unwrapped vs. the wrapped drying test.

From a visual inspection of the data in figure 2.8, it is apparent that the negative portion of the SGP curve (generated during unloading) deteriorates less and maintains a cleaner curve when the sample is wrapped. It is worth noting that the peak SGP values still appeared to decrease over the hour of testing. Statistical analysis will be performed to determine the effectiveness of wrapping the samples.

### 2.8.2 Test Procedures

Baseline drift was an issue in previous experiments, therefore before official testing began a pre-load was applied to the sample to allow the sample to settle into place and for the SGP baseline to stabilize (Fig. 2.9). The pre-load was applied at a displacement rate of  $100 \frac{mm}{min}$  to a target load of 10N. The displacement was held for six seconds before unloading (Table 2.8). This pre-load cycle was repeated ten times before official testing began.

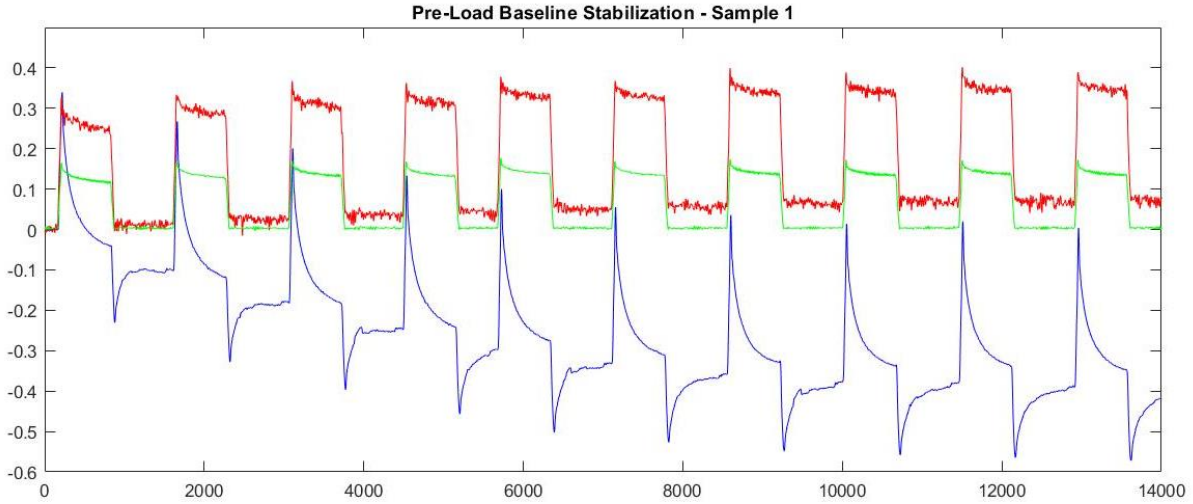


**Figure 2.9:** This graph shows how the pre-load being cycled 10 times stabilizes the baseline as the fluid and electrodes warm up. This pre-load was applied to each sample before testing took place. SGP (blue), strain (red) and force (green).

**Table 2.8:** Pre-load Test Information

| <i>Displacement Rate (<math>\frac{mm}{min}</math>)</i> | <i>Target Force (N)</i> | <i>Time Held (seconds)</i> |
|--|-------------------------|----------------------------|
| 100  | 10                      | 6                          |

### Unwrapped Long Duration Test

The purpose of this test was to monitor how much the magnitude of SGP signal decreased over one hour of intermittent (every 15 minutes) mechanical testing. A total of three tests were performed per sample (Table 2.9). The samples were left to re-hydrate for at least 24 hours after each test. No more than one test was performed per day on an individual sample to ensure sufficient time to re-hydrate before the next test.

For both long duration tests, two tests were performed. The first test held displacement for six seconds and the second for zero seconds (Table 2.9). The purpose of this was to verify that there was 1) consistent maximum SGP, strain, and force magnitudes reached between the zero and six second tests and 2) to see if there was overshoot present in the zero second held tests.

### Wrapped Long Duration Test

To minimize the amount of evaporation of unbound water in the sample during testing, the long duration tests were repeated following the test procedure in Table 2.9, but instead the samples were wrapped in plastic wrap. We hypothesized that the plastic would reduce the amount of air exposure and evaporation of unbound water and therefore keep the sample hydrated for a longer period of time.

### Wrapped Short Duration Test

These tests followed the same testing procedure in Table 2.9, but only held displacement for six seconds and, instead of waiting 15 minutes between tests for a total test duration of approximately 90 minutes, the entire testing period lasted 10 to 15 minutes. The goal of these tests was to see if the decrease in SGP magnitude was caused by a longer testing period, dehydration of the sample during loading, or a combination of the two. We expected that any decrease in SGP magnitude in during this experiment is mostly caused by the loss of water during the bending of the sample itself, rather than the loss of water caused by evaporation.

**Table 2.9:** Drying Test Information

| <i>Test Name</i> | <i>Displacement Rate (<math>\frac{mm}{min}</math>)</i> | <i>Target Force (N)</i> | <i>Time Held (seconds)</i> |
|------------------|--|-------------------------|----------------------------|
| Unwrapped – LD*  | 100  | 30                      | 0 & 6                      |
| Wrapped - LD     | 100  | 30                      | 0 & 6                      |
| Wrapped - SD     | 100  | 30                      | 6                          |

\*long duration

## **2.9 Force Magnitude and Deformation Rate Tests**

### **2.9.1 Background**

Steinberg et al. (Steinberg et al., 1973) performed tests on whole rat femurs. The femurs were stored in saline and kept physiologically moist throughout testing in a chamber of 98% relative humidity. The femurs were subjected to four-point bending under two different loading patterns:

1. Load at a constant deformation rate ( $0.5 \frac{\text{in}}{\text{min}}$ ) until a specific load was reached (1, 2, 3, 4 and 5 lbs.) then immediately unloaded at the same deformation rate (Fig. 2.10).
2. Load at a constant deformation rate ( $0.5 \frac{\text{in}}{\text{min}}$ ) until a specific load was reached (1, 2, 3, 4 and 5 lbs.). Hold that load for 30 seconds. Unload at the same deformation rate (Fig. 2.11).

Steinberg then repeated the tests with varying deformation rates and found a linear relationship between load and SGP at 'high' deformation rates ( $0.5 \frac{\text{in}}{\text{min}}$ ) but a nonlinear relationship at lower deformation rates ( $0.02 - 0.2 \frac{\text{in}}{\text{min}}$ ) (Fig. 2.12a). A nonlinear relationship was also found between deformation rate and SGP for varying loads, with a smaller change in at 'higher' deformation rates (Fig. 2.12b). These experimental results suggest that both higher deformation rates and higher magnitude loads produced greater SGPs until a maximum voltage was reached (or until fracture occurred).

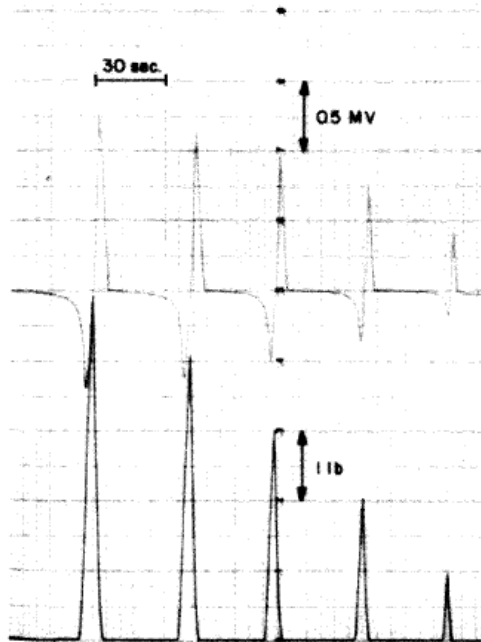


**Figure 2.10:** Data from Steinberg (1973). Recording of electrical potential (top) and load/deformation curve (bottom) from normal femur subjected to sequential loading of 1, 2, 3, 4 and 5 pounds at a deformation rate of  $0.5 \frac{\text{in.}}{\text{min.}}$  with immediate release (read right to left).

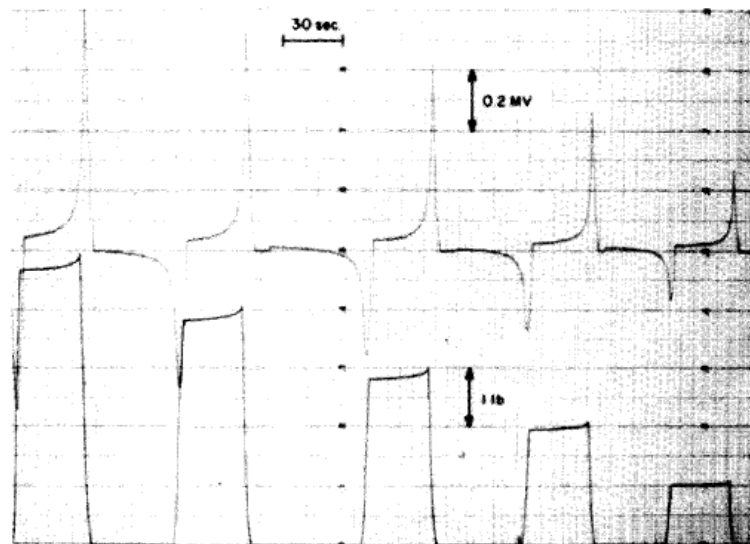


**Figure 2.11:** Data from Steinberg (1973). Recording of electrical potential (top) and load/deformation curve (bottom) from normal femur subjected to sequential loading at  $0.5 \frac{\text{in.}}{\text{min.}}$  with each deformation maintained for 30 seconds prior to release (read right to left).

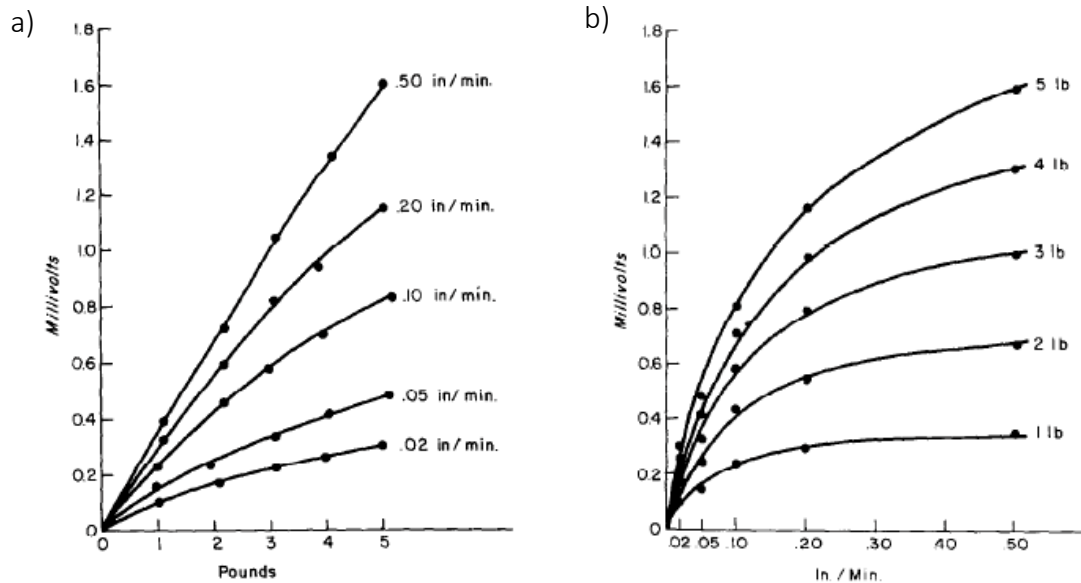


**Figure 2.12:** Data from Steinberg (1973). (a) Graph of peak voltage vs. load at different rates of deformation for normal rat femur. (b) Graph of peak voltage vs. rate of deformation at different loads for normal rat femur.

### 2.9.2 Recreating the Steinberg Tests

Like Steinberg, our main objective of performing these experiments was to observe the effect of varying load magnitudes and deformation rates on SGPs in wet bone. There were some differences in the experiments. Steinberg used whole rat femurs under four-point bending. In an effort to reduce inter-sample variability, I machined relatively uniform samples from bovine cortical bone. Analysis of the machined samples demonstrated that difference in sample thickness did have a significant effect on strain measures and SGPs (section 3.4), but this was accounted for using repeated measures analysis. Due to the stronger and larger bone samples, I was able to increase the range of loading magnitude and deformation rates of the testing procedures. The deformation rate used by Steinberg ranged from  $0.02$  to  $0.5 \frac{\text{in}}{\text{min}}$  ( $0.508$  to  $12.7 \frac{\text{mm}}{\text{min}}$ ). Whereas the bovine cortical bone samples in the current study were loaded at deformation rates of 50, 100, 150 and  $200 \frac{\text{mm}}{\text{min}}$  (Change in Deformation Rate tests), which are considerably higher than those in the original



paper<sup>7</sup>. The Admet materials test system performs irregularly at deformation rates under  $25 \frac{mm}{min}$  (as demonstrated during force calibration experiments; see Appendix 3), therefore, tests were restricted to the use of higher deformation rates. Finally, using machined beams of bovine cortical bone samples enabled strain gauges to be affixed to the bone surfaces to allow for a comparison of strain to SGP.

### **2.9.3 Sample Prep**

The same as in section 2.8.2.

### **2.9.4 Test Procedure**

The tests for change in load magnitude and displacement rate were modified slightly from the drying tests. When performing the drying tests, the same test was repeated five times over a selected time frame. For this round of tests, either load magnitude or deformation rate was increased with each test to measure the effect on the strain and SGP produced in the sample. To accomplish these experimental variations, eight different tests were performed (Table 2.10). Each test was only repeated twice per testing day on each sample. There was a total of three different testing days. Three variations of testing order were used (Table 2.11) to eliminate any biasing effects of possible drying over the testing period. In a pre-load test (test 0) the samples were loaded up to 10N at  $100 \frac{mm}{min}$  for 10 cycles to “warm up” the sample. In tests 1-4 (Change in Load Magnitude tests), the samples were loaded at the same displacement rate ( $100 \frac{mm}{min}$ ) up to a target load of 20, 30, 40, or 50N respectively, held for six seconds and then unloaded. This test was repeated five times for a total of five cycles per test.

---

<sup>7</sup> Although other papers cite using significantly higher deformation rates (Cochran et al., 1968; Gross & Williams, 1982).

**Table 2.10:** Force and Rate Test Information

| <i>Test Type</i>           | <i>Test #</i> | <i>Deformation Rate</i><br>$\frac{mm}{min}$ | <i>Load (N)</i> | <i>Time of Held Displacement (sec)</i> | <i>Cycles per Test (#)</i> |
|----------------------------|---------------|---|-----------------|--|----------------------------|
| Pre-load                   | 0             | 100   | 10              | 6                                      | 10                         |
| Change in Load Magnitude   | 1             | 100   | 20              | 6                                      | 5                          |
|                            | 2             | 100   | 30              | 6                                      | 5                          |
|                            | 3             | 100   | 40              | 6                                      | 5                          |
|                            | 4             | 100   | 50              | 6                                      | 5                          |
| Change in Deformation Rate | 5             | 50  | 30              | 6                                      | 5                          |
|                            | 6             | 100   | 30              | 6                                      | 5                          |
|                            | 7             | 150   | 30              | 6                                      | 5                          |
|                            | 8             | 200   | 30              | 6                                      | 5                          |

**Table 2.11:** Variations of Test Order for the Force and Rate Tests

| <i>Order ID</i> | <i>Round</i> | <i>Test Order</i>      |
|-----------------|--------------|------------------------|
| 1               | 1            | 1, 2, 3, 4, 5, 6, 7, 8 |
|                 | 2            | 8, 7, 6, 5, 4, 3, 2, 1 |
| 2               | 1            | 5, 6, 7, 8, 1, 2, 3, 4 |
|                 | 2            | 4, 3, 2, 1, 8, 7, 6, 5 |
| 3               | 1            | 8, 7, 3, 4, 6, 5, 1, 2 |
|                 | 2            | 2, 1, 5, 6, 4, 3, 7, 8 |

## 2.10 Analysis Methods

Not all signals that were collected were acceptable for analysis. A 'good' test required multiple criteria including: sample was hydrated enough to produce a clean signal with minimal noise (Fig. 2.13a), the sample did not slip out of place while undergoing loading (Fig. 2.13b), and the strain gauges operated as expected (Fig. 2.13c).

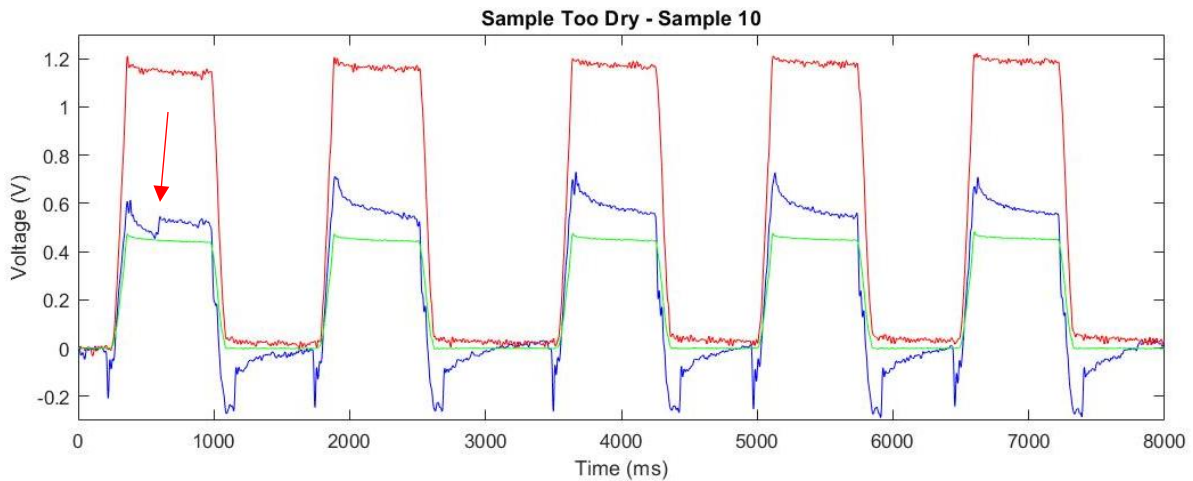


**Figure 2.13a:** An example of a bad test where the sample was not hydrated enough to produce smooth signals as shown by red arrow. SGP (blue), strain (red) and force (green).

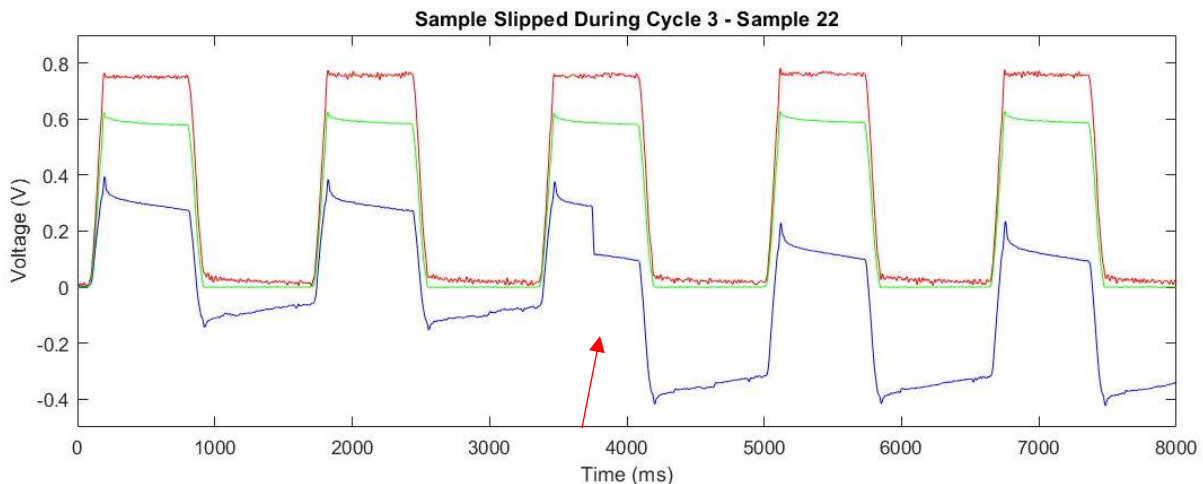


**Figure 2.13b:** Example of a bad test where the sample slipped out of place during the third loading cycle. SGP (blue), strain (red) and force (green).

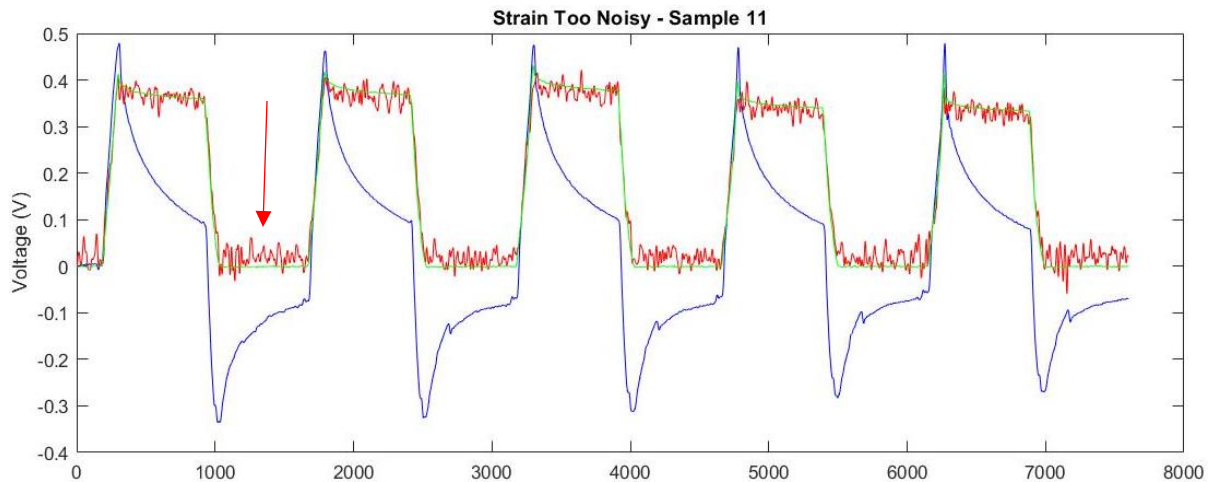


**Figure 2.13c:** Example of a bad test where the strain gauge was producing far too much noise, indicating the strain gauge needed to be replaced. SGP (blue), strain (red) and force (green).

Statistical analysis was performed using R Studio Software. Normality was determined using Shapiro-Wilkins and equality of variances was determined using a Bartlett test. For data sets that were normally distributed, the difference in means were calculated using the Student's t-test, repeated measures ANOVA and a Tukey test was used as a multiple comparison test to determine the difference between months. For non-parametric datasets the Friedman test was used with a pairwise test for multiple comparisons and Wilcoxon Rank Sum for t-tests. A significance level of  $p = 0.05$  was used.

### **2.10.1 Data Processing**

#### **Curve Isolation**

MATLAB programs were written to prepare the data for analysis (code in Appendix 7). For the data that was considered good enough for analysis programs were run on the data to do the following:

1. Zero Baseline
  - Baselines were determined by finding the values collected before testing began. Baseline values were added (or subtracted) to the rest of the signal (Fig. 2.14 (1)).
2. Isolate Test Cycles
  - The cycles for each test were then isolated (Fig. 2.14 (2)).
3. Isolate Positive Curves
  - All<sup>8</sup> the curves were then isolated from the time the peak load was reached until the sample was unloaded 6 seconds later (Fig. 2.14 (3)).

Some cycles were intentionally duplicated within a test. For example, sometimes I neglected to do all five cycles of a test. In that case the last cycle was manually replicated in MATLAB so there was a consistent number of cycles for all tests (R does not handle datasets of varying sizes well). On occasion, there was an issue with excessive noise in one cycle, typically in the SGP/strain signal, and, in that case, they were also replaced.

#### **2.10.2 Values of Interest**

The SGP, strain, and force all followed decaying exponential curves during held displacement. There was a negative SGP produced after unloading that also followed a decaying exponential, but

---

<sup>8</sup> The strain curves were only isolated in the preliminary tests. Curves were not normalized after this test and could not have curves fit to them due to the high level of noise. SGP curves were always isolated.

the magnitude varied dramatically between samples (as seen in figure 2.14 vs. figure 2.15). Because of the irregularity in the magnitude and generally poor quality of the negative SGP signals, they were excluded from analyses.

Initially, the main values of interest were the maximum SGP, strain, and force value collected during each cycle of testing. See figure 2.15 to see a sample of an isolated cycle showing the maximum values for each signal. To analyze the rest of the signal collected following the maximum value, further analysis was performed such as comparing the maximum value to the 'steady-state' value reached before the sample was unloaded. The values and their descriptions can be seen in Table 2.12 and figures 2.16a-2.17b.

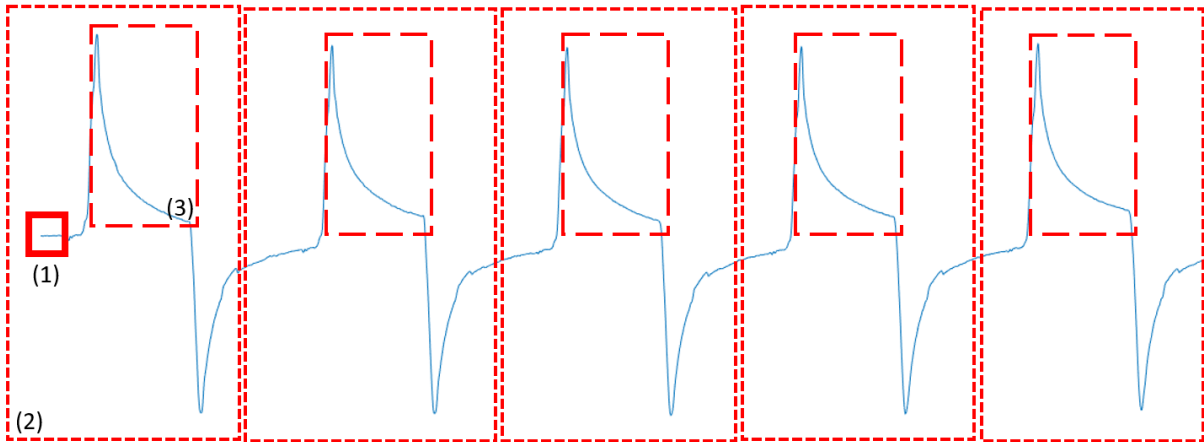


**Figure 2.14:** Diagram showing how the data was processed for curve isolation. The steps were: (1) zero to the baseline of the signal using this value, (2) isolate the five cycles (3) isolate the positive curve from the cycle.

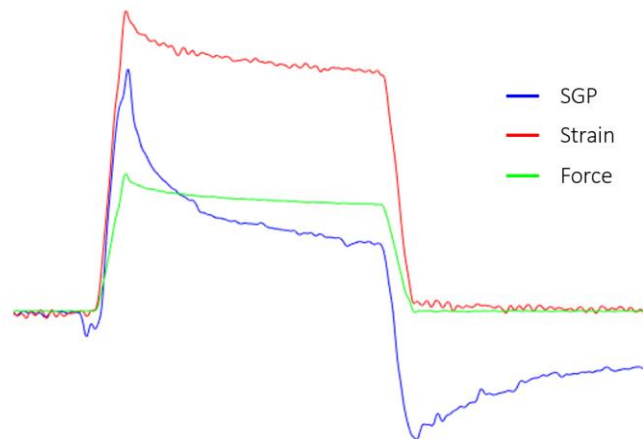


**Figure 2.15:** Example of an isolated cycle from a good test showing real SGP (blue), strain (red) and force (green) data where a sample was loaded/unloaded at  $100 \frac{mm}{min}$  to 30N, with held displacement for six seconds.

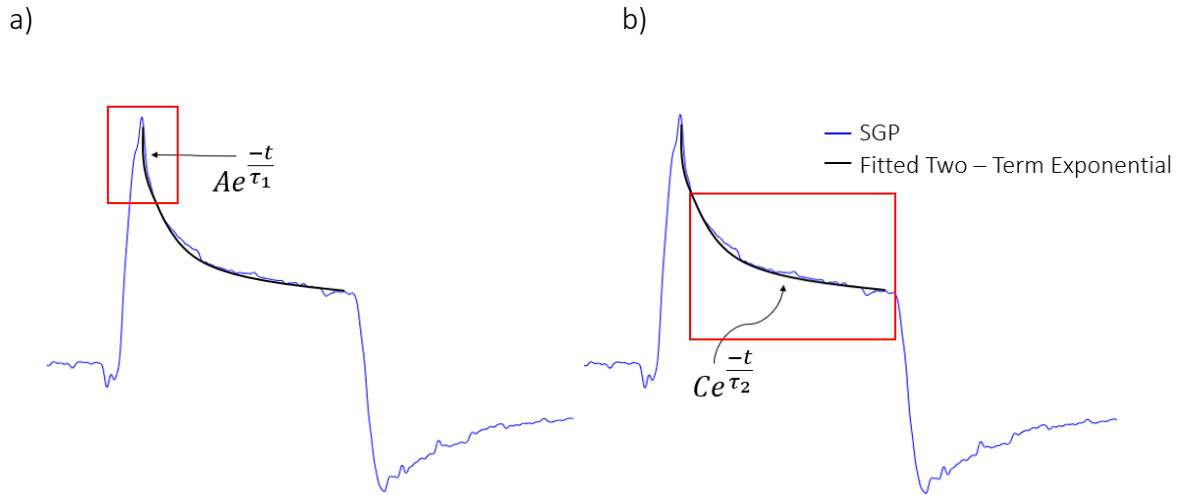


**Figure 2.16a:** The initial, rapidly decaying segment of the exponential curve that is described by the first term in Equation 2.1.

**Figure 2.16b:** The 'steady-state' segment of the decaying exponential curve that is described by the second term in Equation 2.1.

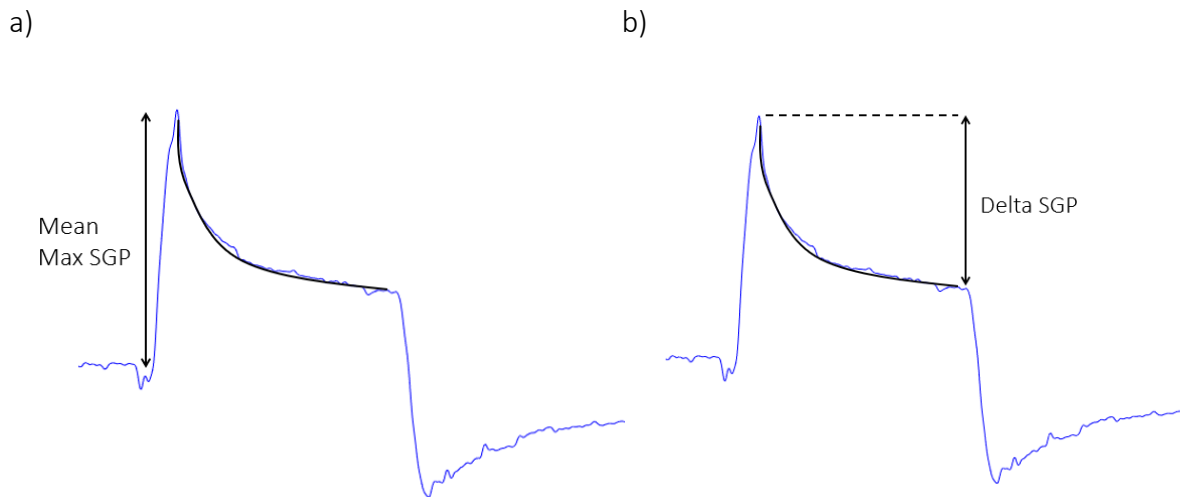


**Figure 2.17a:** The variable called 'Mean Max SGP' describes the peak value that the SGP reaches during deformation. This variable also applies to the mean max values from strain and force curves. The mean comes from the average max value collected over all five cycles collected during one test.

**Figure 2.17b:** The variable called 'Delta SGP' describes the change in the SGP value. This value is the difference between the max SGP value and the value right before the load is released. The mean is the average delta SGP value from all five cycles.



**Table 2.12:** Descriptions of Values Collected from Tests (REFER TO FIGURE 2.16)

| <i>Test Name</i>                                 | <i>Variable Name</i> | <i>Variable Explanation</i>   | <i>Description</i>  |
|--|----------------------|---|---|
| <b>Preliminary Tests</b>                         | Mean Max SGP         | Mean max value of positive SGP from cycle 1 to 5                            | Fig. 2.17a  |
|  | Mean Max Strain      | Mean max value of strain from cycle 1 to 5 *                                | Fig. 2.17a  |
|  | Mean Max Force       | Mean max value of force from cycle 1 to 5 *                                 | Fig. 2.17a  |
| <b>Drying Tests and Magnitude and Rate Tests</b> | Mean Max SGP         | Mean max value of positive SGP for cycles 1 to 5                            | Fig. 2.17a  |
|  | Mean Max Strain      | Mean max value of strain for cycles 1 to 5 *                                | Fig. 2.17a  |
|  | Mean Max Force       | Mean max value of force for cycles 1 to 5 *                                 | Fig. 2.17a  |
|  | Mean Delta SGP       | Mean change in positive SGP after ~ 6 seconds for cycles 1 to 5             | Fig. 2.17b  |
|  | Max SGP Ratio        | Mean ratio between the first (test 1) and last (test 5) mean max SGP values | $\frac{\text{Test 1 Max SGP}}{\text{Test 5 Max SGP}}$     |
|  | Delta SGP Ratio      | Mean ratio between the first (test 1) and last (test 5) mean change in SGP  | $\frac{\text{Test 1 Delta SGP}}{\text{Test 5 Delta SGP}}$ |

\*strain and force were not consistently collected during the drying tests as they were not factors of interest

### 2.10.3 Curve Analysis – Fitting the Two-Term Decaying Exponential

To explore the quantitative relationship between SGPs and strain, I fit a mathematical equation to the SGP signals collected during testing<sup>9</sup>. A typical signal that was collected during one cycle of testing can be seen in figure 2.15. A two-term decaying exponential equation (equation 2.1) was determined to be the best option for curve fitting. The Curve Fitting MATLAB Application (MATLAB R2018a) was used to fit various equations to the isolated curves. The two terms in this equation are associated with different segments of the isolated curve. The first term  $Ae^{\frac{-t}{\tau_1}}$  quantifies the initial, steeper part of the curve, and the second term  $Ce^{\frac{-t}{\tau_2}}$  quantifies the region where the curve reaches a more steady-state (Fig. 2.16a-b). All four variables in equation 2.1 were examined. The

<sup>9</sup> Equations were also fit to the strain curves for the preliminary tests to observe how sample thickness affected both strain and SGP signals.

A and C-coefficients represent the magnitude of the signal (the gain) at the beginning of their respective decaying exponentials<sup>10</sup>, and  $\tau_1$  and  $\tau_2$  are the respective time constants (Table 2.13). These coefficients and time constants were compared between samples.

$$V(t) = Ae^{\frac{-t}{\tau_1}} + Ce^{\frac{-t}{\tau_2}}$$

**Equation 2.1:** Two-term decaying exponential equation that was fit to the curves.

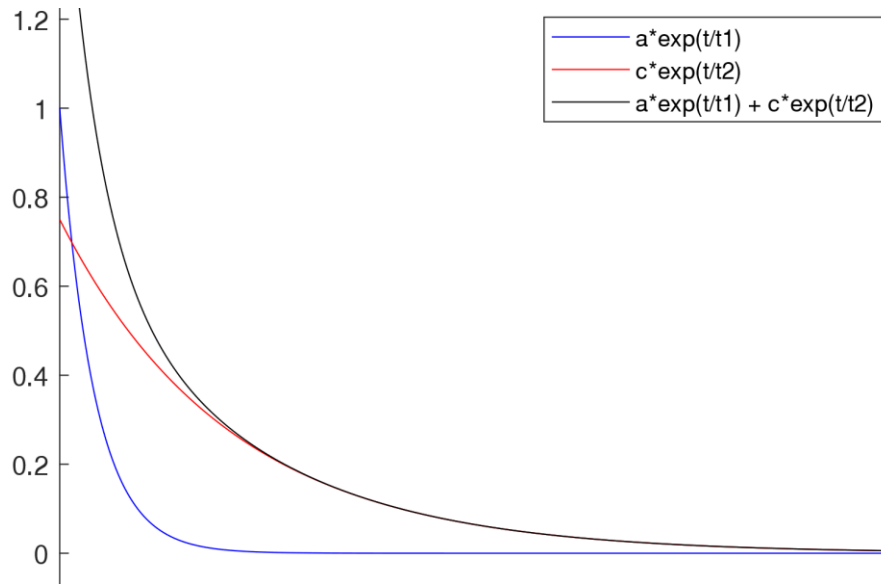
**Table 2.13:** What the Values in Equation 2.1 Represent

| <i>Variable</i> | <i>Variable Explanation</i>                          |
|-----------------|--|
| A               | Value at peak load AKA max value                     |
| C               | Steady-state value at start of second part of curve  |
| $\tau_1$        | Time constant associated with A/first part of curve  |
| $\tau_2$        | Time constant associated with B/second part of curve |

---

<sup>10</sup> Note that the mean max SGP value is the sum of the A and C-coefficients. See figure 2.17a-b.

a)



b)

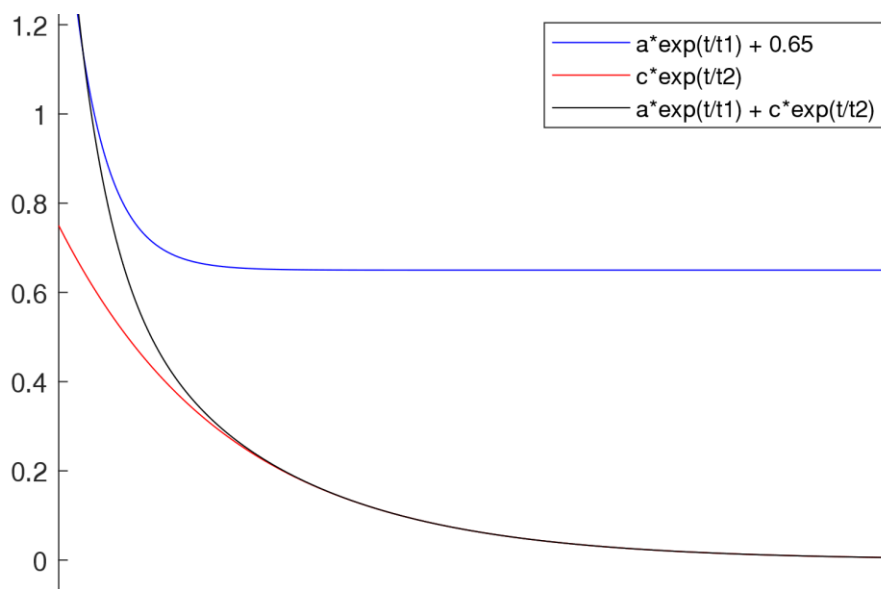


**Figure 2.18a:** Example of two single-term exponentials (blue, red) and the sum of the two (black) to create the two-term exponential ( $a = 1$ ,  $t_1 = -4$ ,  $c = 0.75$ ,  $t_2 = -20$ ).

**Figure 2.18b:** Same two equations as in the previous figure, but the first term (blue) is offset by 0.65 to show its fit with the initial part of the two-term exponential equation.

### What do the Tau Values Quantify?

The tau values are time constants that mathematically describe how a first-order linear time-invariant system (LTI system) responds to a step input, assuming an exponential decay ( $e^{-\frac{t}{\tau}}$ ). The time constant itself represents the amount of time it takes for the system to decrease to  $\sim 36.8\%$  (i.e. when  $t = \tau$ ,  $e^{-1} = 0.368$ ) of its maximum to its asymptotic value or, in simpler terms, how rapidly the function decays over time (Fig. 2.18a-b, 2.19b).

#### 2.10.4 RC Circuits and Stress Relaxation

The decaying exponential waveform obtained from wet bone (as seen in figure 2.16a-b) is similar to that in an RC circuit (Fig. 2.19b) where a capacitor (C) is discharging through a resistor (R) (Fig. 2.19a). An RC circuit is a first-order LTI system (as discussed in the previous paragraph) and, since the wet bone samples produced a similar voltage in response to a step input, we can assume the samples behaved like a first-order LTI system. Because of this, I compared the two mathematically.

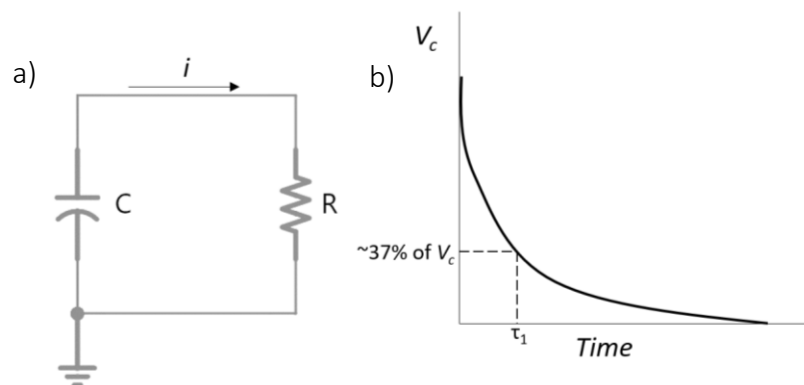


**Figure 2.19a:** A simple RC circuit.

**Figure 2.19b:** Response from an RC circuit, showing the first tau value.

## RC Time Constants

In an RC circuit, the time constant  $\tau$  is the product of the resistance and capacitance of the system ( $\tau = RC$ ), indicating that the speed at which the capacitor charges/discharges is proportional to

$$V_c(t) = V_0 e^{-t/\tau}$$

**Equation 2.2:** Equation RC circuit equation where  $V_0$  is the initial voltage of the capacitor and  $\tau = RC$ .

the resistance and capacitance. Equation 2.2 describes an RC circuit where the capacitor is discharging through the resistor, where  $V_0$  is the initial voltage of the capacitor. Note the similarity between equation 2.1 and equation 2.2. Both contain decaying exponentials, but the equation we are using for curve-fitting our SGP signals has two terms. This brings about the question as to what the two terms represent, which is examined through testing and analysis and discussed in Chapter 4.

## 3 Results

### 3.1 Dry vs. Wet Tests

In wet bone samples the SGP, strain, and force all followed decaying exponential curves during the held displacement. SGP, strain, and force curves were similar in terms of shape and duration, but there was a small negative SGP produced after unloading.

Dry bone samples did not produce SGPs like those found in the wet bone samples. There was a lot of baseline noise and voltage spikes were produced upon loading/unloading (Fig. 3.1).

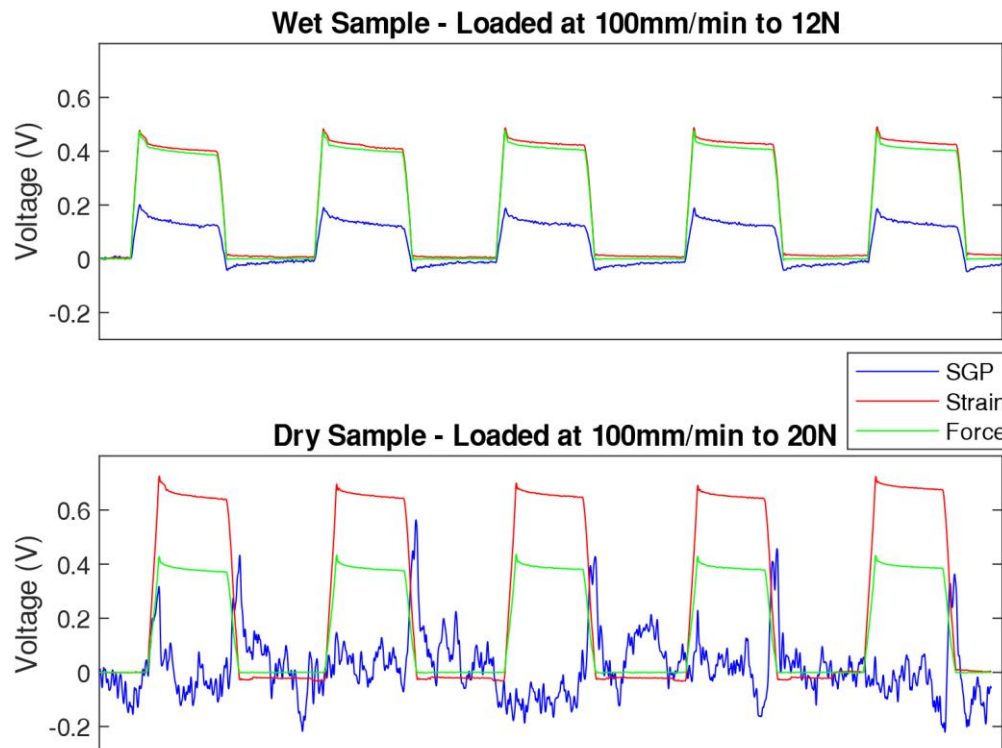


**Figure 3.1:** Difference in SGPs collected from a dry and a wet sample. Note that the difference in strain magnitude is due to this data being from two samples of different thicknesses.

### 3.2 Charge Amplifier Tests

Before ethanol drying, sample 12 produced a good SGP signal which was successfully collected by the charge amplifier circuit. After ethanol drying, there was no signal collected at all (Fig. 3.2).

Note that sample 12 was much thinner than the other samples (~ 2 mm thick), and so a much larger strain was produced in comparison.

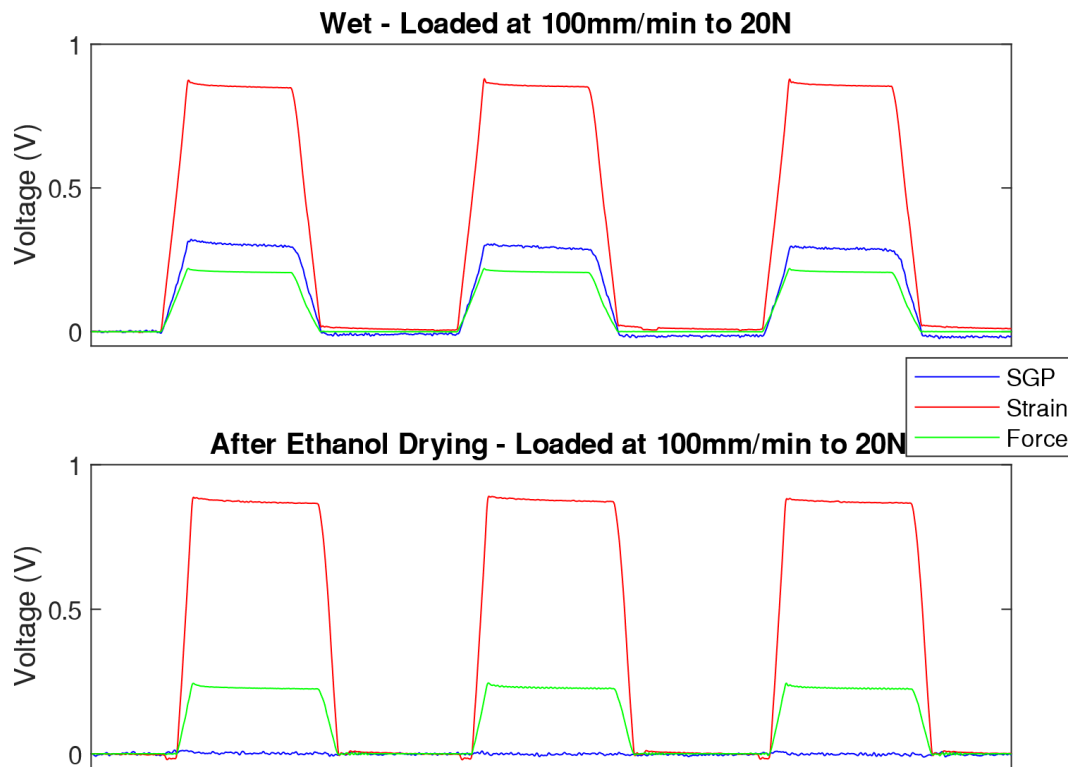


**Figure 3.2:** Difference in SGPs collected from sample 12 before and after drying with ethanol. Both were collected using the charge amplifier circuit.

### 3.3 Evaporation Tests

An example of the SGP signals collected from a sample before and after the evaporation process can be seen in figure 3.3. All samples in this experiment produced similar SGP signals as those shown in figure 3.3 before and after drying. There is a clear SGP signal before drying and a very noisy 'SGP' signal collected after drying. The noisy SGP signals collected from the samples post-air drying are like those seen in the desiccated samples in the dry vs. wet tests (Fig 3.1).

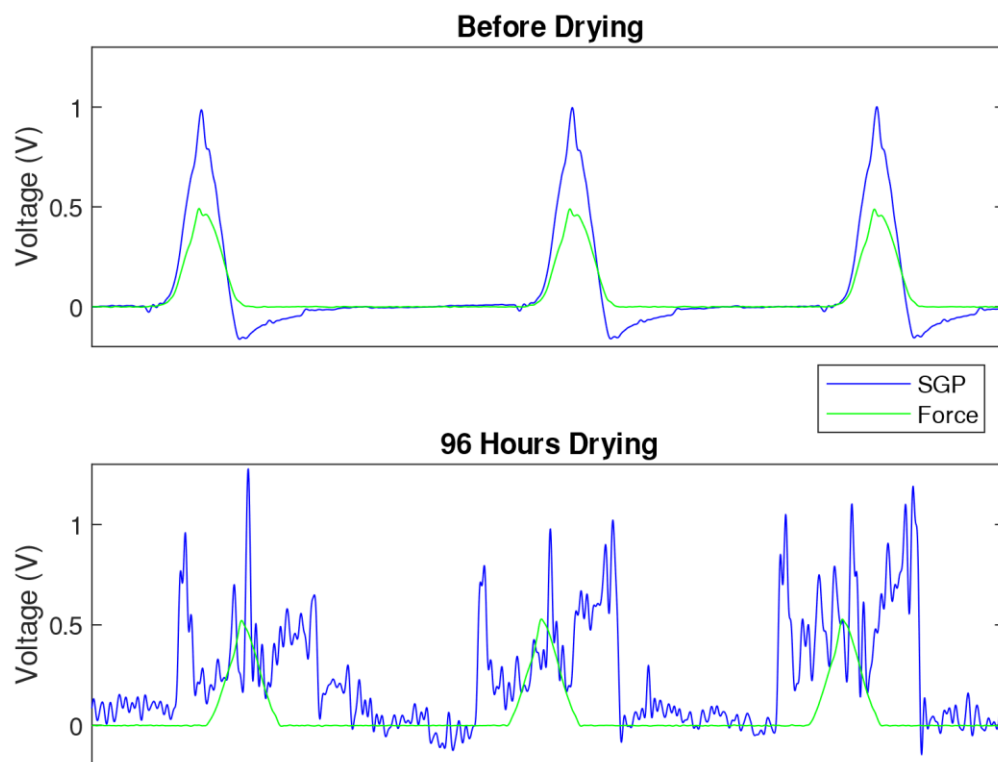


**Figure 3.3:** SGP signals collected from sample 10 before and after the drying period. Clean SGP produced in the sample before drying, but only noise from movement of the load cell is collected after the drying process. Strain was not measured, but force was to show that the sample was indeed being loaded but there was no 'good' SGP signal being collected.



### 3.4 Unified Sample Preparation Tests

No significant differences were found between the three groups for any of the values collected during this test: mean max SGP, mean delta SGP, mean max strain, and  $\tau_1$  and  $\tau_2$  for both SGP and strain curves.

One good test for each sample was used for evaluation of the samples. The maximum SGP, strain, and force values were collected from each cycle and curves were fit to each cycle to find the tau values. A linear model was fit to the max SGP and strain values collected from the test as well as  $\tau_1$  and  $\tau_2$  values (Figs. 3.4b - 3.7b). A linear model was also fit for samples that were less than 3.15 mm thick (Table 3.1), to assess if the two thicker samples somehow skewed the data (Figs. 3.4a – 3.7a). For the max SGP and strain data, both linear models had negative slopes, where SGP and strain decreased with increasing sample thickness. For the tau values,  $\tau_1$  for SGP decreased with increasing  $\tau_1$  for strain and  $\tau_2$  for SGP increased with increasing  $\tau_2$  for strain.

**Table 3.1:** Average Thicknesses for All Samples vs Samples < 3.15 mm

|                              | Thickness (mm)<br>[mean ± std] | Slope of line<br>( $R^2$ ) |                      |                                  |                                  |
|------------------------------|--------------------------------|----------------------------|----------------------|----------------------------------|----------------------------------|
|                              |                                | Mean Max SGP               | Mean Max Strain      | SGP $\tau_1$ vs. Strain $\tau_1$ | SGP $\tau_2$ vs. Strain $\tau_2$ |
| <i>‘Thinner’<br/>Samples</i> | 2.9 ± 0.2                      | m = -0.15<br>(0.03)        | m = -325.7<br>(0.1)  | m = -0.071<br>(-0.009)           | m = 0.014<br>(0.15)              |
| <i>All<br/>Samples</i>       | 3.02 ± 0.4                     | m = -0.06<br>(0.008)       | m = -342.2<br>(0.32) | m = -0.083<br>(-0.003)           | m = 0.018<br>(0.19)              |

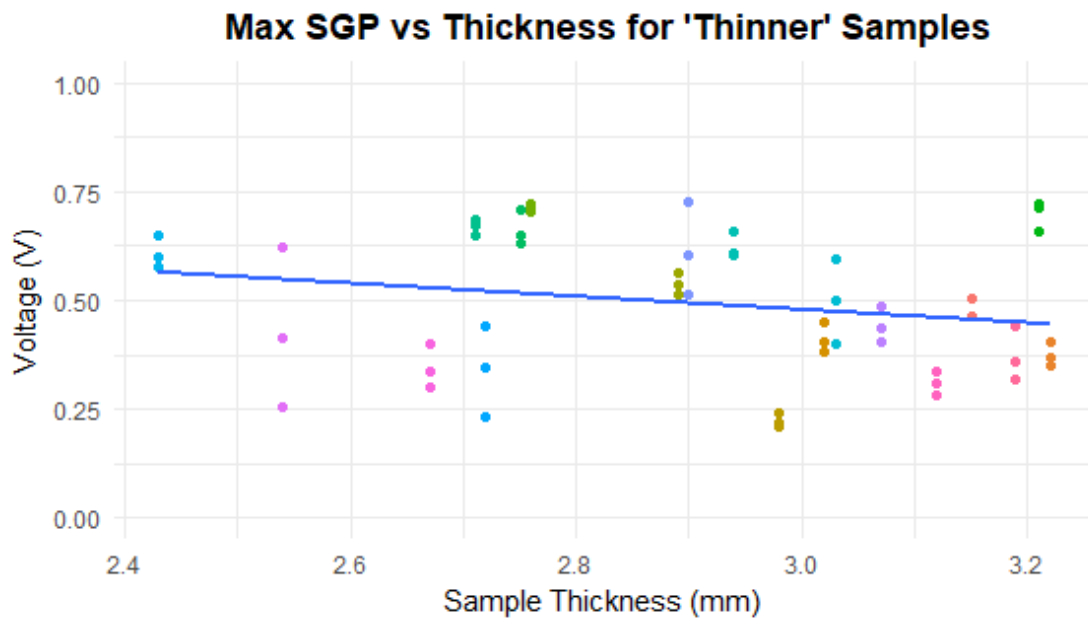


**Figure 3.4a:** A linear model fit to the max SGP values for samples thinner than 3.15mm. SGP decreases with increasing sample thickness, but  $R^2$  value is very small.

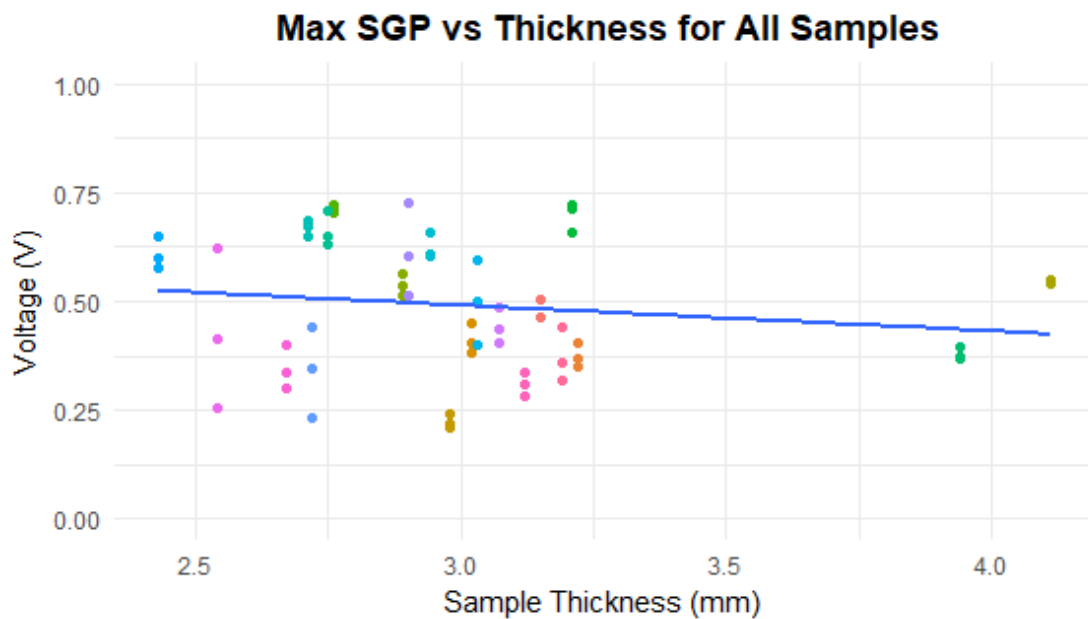


**Figure 3.4b:** A linear model fit to the max SGP values for all samples. SGP decreases with increasing sample thickness, but  $R^2$  value is very small.

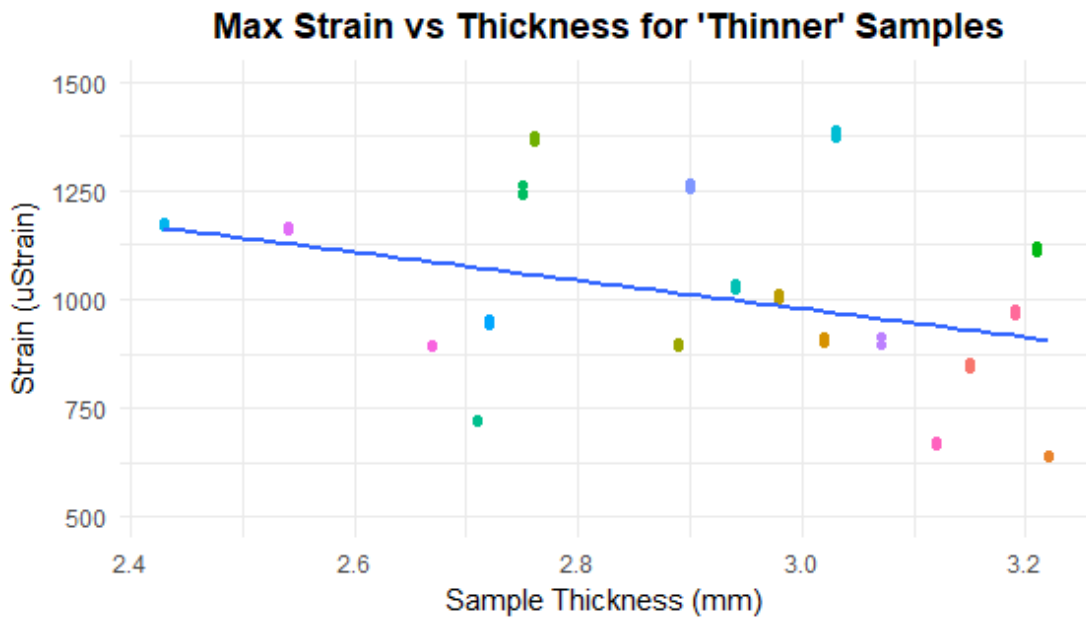


**Figure 3.5a:** A linear model fit to the max strain values for samples thinner than 3.15mm. Strain decreases with increasing sample thickness.

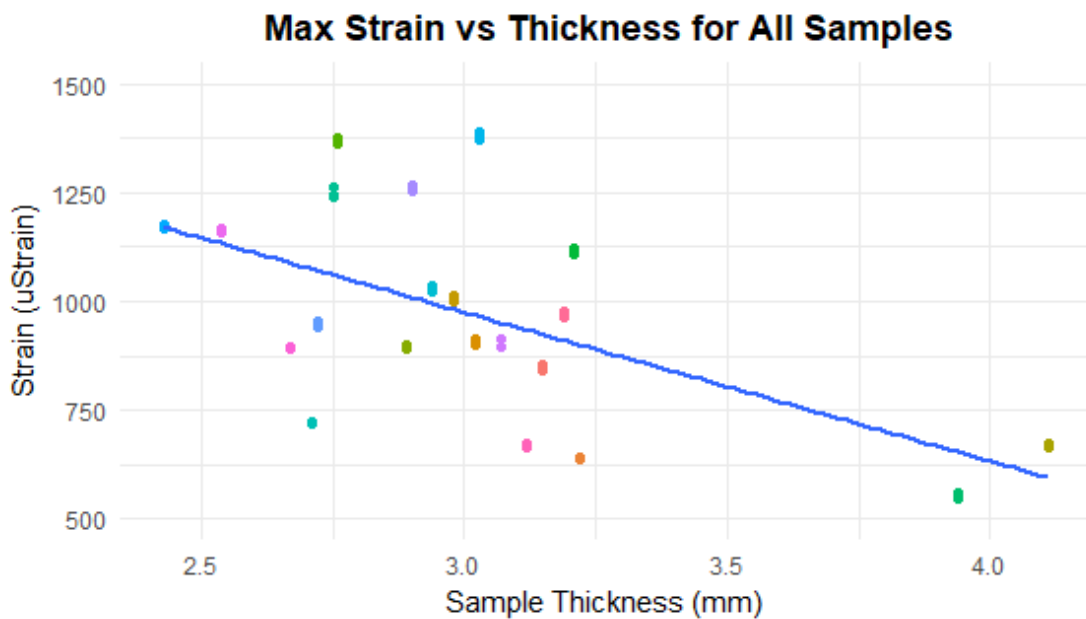


**Figure 3.5b:** A linear model fit to the max strain values for all samples. Strain decreases with increasing sample thickness.

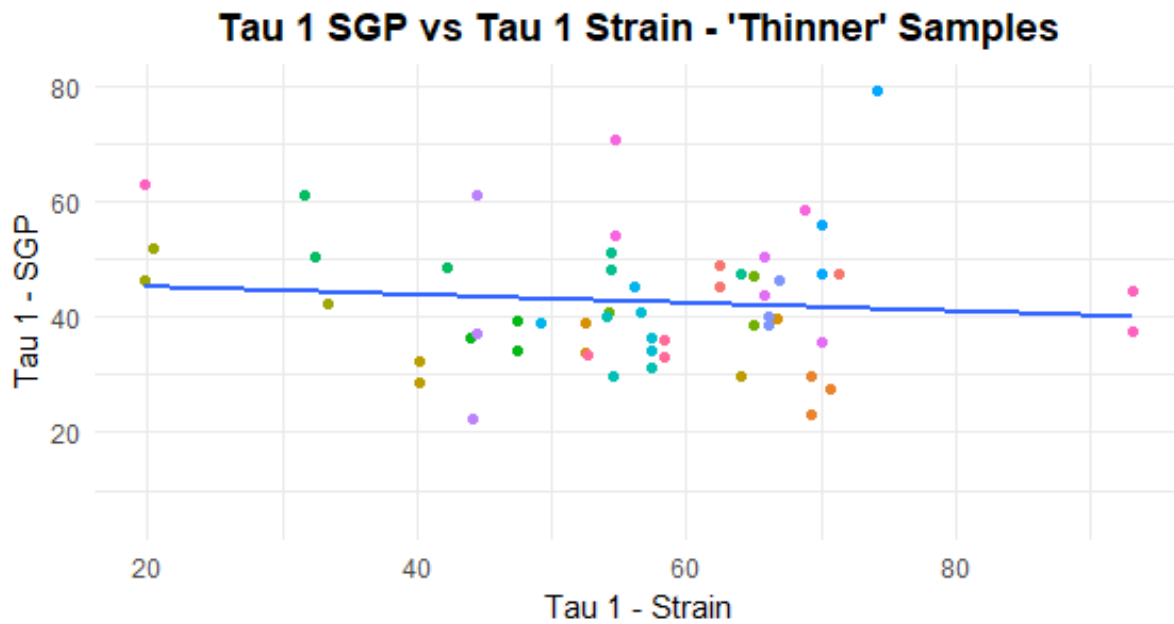


**Figure 3.6a:** A linear model fit to the SGP and strain  $\tau_1$  values for samples thinner than 3.15mm.  $\tau_1$  for SGP decreased with increasing  $\tau_1$  for strain.

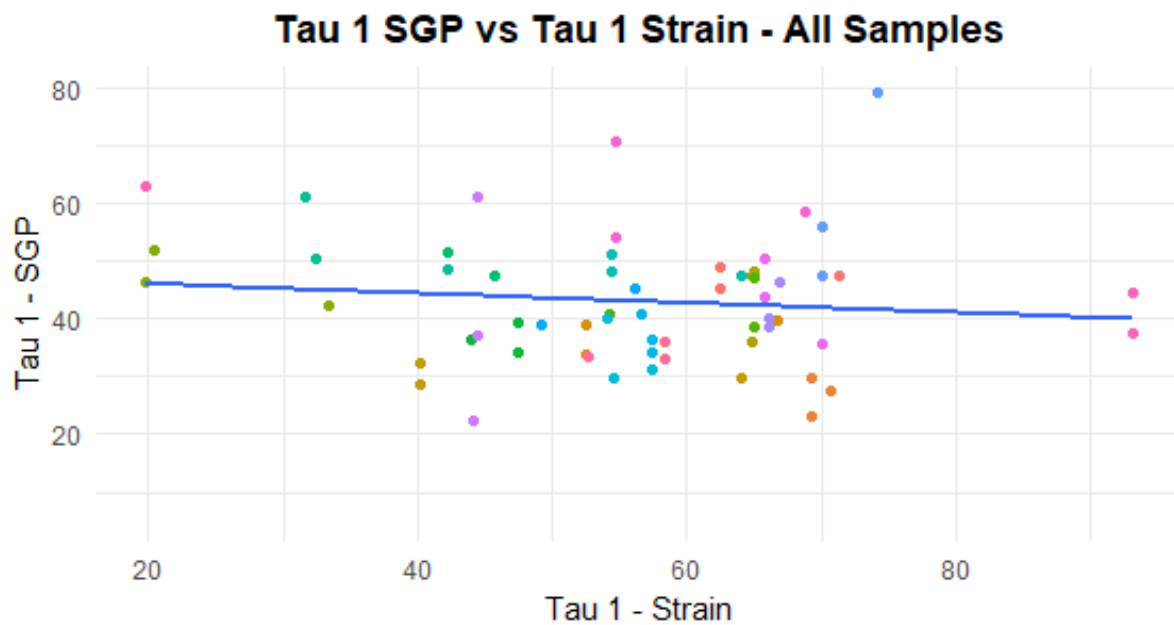


**Figure 3.6b:** A linear model fit to the SGP and strain  $\tau_1$  values for all samples.  $\tau_1$  for SGP decreased with increasing  $\tau_1$  for strain.

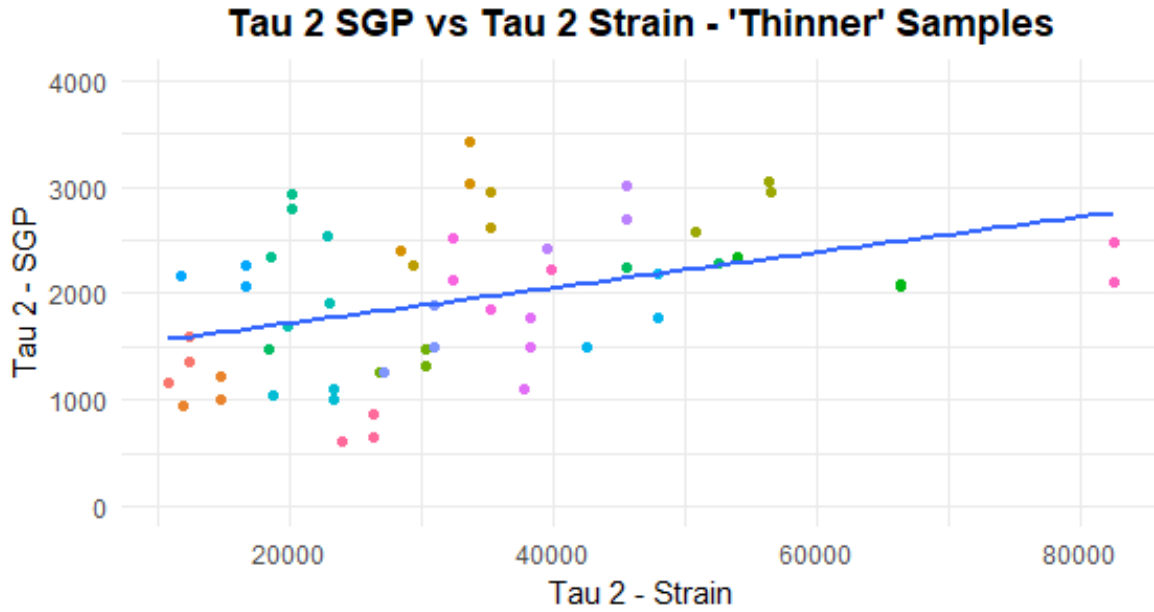


**Figure 3.7a:** A linear model fit to the  $\tau_2$  SGP and strain values for samples thinner than 3.15mm.  $\tau_2$  for SGP increased with increasing  $\tau_2$  for strain.

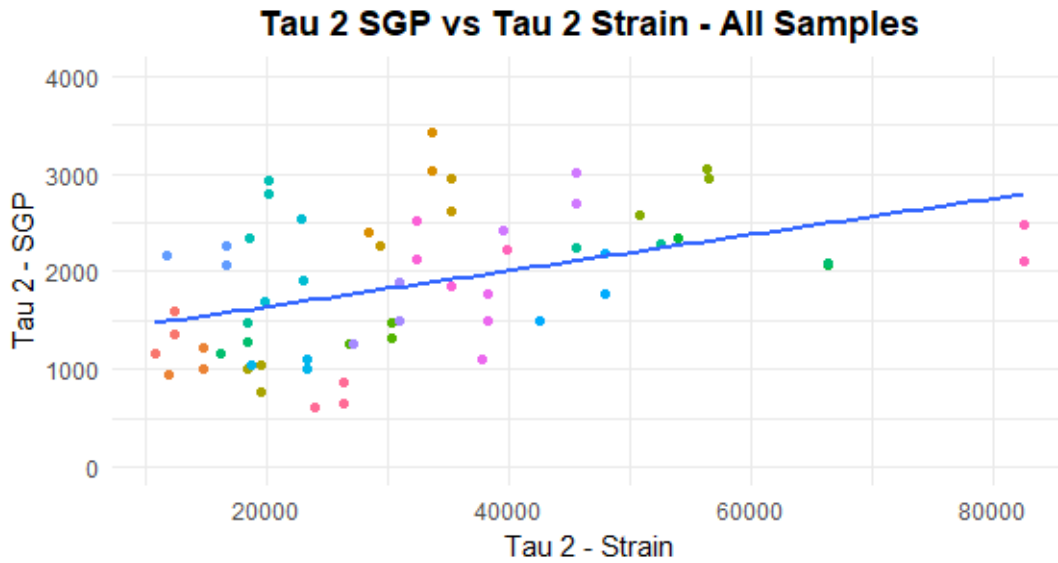


**Figure 3.7b:** A linear model fit to the  $\tau_2$  SGP and strain values for all samples.  $\tau_2$  for SGP increased with increasing  $\tau_2$  for strain.

### **3.5 Drying Tests**

To assess the differences between the three drying tests, student's t-test and repeated measures ANOVA were performed. The data sets were found to be normally distributed. There were two comparisons made for the t-tests: 1) unwrapped vs. wrapped for long duration tests and 2) the wrapped long duration test vs. the wrapped short duration tests. For each comparison, the values of interest were the mean max SGP, the mean delta SGP, their ratios over the test period (recall table 2.12), and the four values collected from fitting the two-term exponential to the SGP curve: A-coefficient, C-coefficient,  $\tau_1$  and  $\tau_2$ .

On those same values, repeated measures ANOVA was conducted on the five tests within the testing period for each experiment. The same values of interest were compared using this test and were examined in the t-tests.

#### **3.5.1 Force Variations**

It is important to note that both long duration tests went through two different tests where the only difference was the time of held displacement (zero and six seconds). From visual inspection, there is a clear difference in the variance (i.e. the box plots are taller showing greater test variance) of the targeted force between the long and short duration tests (Fig. 3.8). The reason for the increased variance is due to the overshoot associated with the zero second held displacement tests. Figure 3.9 clearly shows the six second held displacement tests produced less overshoot for the targeted 30N load compared to the zero second held displacement tests. Although it is not a very large overshoot, it contributed to the increase in variance of the boxplots in the long duration tests in figure 3.8. This was also seen in the Force Magnitude and Rate tests when the rate of deformation was increased.

Due to this variation caused by force overshoot, only the data collected from the six second held tests was used for statistical analysis to compare the three experiments. This ensured a more consistent target force was reached for all three experimental conditions.

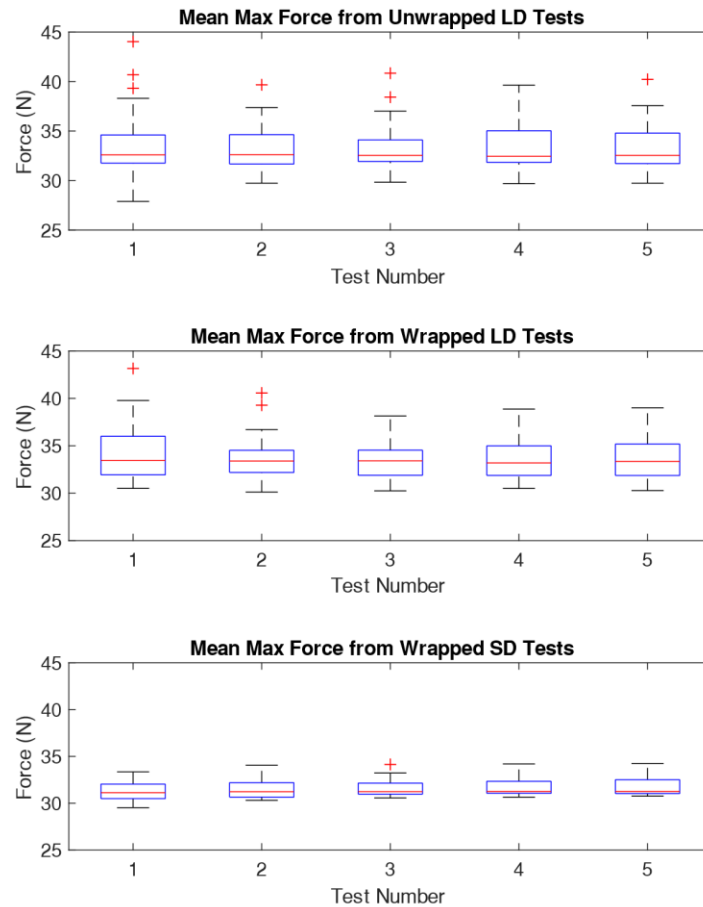


**Figure 3.8:** Boxplots showing that the force consistently reached approximately 30N during the Drying tests. Wrapped short duration tests had less variation because they were only ever in held displacement for six seconds.

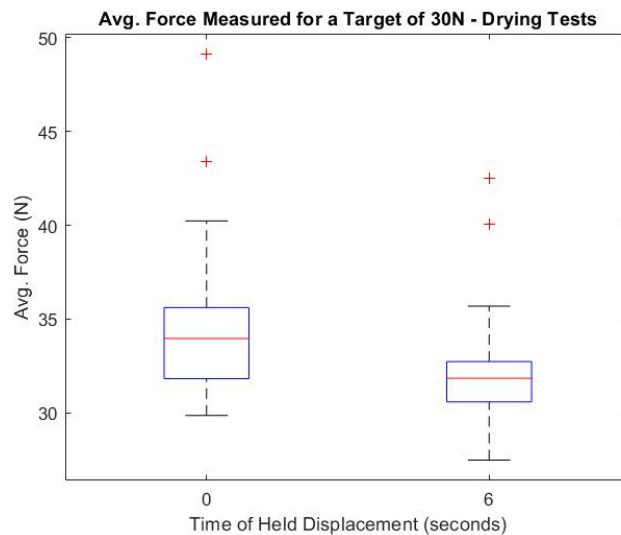


**Figure 3.9:** Overshoot in target force from the zero second held displacement tests caused the variation in the wrapped and unwrapped long duration tests.



### 3.5.2 Results from Statistical Analysis

Mean max SGPs (Fig. 3.10a-b) and A-coefficients (Fig. 3.16a-b) for both long duration experiments decreased significantly with each test over the testing period. The wrapped short duration experiments maintained a mean max SGP that did not significantly differ over the entire testing period (Fig. 3.10c). The A-coefficient decreased significantly from the start to the end of the testing period, but not from test to test like in the long duration experiments (Fig. 3.16c). For all three experiments, the C-coefficient had a trend to decrease over the tests with a significant decrease from the first to the last test (Fig. 3.17a-c).

Looking at the t-test results that compare the mean max SGP from each test between the three experiments (Table 3.2a-b), there was no significant difference between the wrapped long duration and short duration tests, but tests one, two and five were significantly different ( $p < 0.001$ ) for the wrapped and unwrapped long duration tests. The same result was found for the C-coefficient (Table 3.7a-b). Almost all the A-coefficients differed significantly between the three experiments (Table 3.6a-b).

The mean delta SGPs tended to decrease significantly over time for all three experiments (Fig. 3.11a-b). A significant difference was found between all tests (except the first test) for all three experiments (Table 3.3a-b). The ratio of mean max SGP from test one to test five was only significantly different in the wrapped short duration tests (Fig. 3.12). The same result was found for the ratio of delta SGP (Fig. 3.13).

$\tau_1$  was unchanged in the wrapped short duration test and gave no conclusive result for both wrapped and unwrapped long duration tests (Fig. 3.14a-c). The t-test results for  $\tau_1$  showed a

significant difference between the wrapped long and short duration tests but no difference between the unwrapped and wrapped long duration tests (Table 3.4a-b).

$\tau_2$  from SGP curves for wrapped short duration tests increase significantly over the testing period, but the long duration tests increase more dramatically than the short duration (Fig. 3.15a-c). A significance difference was found for almost all tests between all three experiments (Table 3.5a-b).

Overall, the short duration tests had a much less drastic change in values compared to the long duration tests.

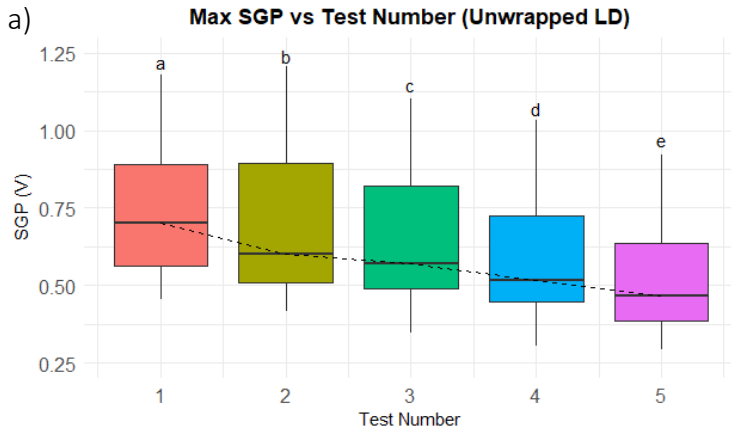


**Table 3.2a:** T-Test Results Comparing Max SGP Between Wrapped and Unwrapped Long Duration Tests

| Test Number   | p-value | Different? |
|---------------|---------|------------|
| 1             | < 0.001 | Y          |
| 2             | < 0.001 | Y          |
| 3             | 0.44    | N          |
| 4             | 0.07    | N          |
| 5             | < 0.001 | Y          |
| 1v5 unwrapped | < 0.001 | Y          |
| 1v5 wrapped   | < 0.001 | Y          |

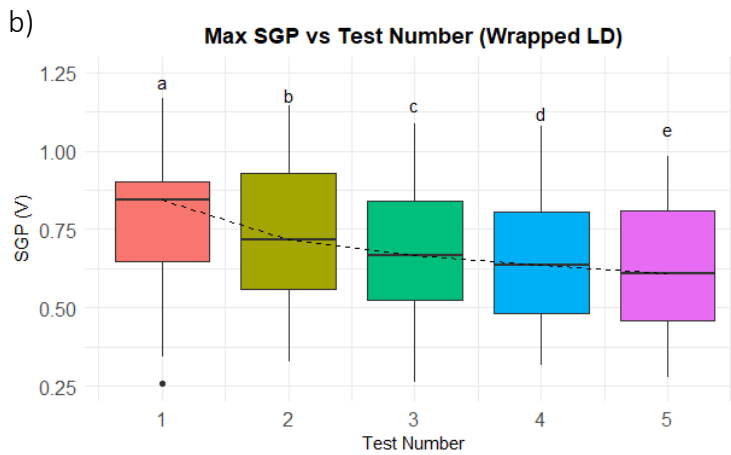


**Table 3.2b:** T-Test Results Comparing Max SGP Between Wrapped Long and Short Duration Tests

| Test Number    | p-value | Different? |
|----------------|---------|------------|
| 1              | 0.72    | N          |
| 2              | 0.29    | N          |
| 3              | 0.86    | N          |
| 4              | 0.62    | N          |
| 5              | 0.31    | N          |
| 1v5 wrapped LD | < 0.001 | Y          |
| 1v5 wrapped SD | 0.188   | N          |

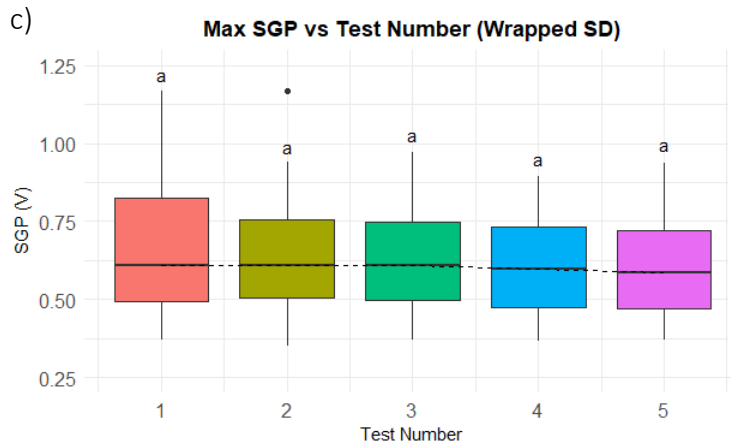


**Figure 3.10a:** Mean max SGP for unwrapped long duration tests decreases significantly with each test over the testing period.

**Figure 3.10b:** Mean max SGP for wrapped long duration tests decreases significantly with each test over the testing period.

**Figure 3.10c:** Mean max SGP for wrapped short duration tests remains unchanged over the testing period.

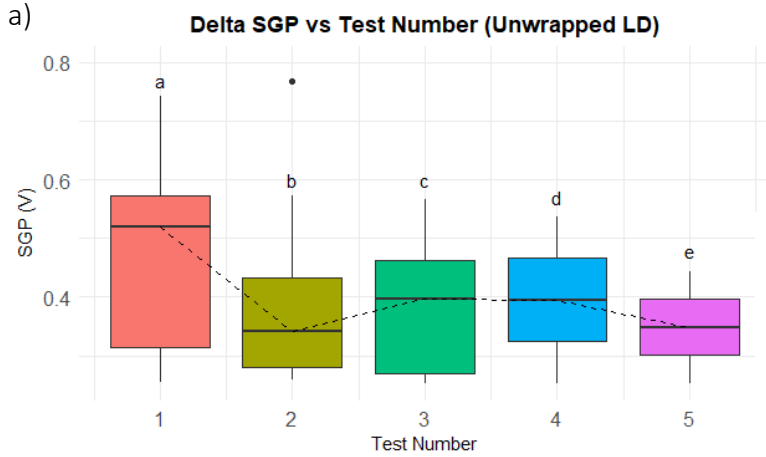


**Table 3.3a:** T-Test Results Comparing Max Delta SGP Between Wrapped and Unwrapped Long Duration Tests

| Test Number   | p-value | Different? |
|---------------|---------|------------|
| 1             | 0.25    | N          |
| 2             | < 0.001 | Y          |
| 3             | < 0.001 | Y          |
| 4             | < 0.001 | Y          |
| 5             | < 0.001 | Y          |
| 1v5 unwrapped | < 0.001 | Y          |
| 1v5 wrapped   | < 0.001 | Y          |

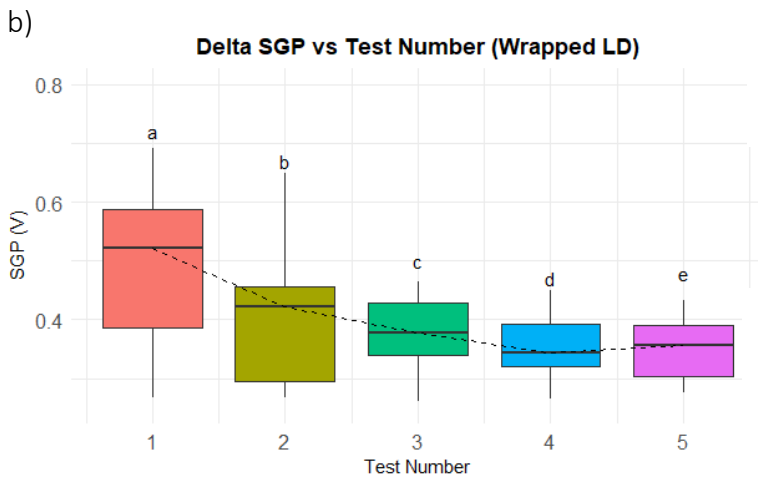


**Table 3.3b:** T-Test Results Comparing Max Delta SGP Between Wrapped Long and Short Duration Tests

| Test Number    | p-value | Different? |
|----------------|---------|------------|
| 1              | 0.91    | N          |
| 2              | < 0.001 | Y          |
| 3              | < 0.001 | Y          |
| 4              | < 0.001 | Y          |
| 5              | < 0.001 | Y          |
| 1v5 wrapped LD | < 0.001 | Y          |
| 1v5 wrapped SD | < 0.001 | Y          |



**Figure 3.11a:** Mean delta SGP for unwrapped long duration tests are significantly different with each test over the testing period.

**Figure 3.11b:** Mean delta SGP for wrapped long duration tests are significantly different with each test over the testing period.

**Figure 3.11c:** Mean delta SGP for wrapped short duration tests are significantly different with each test over the testing period.

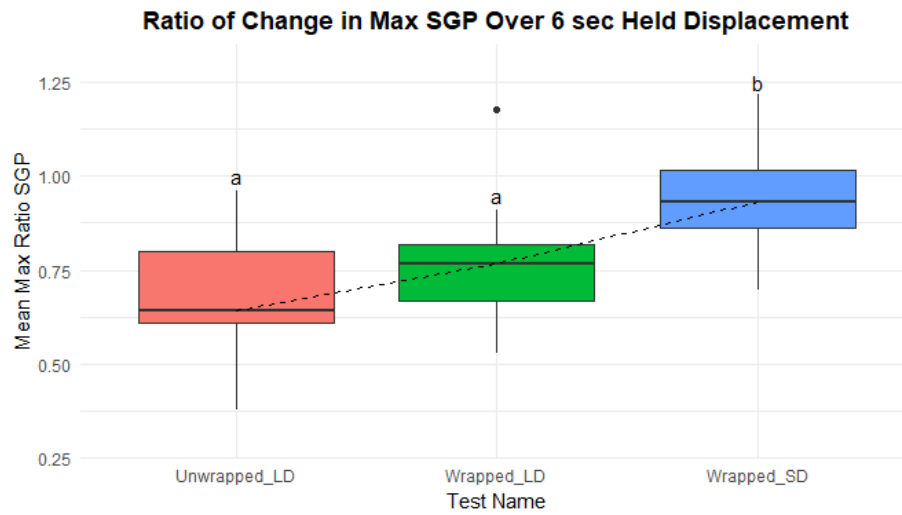


**Figure 3.12:** Max SGP ratio for wrapped and unwrapped long duration drying tests are not significantly different, but the wrapped short duration test is significantly different.

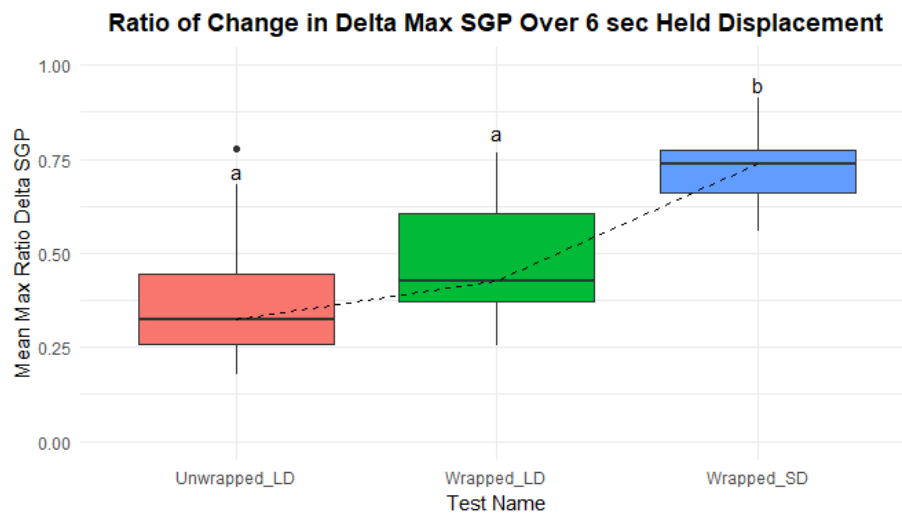


**Figure 3.13:** Delta SGP ratio for wrapped and unwrapped long duration drying tests are not significantly different, but the wrapped short duration test is significantly different.

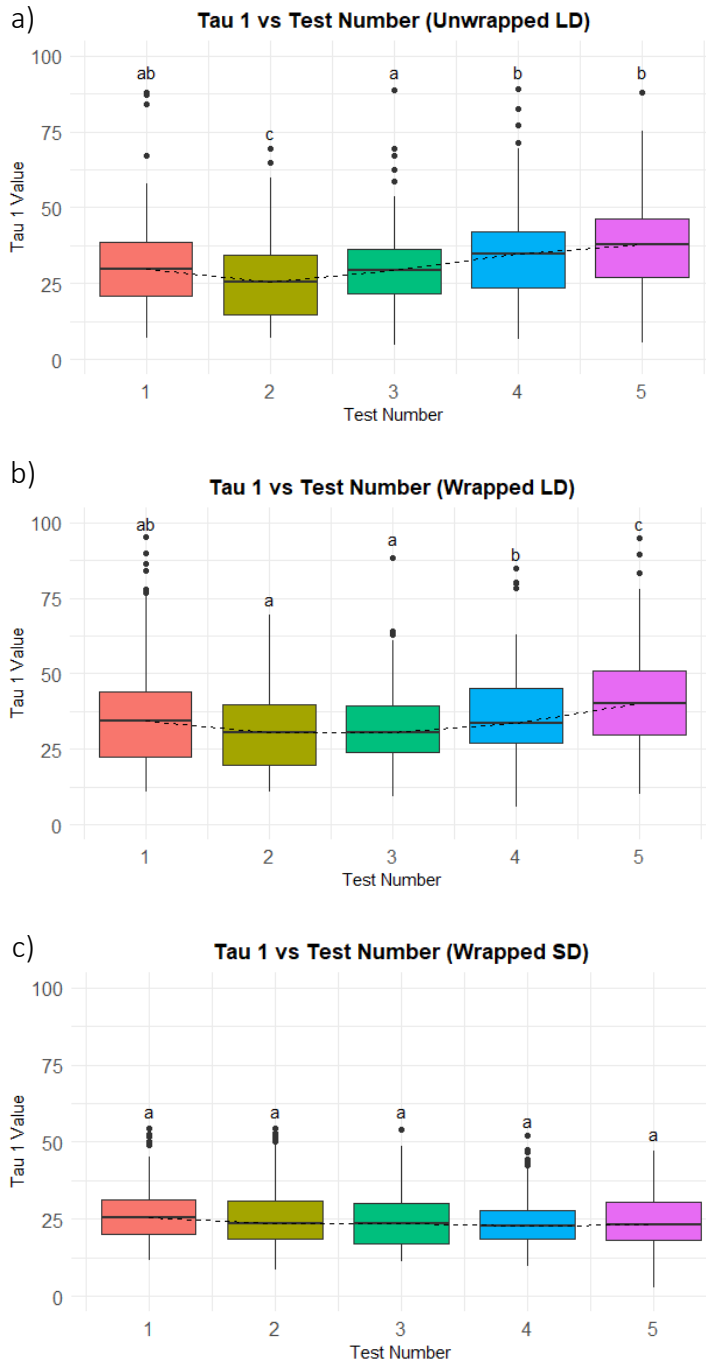


**Table 3.4a:** T-Test Results Comparing  $\tau_1$  of SGP Between Wrapped and Unwrapped Long Duration Tests

| Test Number   | p-value | Different? |
|---------------|---------|------------|
| 1             | 0.42    | N          |
| 2             | .0068   | Y          |
| 3             | 0.1     | N          |
| 4             | 0.79    | N          |
| 5             | 0.42    | N          |
| 1v5 unwrapped | 0.1     | N          |
| 1v5 wrapped   | 0.059   | N          |

**Table 3.4b:** T-Test Results Comparing  $\tau_1$  of SGP Between Wrapped Long and Short Duration Tests

| Test Number    | p-value | Different? |
|----------------|---------|------------|
| 1              | < 0.001 | Y          |
| 2              | .0015   | Y          |
| 3              | < 0.001 | Y          |
| 4              | < 0.001 | Y          |
| 5              | < 0.001 | Y          |
| 1v5 wrapped LD | 0.059   | N          |
| 1v5 wrapped SD | 0.01    | N          |

**Figure 3.14a:**  $\tau_1$  from SGP curves for unwrapped long duration tests decreases over the testing period but not from test to test.

**Figure 3.14b:**  $\tau_1$  from SGP curves for wrapped long duration tests decreases over the testing period but not from test to test.

**Figure 3.14c:**  $\tau_1$  from SGP curves for wrapped short duration tests remains unchanged over the testing period.

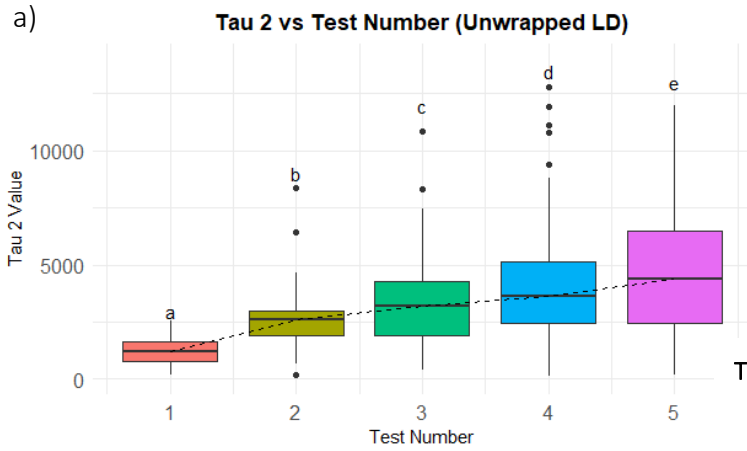


**Table 3.5a:** T-Test Results Comparing  $\tau_2$  of SGP Between Wrapped and Unwrapped Long Duration Tests

| Test Number   | <i>p</i> -value | Different? |
|---------------|-----------------|------------|
| 1             | 0.6             | N          |
| 2             | < 0.001         | Y          |
| 3             | < 0.001         | Y          |
| 4             | < 0.001         | Y          |
| 5             | < 0.001         | Y          |
| 1v5 unwrapped | < 0.001         | Y          |
| 1v5 wrapped   | < 0.001         | Y          |

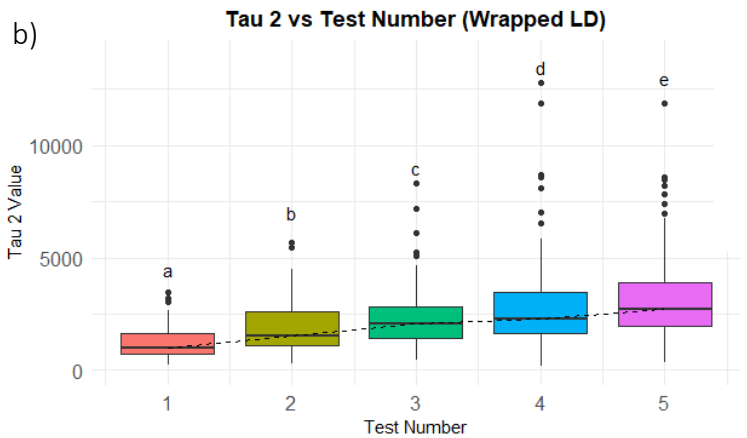


**Table 3.5b:** T-Test Results Comparing  $\tau_2$  of SGP Between Wrapped Long and Short Duration Tests

| Test Number    | <i>p</i> -value | Different? |
|----------------|-----------------|------------|
| 1              | 0.038           | Y          |
| 2              | < 0.001         | Y          |
| 3              | < 0.001         | Y          |
| 4              | < 0.001         | Y          |
| 5              | < 0.001         | Y          |
| 1v5 wrapped LD | < 0.001         | Y          |
| 1v5 wrapped SD | < 0.001         | Y          |

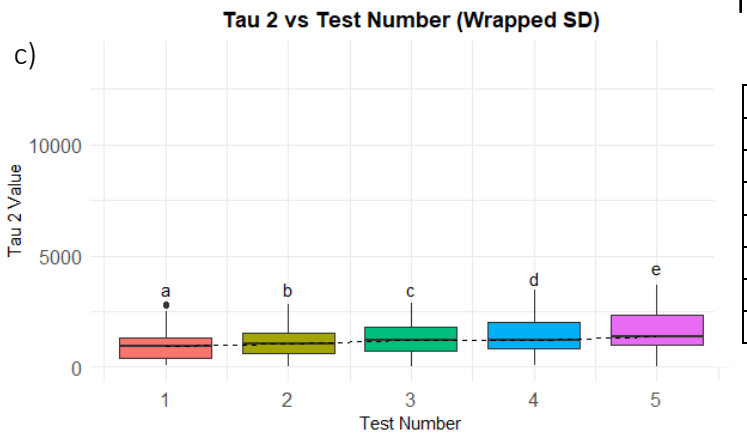


**Figure 3.15a:**  $\tau_2$  from SGP curves for unwrapped long duration tests increase significantly over the testing period.

**Figure 3.15b:**  $\tau_2$  from SGP curves for wrapped long duration tests increase significantly over the testing period.

**Figure 3.15c:**  $\tau_2$  from SGP curves for wrapped short duration tests increase significantly over the testing period.

a) **A Coeff vs Test Number (Unwrapped LD)**

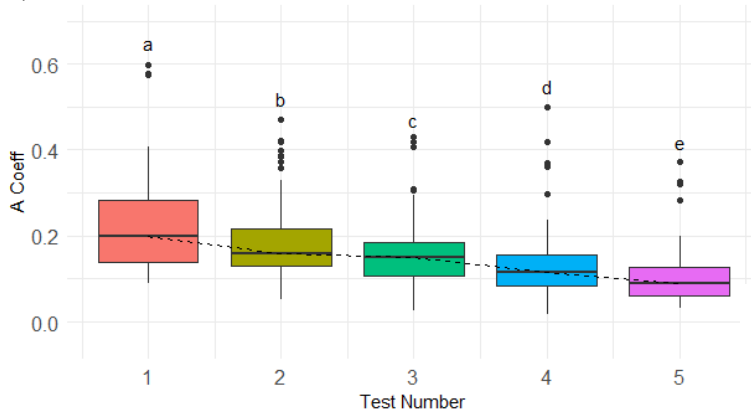


**Table 3.6a:** T-Test Results Comparing A Coefficient of SGP Between Wrapped and Unwrapped Long Duration Tests

| Test Number   | p-value | Different? |
|---------------|---------|------------|
| 1             | < 0.001 | Y          |
| 2             | .0034   | Y          |
| 3             | < 0.001 | Y          |
| 4             | < 0.001 | Y          |
| 5             | < 0.001 | Y          |
| 1v5 unwrapped | < 0.001 | Y          |
| 1v5 wrapped   | < 0.001 | Y          |

b) **A Coeff vs Test Number (Wrapped LD)**

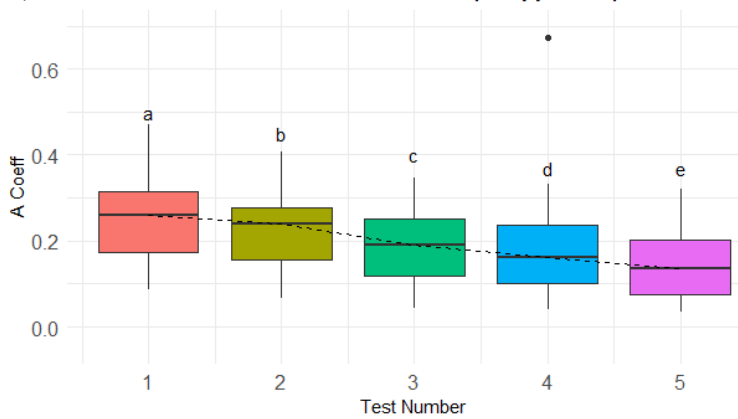


**Table 3.6b:** T-Test Results Comparing A Coefficient of SGP Between Wrapped Long and Short Duration Tests

| Test Number    | p-value | Different? |
|----------------|---------|------------|
| 1              | < 0.001 | Y          |
| 2              | 0.87    | N          |
| 3              | 0.04    | Y          |
| 4              | .0054   | Y          |
| 5              | < 0.001 | Y          |
| 1v5 wrapped LD | < 0.001 | Y          |
| 1v5 wrapped SD | 0.098   | N          |

c) **A Coeff vs Test Number (Wrapped SD)**

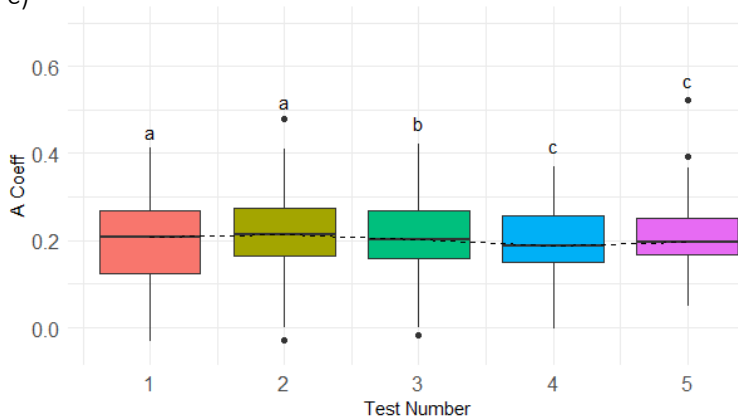


**Figure 3.16a:** A-coefficients from SGP curves for unwrapped long duration tests decrease significantly with each test over the testing period.

**Figure 3.16b:** A-coefficients from SGP curves for wrapped long duration tests decrease significantly with each test over the testing period.

**Figure 3.16c:** A-coefficients from SGP curves for wrapped short duration tests decrease significantly over the testing period.



a) **C Coeff vs Test Number (Unwrapped LD)**

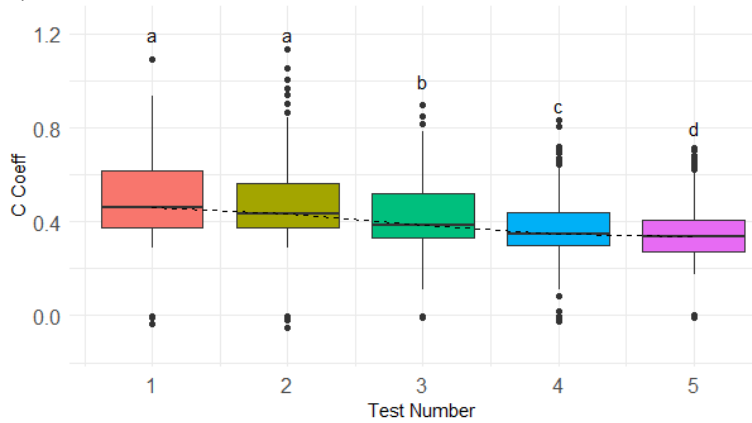


**Table 3.7a:** T-Test Results Comparing C Coefficient of SGP Between Wrapped and Unwrapped Long Duration Tests

| Test Number   | p-value | Different? |
|---------------|---------|------------|
| 1             | < 0.001 | Y          |
| 2             | .0052   | Y          |
| 3             | 0.82    | N          |
| 4             | 0.41    | N          |
| 5             | 0.016   | Y          |
| 1v5 unwrapped | < 0.001 | Y          |
| 1v5 wrapped   | < 0.001 | Y          |

b) **C Coeff vs Test Number (Wrapped LD)**

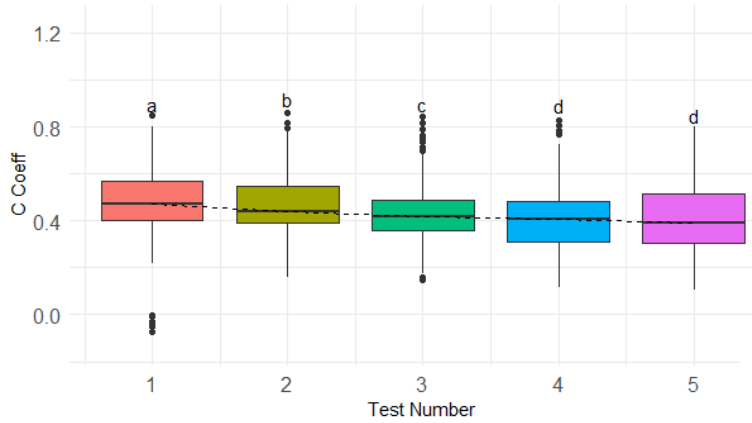


**Table 3.7b:** T-Test Results Comparing C Coefficient of SGP Between Wrapped Long and Short Duration Tests

| Test Number    | p-value | Different? |
|----------------|---------|------------|
| 1              | 0.15    | N          |
| 2              | 0.12    | N          |
| 3              | 0.88    | N          |
| 4              | 0.86    | N          |
| 5              | 0.88    | N          |
| 1v5 wrapped SD | < 0.001 | Y          |
| 1v5 wrapped SD | < 0.001 | Y          |

c) **C Coeff vs Test Number (Wrapped SD)**

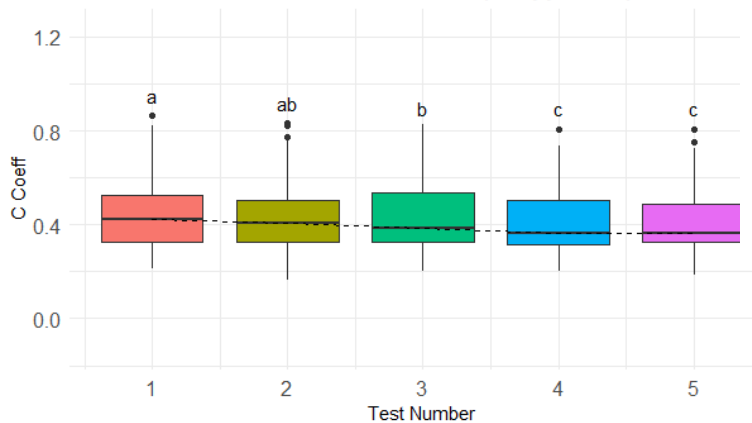


**Figure 3.17a:** C-coefficients from SGP curves for unwrapped long duration tests decrease significantly with each test over the testing period.

**Figure 3.17b:** C-coefficients from SGP curves for wrapped long duration tests decrease significantly with each test over the testing period.

**Figure 3.17c:** C-coefficients from SGP curves for wrapped short duration tests decrease significantly over the testing period.

### **3.1.6 Force Magnitude and Rate Tests**

#### **Overshoot**

Although the target force was 20, 30, 40 and 50N, the Admet material test system typically overshoot the target by about 2N (Fig. 3.18a). There was more obvious overshoot during the rate tests with increasing displacement rate. As seen in (Fig. 3.18b), even though the target force was 30N, the higher deformation rates led to more overshoot and thus a significant difference in the max force for the rate tests. This overshoot in the rate tests also affected the mean max strain values, which were also significantly different from each other (Fig. 3.19a-b).

#### **Test Two vs. Test Six**

Test two and test six of the Magnitude and Rate tests were the exact same test (Table 2.11) – a deformation rate of  $100 \frac{mm}{min}$  to a target of 30N. The purpose of the redundancy was to allow for a way to verify if there was consistency in the SGPs over the testing period for the various testing orders. I expected these two tests to produce the same results since they were the same test. There was no significant difference found in the measures of mean max SGP and mean delta SGP between test two and test six.

#### **SGP vs Load**

Mean max SGP increased significantly with increasing load (Fig. 3.20b). Mean delta SGP also increased significantly with increasing load, but not as drastically as the mean max SGP when the y-axis range difference is taken into consideration (Fig. 3.21b). The A-coefficient remained relatively unchanged with increased force (Fig. 3.24a) but the C-coefficient increases significantly with increasing force (Fig. 3.25a). Like the coefficients,  $\tau_1$  seems to remain constant with increasing force (Fig. 3.22a) and  $\tau_2$  increased significantly with increasing force (Fig. 3.23a).

### **SGP vs Deformation Rate**

It was difficult to tell if increased loading rate caused a difference in mean max SGP in the rate tests due to the overshoot. If I ignored the possible effect of overshoot, the mean max SGP significantly increased over the first three rate tests, but the last two rate tests were not significantly different (Fig. 3.20b). The mean delta SGP increased significantly with increasing deformation rate (Fig. 3.21b). The A-coefficient increased significantly with increasing deformation rate (Fig. 3.24b) whereas the C-coefficient remained unchanged with increasing loading rate (Fig. 3.25b) but increased significantly with increasing force magnitude (Fig. 3.25a).  $\tau_1$  decreased significantly with increasing deformation rate (Fig. 3.22b) whereas  $\tau_2$  remains constant with increasing deformation rate (Fig. 3.23b).

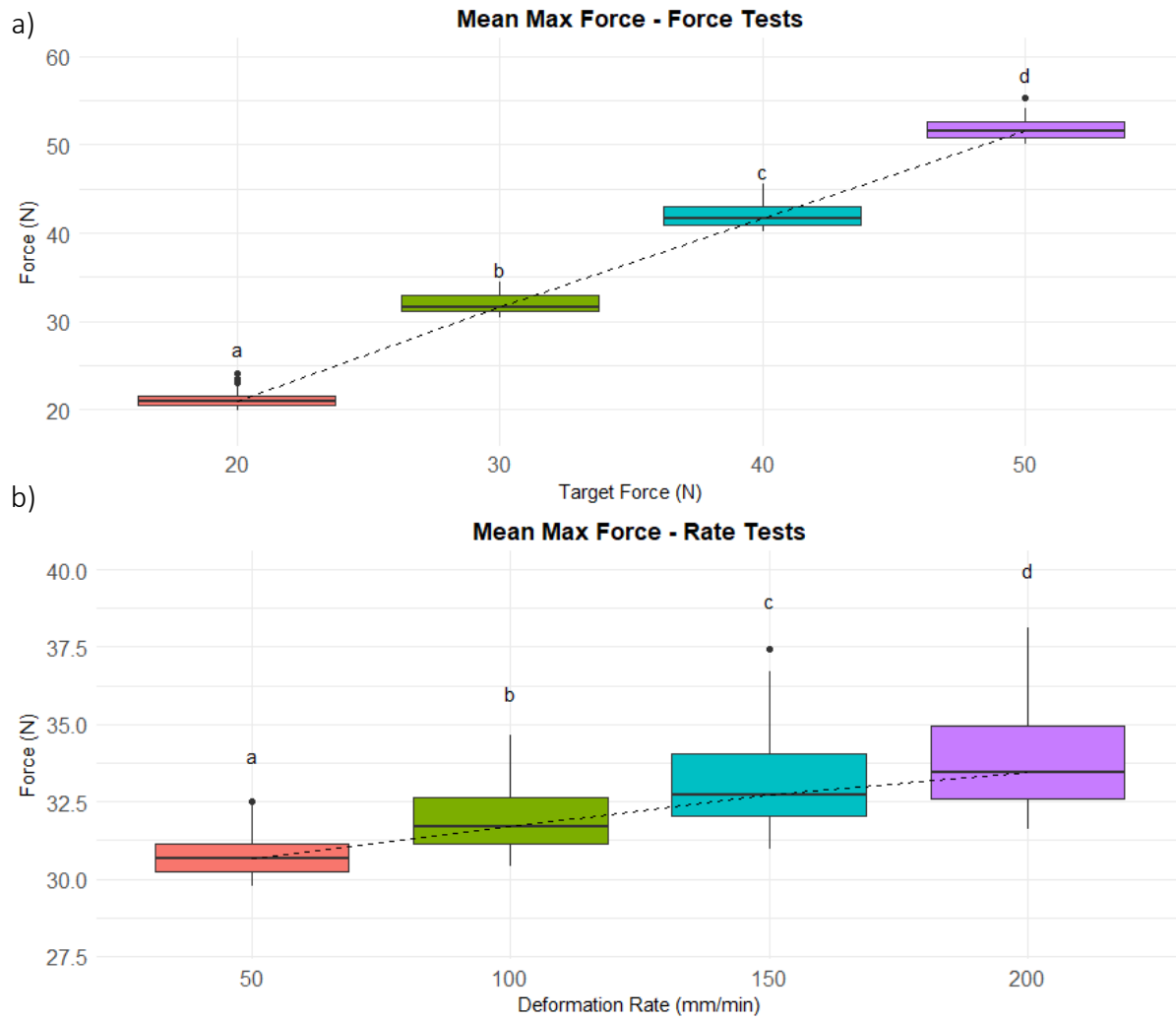


**Figure 3.18a-b:** Overshoot seen in both tests. In the force tests the Admet typically overshoot by about 2N. In the rate tests there was a larger overshoot seen with a higher deformation rate.

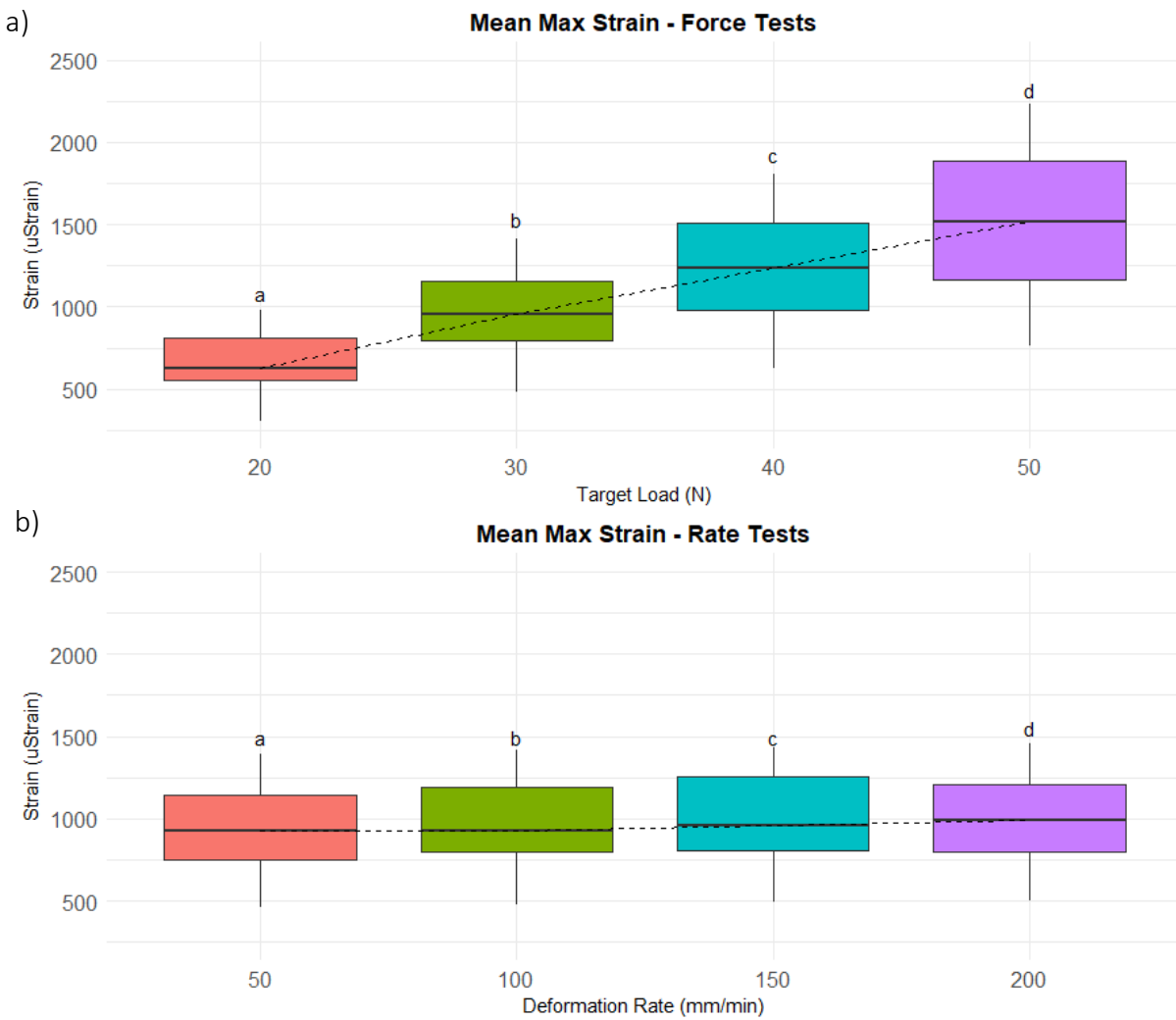


**Figure 3.19a-b:** As expected, in the force tests strain increased significantly with increasing force, but, like the max force, the strain also increased significantly due to overshoot in the rate tests.

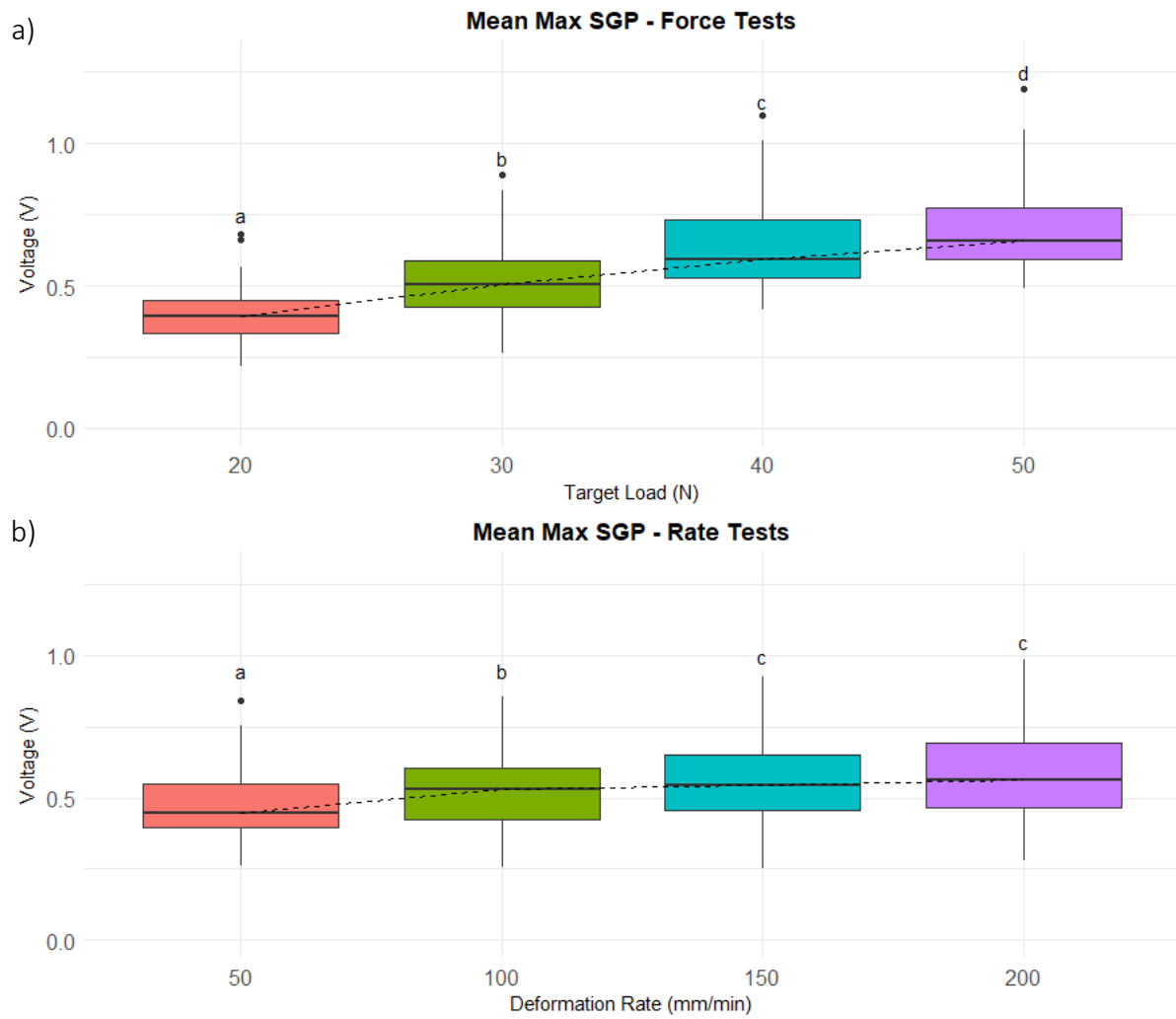


**Figure 3.20a-b:** The max SGP value increases significantly with increasing load in the force tests. It is difficult to tell if increased loading rate was the cause of the difference in max SGP in the rate tests due to the overshoot.

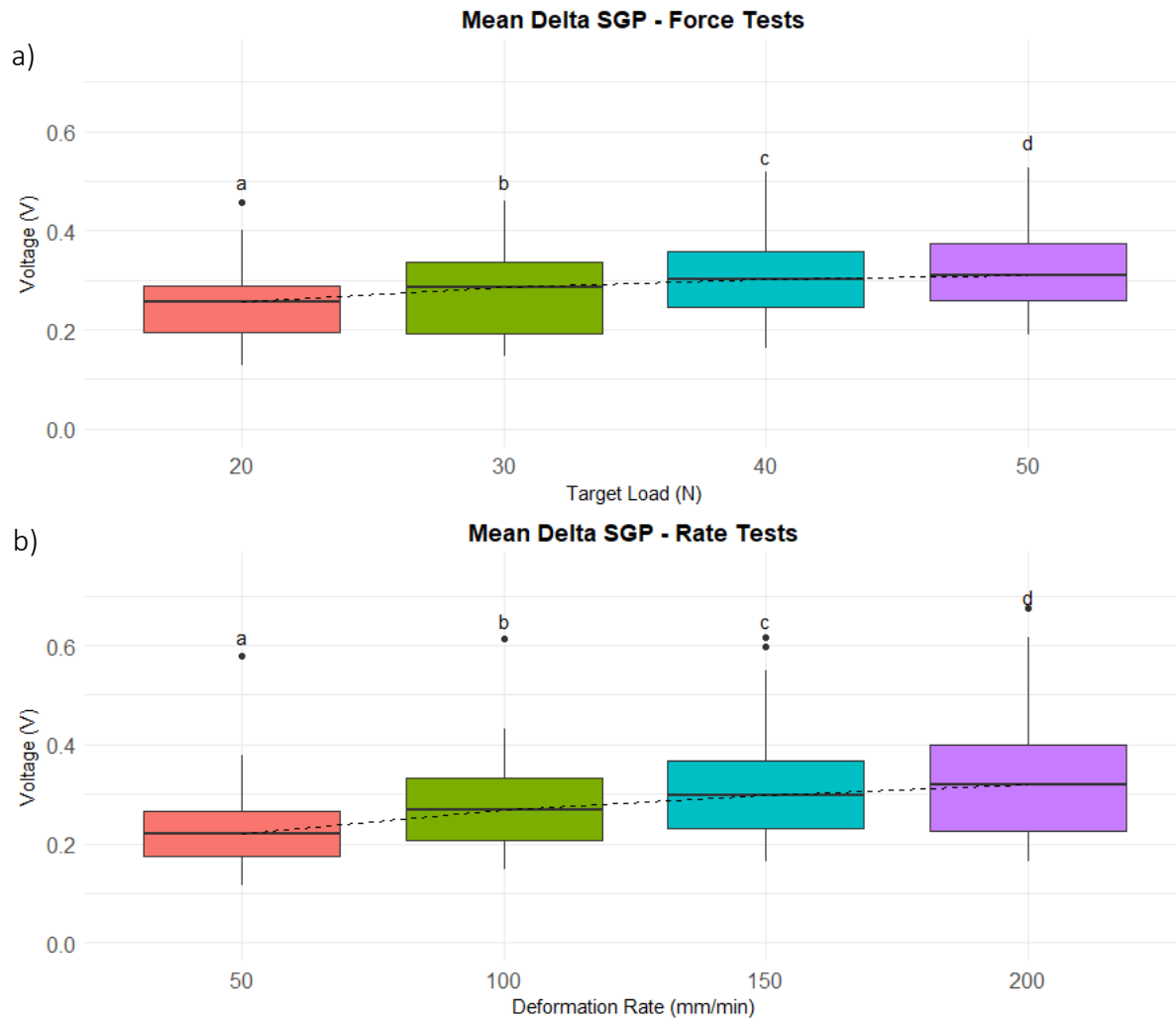


**Figure 3.21a-b:** The delta SGP value increases significantly with increasing load in the force tests and increasing deformation rate in the rate tests.

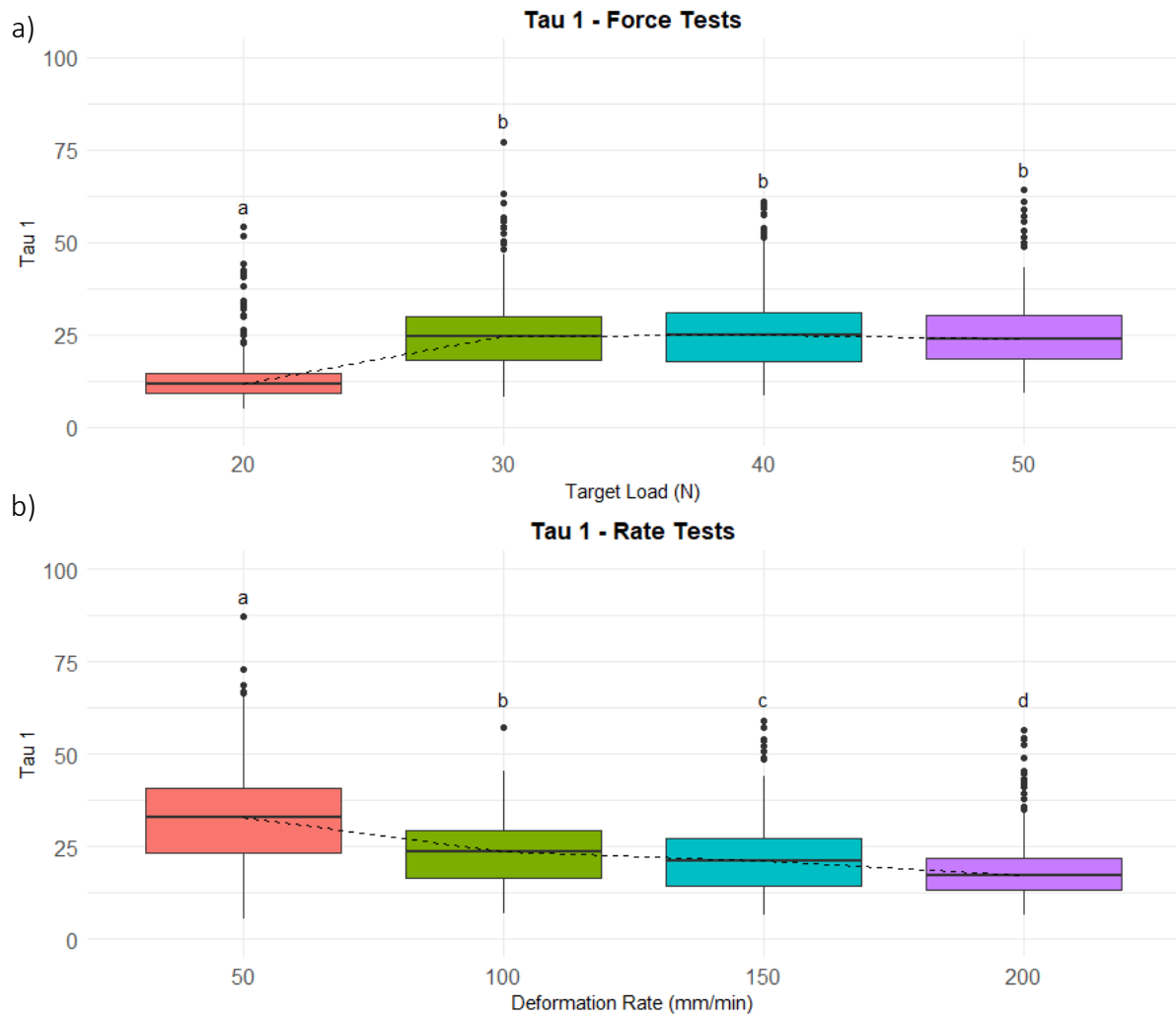


**Figure 3.22a-b:**  $\tau_1$  does not increase significantly (tests 2-4) with increasing load in the force tests and decreases significantly with increasing deformation rate in the rate tests.



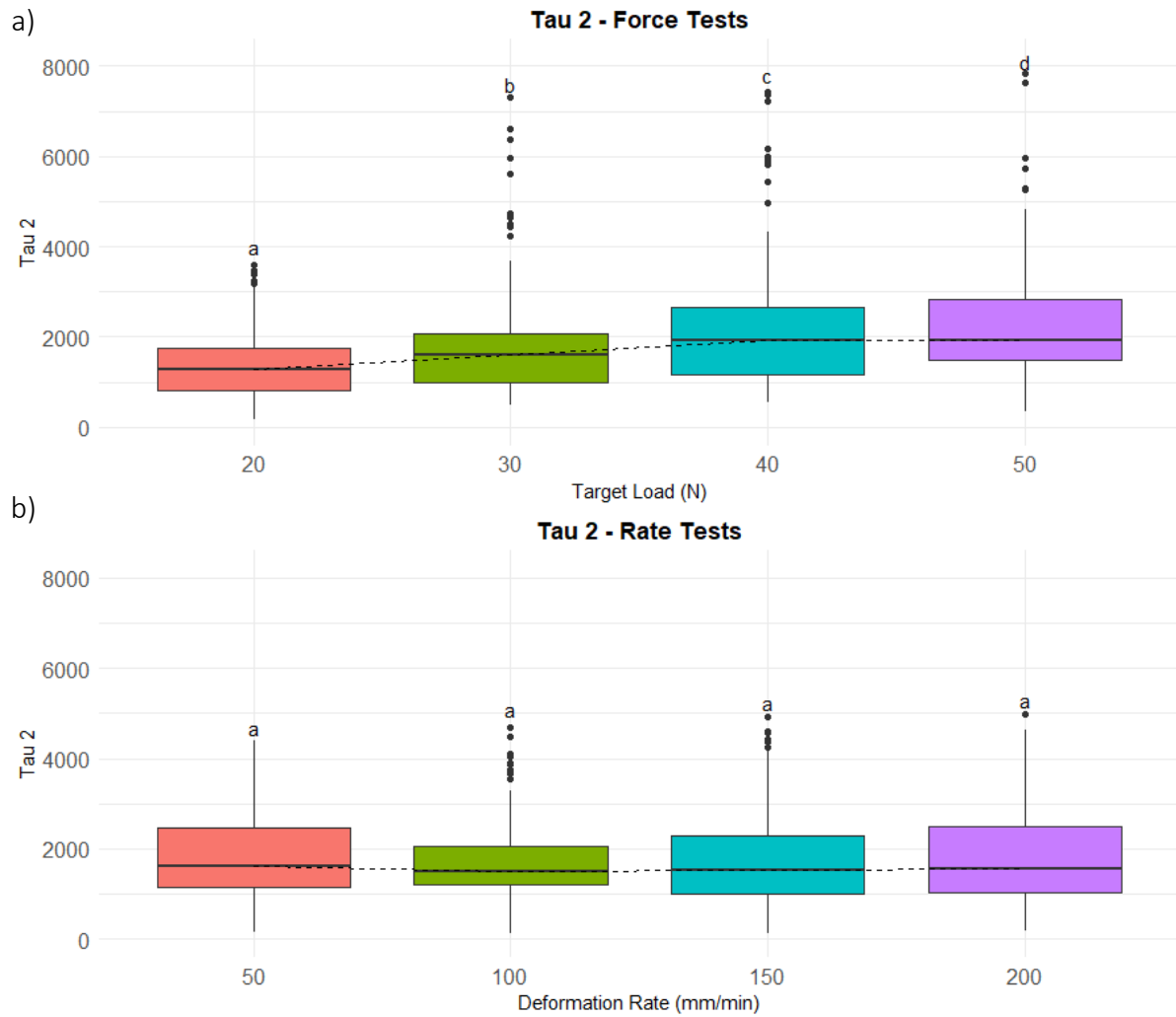


**Figure 3.23a-b:**  $\tau_2$  increases significantly with increasing load in the force tests and is unchanged for increasing deformation rate in the rate tests.

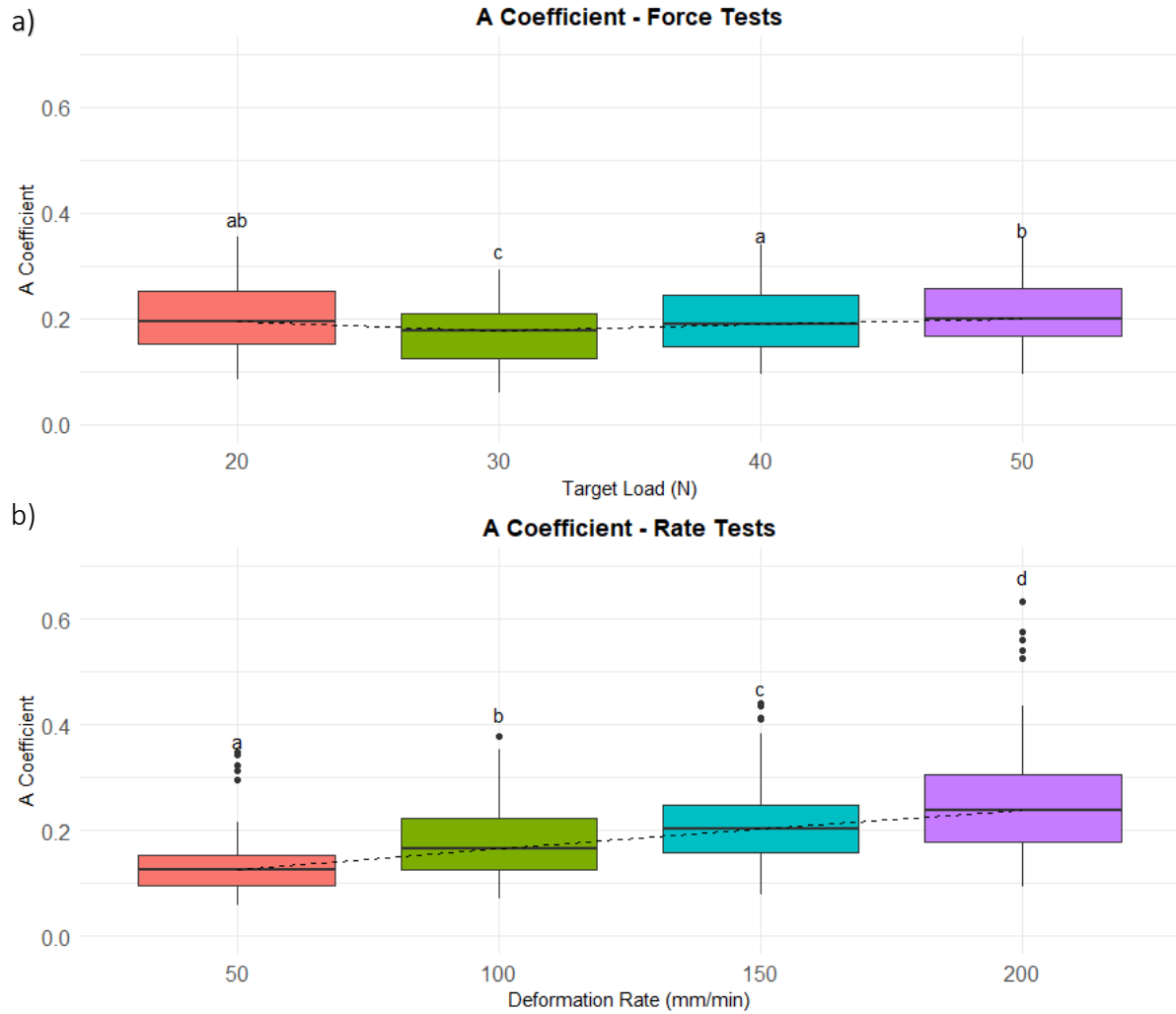


**Figure 3.24a-b:** The A-coefficient does not give conclusive results for the force tests but increases significantly with increasing deformation rate in the rate tests.

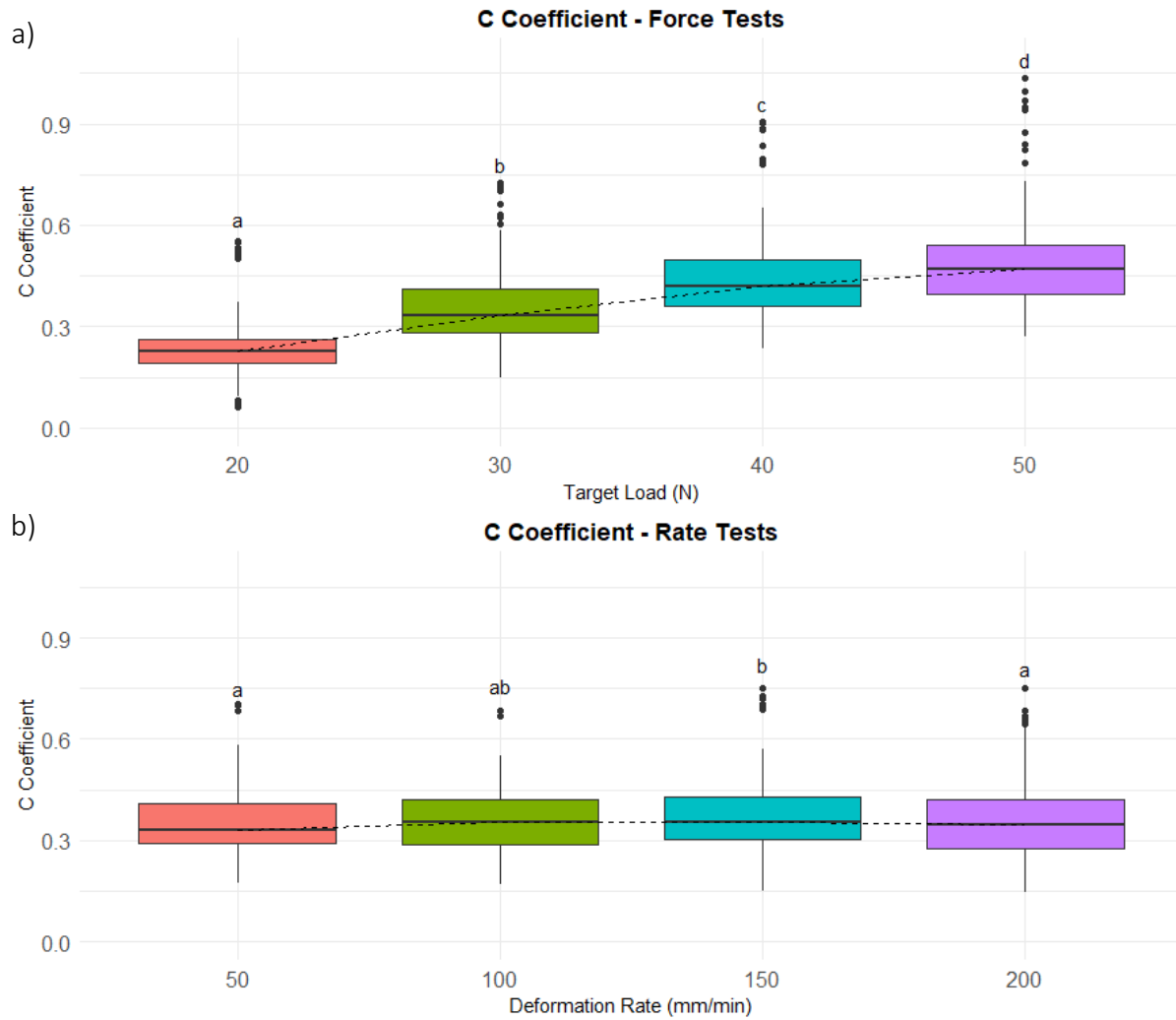


**Figure 3.25a-b:** The C-coefficient increases significantly with increasing load in the force tests and remains relatively constant for increasing deformation rate in the rate tests.

## **4 Discussion**

By performing these experiments, we sought out to collect SGPs produced by both piezoelectricity and streaming potentials in dry and wet bone. Once the signals were collected, we aimed to analyze their dependence on hydration level, load and deformation rate.

Without any gain, the magnitude of the SGP signals ranged from about 1 – 5 mV. This is within the range of SGP magnitudes found by other authors (Appendix 6). Similar to Cochran (Cochran et al., 1968), the magnitude of SGP within each sample tended to vary inexplicably with the testing day despite identical sample preparation and test procedure.

The negative voltages were typically of smaller magnitudes than the positive ones, although occasionally they were of equal magnitude (Fig. 2.14). Cochran also noted that if held deformation was released before the positive signal had sufficient time to decay to zero, the magnitude of the negative signal was smaller than it would have been granted the positive signal had time to fully decay (Cochran et al., 1968). Since none of the signals measured during any of my experiments decayed to zero this is not an adequate explanation. It is more likely the fact that there was more pressure within the sample during loading (before stress-relaxation occurred) than after the load was released and the sample returned to its original state.

### **4.1 Effect of Dehydration**

The SGP signals deteriorated as the samples became less hydrated – possibly due to the loss of ionic fluid that produce streaming potentials.

#### 4.1.1 Dry vs Wet

There was a clear difference between the SGPs produced by the wet and dry samples (Fig. 3.1). The wet samples produced decaying exponential curves during held displacement and the dry samples produced only noisy signals. Voltage spikes were visible during loading/unloading and are likely caused by motion artifact from the load cell (like in figure 2.5).

What was odd about these noisy signals is that they were of a greater magnitude than the SGP signal collected from the wet samples, yet they were not present in the wet SGP signals. This could have been due to two factors that were directly related. The first factor being that it is possible that the SGP circuit did not properly reject this common-mode noise from the dry samples. This noisy signal may be much larger in the top electrode compared to the bottom electrode due to the increased resistivity of the dried bone sample, thus producing a potential difference that was picked up by the SGP circuit.

There are some studies that explored the effect of hydration levels on the resistivity of bone. In particular, Eriksson measured the electrical resistance in freshly excised bone as it air-dried (Eriksson, 1974). In this study they measured resistance in three different directions: longitudinally (the z-direction along the long axis of the bone) and transversely (x and y-axes). Although it makes sense that there would be less resistance along the longitudinal direction due to Haversian canals, they discovered that at a certain point there was a dramatic increase in longitudinal resistivity, which they associated with collagen-bound water (Fig. 4.1). Additionally, in that paper they also approximated that unbound water (i.e. water that can contribute to streaming potentials) makes up only 2% of the total wet bone mass (Eriksson, 1974). Since our bones were all cut with the longitudinal axis of the bone laying along the long axis of our beams, this is invaluable information.

If there is a point of dehydration where 1) the electrical resistance of the sample dramatically increases and 2) only 2% of unbound water in bone contributes to streaming potential SGPS, it would make sense why our air-dried samples were producing such poor SGP signals.

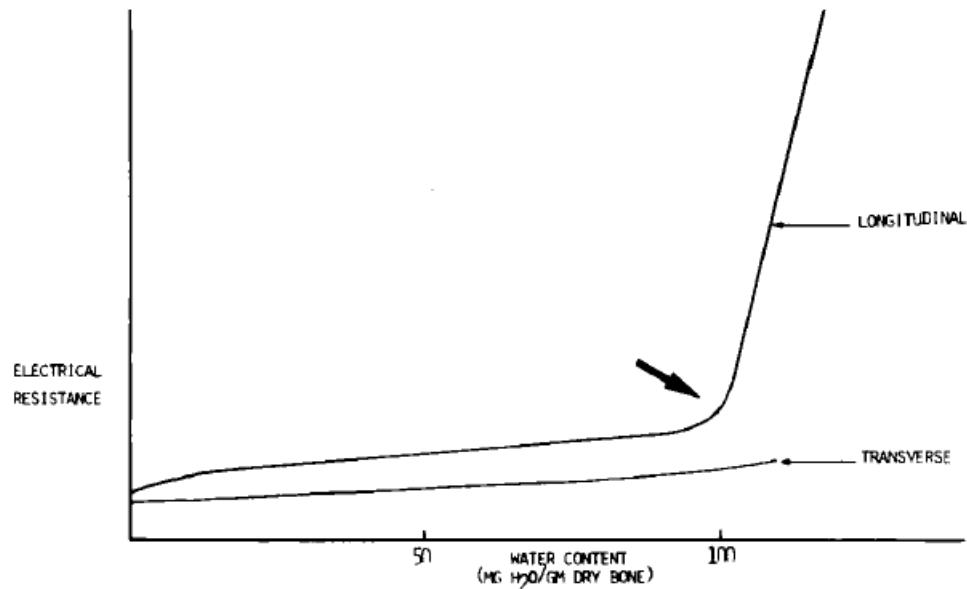
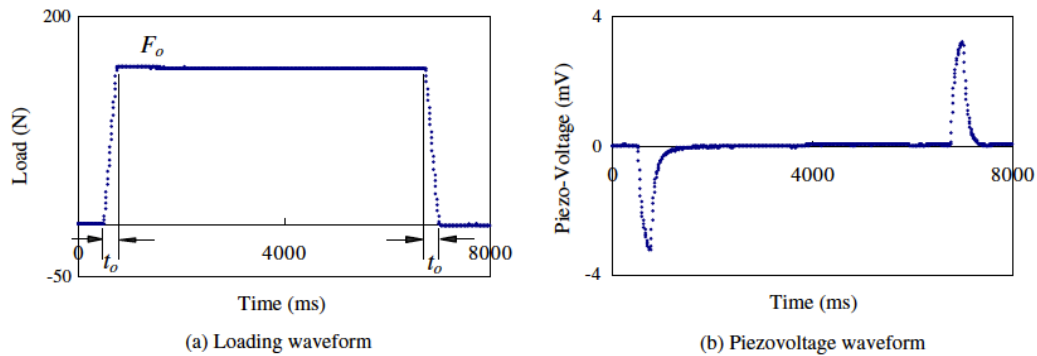


**Figure 4.1:** Plot from Eriksson's study (1974) of longitudinal and transverse electrical resistances as a function of water content. Longitudinal resistance exhibits a pronounced increase at 100 mg of H<sub>2</sub>O per gram of dry bone (indicated by arrow) (Eriksson, 1974).

In 2011, Hou published a paper on the SGPs in air-dried bone (Hou et al., 2011). The experimental setup in this paper was almost identical to my test setup. The biggest difference was that they held load constant instead of displacement. Their results are shown in figure 4.2a-b. The dry bone signal that I collected did not look at all like the spikes Hou found in their experiments. The signals collected by Hou et al. look very similar to some of the signals collected in wet bone by other researchers Appendix 6, but it is also very similar to the signals Williams and Breger collected from quartz, a known piezoelectric material, when subjected to a step load (Williams & Breger, 1975).



**Figures 4.2a-b:** Results from experiments loading air-dried bone sample show a negative spike upon loading and a positive spike upon unloading. This does not appear to be electrode artifact (Hou et al., 2011)

Furthermore, there are numerous examples of piezoelectric SGPs collected from dry bone in previous research (Anderson & Eriksson, 1970; Eiichi Fukada & Yasuda, 1957; Marino & Becker, 1974; Marino et al., 1971; McElhaney, 1967). Since dry collagen is a known piezoelectric material it is not clear why no SGP signals were obtained from our dried samples. This could be due to different methods for collecting the SGP signal itself (not all papers had clearly defined methods, especially in terms of electrical systems) and different methods used for drying the samples.

Heating biological tissue samples for drying can denature proteins in the tissue, which would cause a change in the piezoelectric signal. In the scientific literature there have been many different claims about the temperatures at which collagen is denatured. Hiratai stated that collagen denatured above 60°C (Hiratai et al., 2014), Marino mentions that the proteins within bone become denatured at around 64°C (Marino et al., 1967), Noris-Suarez claimed it denatured between 60-250°C (Noris-Suárez et al., 2007), and Shamos said that collagen fibers began shrinking at 100-120°C (Shamos & Lavine, 1964). Due to a wide variety of drying methods, defined temperatures at which collagen is denatured and ambiguous definitions of 'dry bone', it is unclear

how each drying method affects not just the water content but also the structure of the bone itself. Many different methods were used to dry bone samples such as baking, boiling, exposure to silica gel, or simply air-drying (Anderson & Eriksson, 1970; Marino & Becker, 1975; McElhaney, 1967) etc.). There has yet to be a comprehensive study as to how each of these drying methods affect the different properties of bone (i.e. mechanical, electrical properties). For this experiment, the samples were dried at 33°C, a temperature that is much lower than many used in the literature, so it is unlikely that the collagen fibers were denatured at such a low temperature. So, it was unclear as to why I was not able to collect signals similar to those found in the literature.

We did not give up on trying to measure a voltage signal from the dried bone just yet. We were measuring the SGPs using a voltage amplifier, and since piezoelectricity is a charge rather than a potential difference, we then attempted to measure piezoelectric charge from a dried sample using a charge amplification circuit.

#### **4.1.2 Charge Amplifier Tests**

Now that the sample was ethanol-dried, there was virtually no unbound water left in the sample and therefore no possibility of a streaming potential-induced SGP, the only source of SGP within the sample would come from the piezoelectric SGP produced by dry collagen. Additionally, most of the bound water should have also been removed through the ethanol-drying process leaving the collagen fibers dry enough to produce a piezoelectric charge. Still, no piezoelectric signal was collected. This could be due to the fact that I used a different circuit, a circuit that was collecting charge rather than voltage<sup>11</sup>. It is also worth noting that there was no differential amplification of

---

<sup>11</sup> Just a reminder that this was the only experiment that used the charge amplifier circuit. All other experiments used the SGP circuit.



the charge in the charge amplifier circuit, but there was still a high input resistance of ( $10^{12} \Omega$ ). Also, the charge amplifier circuit had a single-ended input whereas the SGP circuit had a differential input.

Because there was no gain in the charge amplifier it is likely the signal was just too small to be seen in figure 3.2. After I realized this I amplified the signal ( $G = 1000$ ) in MATLAB and this signal was produced (Fig. 4.3). Again, there was still no piezoelectric charge collected by the charge amplifier circuit similar to those seen in other papers.

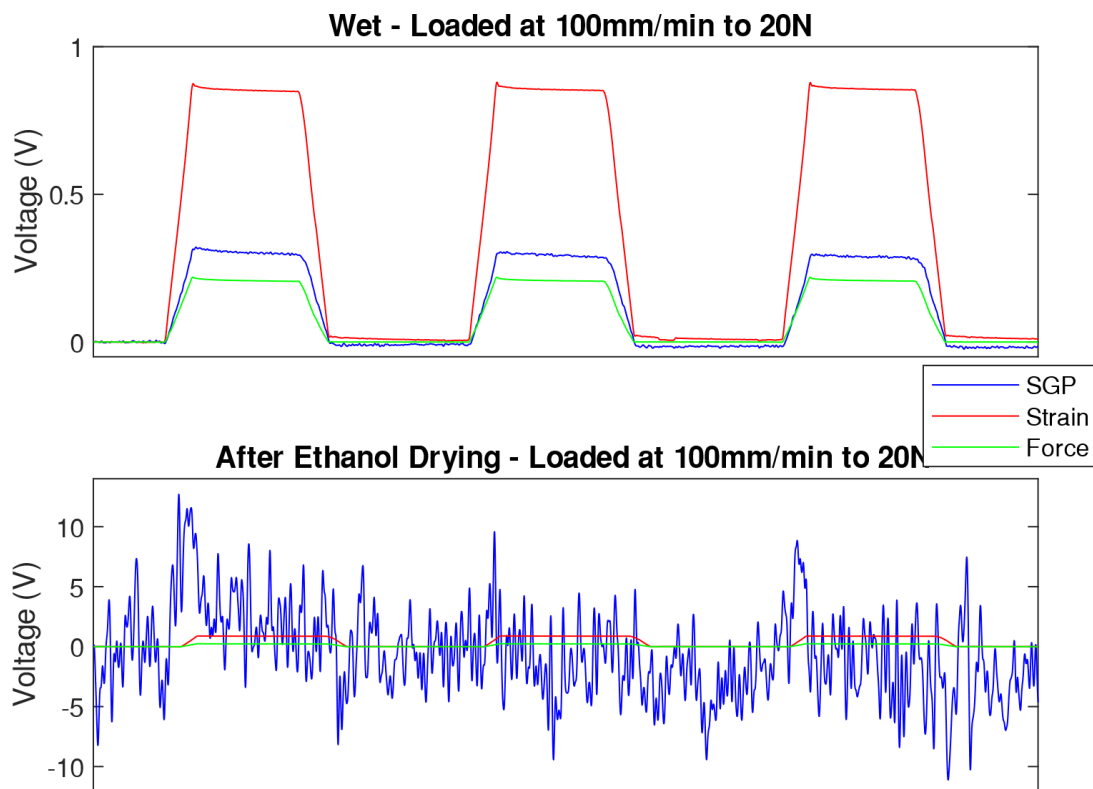


**Figure 4.3:** Amplified signal from figure 3.2. Still no piezoelectric charge collected by charge amplifier. Purely a noisy signal.

### **4.1.3 Evaporation Tests**

The results from this test were similar to those in the dry vs. wet experiment. The signal collected after drying was likely caused by the movement of the load cell and load cell wires, like the one in figure 2.6, except there was no held displacement in this experiment.

Overall, the evaporation tests demonstrate that once the unbound water is removed from the bone sample, there is virtually no SGP signal collected from the bone. Therefore, it is reasonable to assume that the signal being collected from the wet sample is primarily caused by the movement of ionic fluid within the bone sample.

### **4.1.4 Drying Experiments**

The results from these experiments demonstrated how the samples dry out over time and that taking various measures to prevent evaporation of fluid keeps the samples more hydrated during testing.

#### **Test One – 0 Minutes**

The first test, at time zero, was expected to produce similar results (i.e. not be significantly different) across all experiments. This was expected because, prior to testing, all samples were prepared the same way. All samples were stored in the fridge for at least 24 hours before testing, and once removed from the fridge testing began no longer than 30 minutes after removal. Any difference might be due to the additional time taken to apply plastic wrap to the samples during the wrapped tests.

Looking at figure 3.16a-c and table 3.4a-b for the mean max SGP value across the three different experiments, only the unwrapped long duration test one was significantly different ( $p < 0.001$ ). As

mentioned in the previous paragraph, this might be due to the time it took to wrap the samples in preparation for the wrapped experiments. Similar results were found for the C-coefficient ( $p < 0.001$ ).  $\tau_1$  and  $\tau_2$  produced opposite results, where the two long duration experiments produced tau values that were not significantly different ( $p = 0.42$  and  $p = 0.6$ ), whereas the tau values from the short duration experiments were significantly different ( $p < 0.001$  and  $p = 0.038$ ). This result may be due to the short duration tests producing tau values that are shorter than the long duration tests. The wrapped, short duration tests likely keep the sample more hydrated and thus better maintain the viscoelastic properties of bone causing the fluid to move around more efficiently.

If we now look at figure 3.11a-c and table 3.3a-b for the mean delta SGP value across the three different experiments, no significant differences were observed ( $p = 0.25$  and  $p = 0.91$ ). On the contrary, the A-coefficient was significantly different in test one across all three experiments ( $p < 0.001$ ).

### **Test Five – 60 Minutes**

The final test, at the end of the hour of testing, was expected to indicate whether the sample had dried significantly over the test period. It was expected that test five for the short duration experiments would likely not be significantly different from test one of the same experiment, but that test five would be significantly different across all three experiments as both the wrapping of the samples and the shortening of the testing period should counteract the effect of drying in the samples.

The wrapped and unwrapped long duration test five should have significantly different values if the wrapping aided in preventing evaporation of unbound water during testing. As expected, the

mean max SGP, delta SGP,  $\tau_2$ , A and C-coefficient for both long duration test fives were all significantly different ( $p < 0.001$ ). Only the  $\tau_1$  value was the same ( $p = 0.42$ ). The effect of a shorter testing period in addition to wrapping should certainly differ significantly from the long duration test five values. For the short duration wrapped tests, the delta SGP,  $\tau_1$ ,  $\tau_2$ , and A-coefficient were significantly different ( $p < 0.001$ ) but the mean max SGP and C-coefficient were not significantly different ( $p = 0.31$  and  $p = 0.88$ ). The effect of a shorter testing period in addition to wrapping did not affect the max SGP and C-coefficient which means that wrapping helped to maintain the magnitude of the SGP signal regardless of time.

### **Test One vs. Test Five**

Mean max SGP and the A-coefficient were both significantly different from test one to test five for both long duration experiments ( $p < 0.001$ ) but was not significantly different for the short duration experiment ( $p = 0.098$ ). This suggests that by shortening the testing period, regardless of whether the sample is wrapped or not, maintains the magnitude of the SGP peak value. In order to conclude that shorter duration testing is better for maintaining sample hydration during testing, the C-coefficient, which represents the magnitude of the steady-state part of the curve must respond in the same way as the max SGP. Looking at (Table 3.7a-b) we can see that there was a significant difference between the first and last test for all three experiments ( $p < 0.001$ ). The same result was seen for the  $\tau_2$  values. This suggests that the steady-state value decreases regardless of the amount of evaporation that may take place. The results from the mean delta SGP value from test one to test five supports this conclusion as it also was significantly different for all experiments ( $p < 0.001$ ).

Interestingly,  $\tau_1$  was not found to be significantly different from test one to five for all of the experiments ( $p = 0.1$  and  $p = 0.059$ ). This value may be independent of sample hydration and may depend on stress-relaxation. This hypothesis was explored further in the force and rate test results.

#### **4.1.6 Overall**

The main findings from these experiments are as follows:

- The short duration wrapped test maintained a max SGP that did not significantly differ with each test over the testing period, whereas both long duration tests produced SGPs which were significantly different. This suggests that shortening the testing period helps maintain hydration levels better than the longer duration tests, even if the sample is wrapped throughout the testing period. The significant decrease in the C-coefficient over time also supports this.
- Although there is a clear difference between, and seemingly a decrease in, delta SGP over the testing period regardless of experimental procedure, it seems as though there is less of a decrease if the sample is wrapped and tested for a shorter period of time. There may be an asymptotic delta SGP value reached but this can not be concluded without performing these tests for a longer time period.
  - The wrapped short duration test has a significantly larger ratio for both max SGP and delta SGP in comparison to the long duration tests. This suggests that there is a larger difference between the first and last mean max SGP and delta SGP values when the sample is more hydrated. This is the reason why I decided to wrap the

samples in the first place, because I noticed a more prominent decaying exponential. More hydrated samples produce more rapidly decaying exponentials.

- $\tau_1$  did not vary much in the long duration tests, but there was significantly more of a variation in comparison to the wrapped short duration.  $\tau_1$  hardly changed at all over the shorter testing period for the wrapped samples. This shows that wrapping the sample and shortening the testing period caused less of a change in  $\tau_1$  over time, but in the end, there was no significant difference in  $\tau_1$  from the start to the end of the testing period for all three experiments.
- $\tau_2$  clearly increases over time. It increased more when the sample was tested for a longer time period and even more when that sample was also unwrapped. Wrapping the sample had a clear effect on  $\tau_2$ , although it appeared to increase over time regardless.
  - An increase in  $\tau_2$  was also seen in the unified sample preparation tests (Fig 3.7b), but, in that case, an increase in  $\tau_2$  for SGP was associated with a larger  $\tau_2$  value for strain. Based off these results, the reason behind the increase in  $\tau_2$  is likely due to the rate at which fluid was able to return to a steady-state value during held displacement.
- According to the post-hoc repeated measures results, all samples from the wrapped short duration tests maintained more consistent values over the testing period. The exception was mean delta SGP, although it did seem to decrease less.

The results from the drying experiments clearly demonstrated how SGPs diminished as the unbound water within the sample evaporated and how wrapping the samples helped maintain hydration levels<sup>12</sup>.

There have been multiple papers that have studied the effect of hydration levels on SGPs as well as the effect of changing fluid conductivity, viscosity, etc. (Gross & Williams, 1982; Guzelsu & Walsh, 1990; Pienkowski & Pollack, 1983; Pollack, Salzstein, & Pienkowski, 1984). Although the effect of hydration levels on SGPs has been less explored, the papers that do observe its effects mostly noted the change in the dielectric constant (Marino et al., 1967) or d-coefficient (Anderson & Eriksson, 1970; Bur, 1976; E Fukada, Ueda, & Rinaldi, 1976; Eiichi Fukada & Yasuda, 1964; Marino & Becker, 1975; Netto & Zimmerman, 1975; Reinish & Nowick, 1975) in the bone sample. To my knowledge, there are no studies that have explored the effect of drying on the SGP magnitude with respect to time.

## **4.2 Effect of Sample Thickness**

Thicker samples experienced less strain than thinner samples when the same force was applied to both. Higher strains led to larger SGPs. Both tau values for SGP and strain increased with increasing strain.

### **4.2.1 Unified Sample Preparation Test**

By performing this test on all the samples, it was determined that there was no significant difference between the three groups (S16 wet, S16 dry and S17). This indicates that desiccating

---

<sup>12</sup> I would like to point out another method used to maintain hydration levels. Other papers report performing their tests within testing chambers of over 98% relative humidity (RH) (Cochran et al., 1968; Steinberg et al., 1973). Due to our lack of such a chamber in the lab we did not use this method.

the samples at 30°C did not affect their ability to be rehydrated with saline and that the fresher samples behaved similarly to the samples prepared a year prior.

Looking at figure 4.4, imagine we have two beams of difference thicknesses. If we apply the exact same amount of force to the end of both beams, in a cantilever bending set up, the thinner beam will bend much more than the thicker beam. Now, thinking in terms of strain, the thinner sample will undergo much more strain (bending) compared to the thicker sample. Based off the results in (Fig. 3.6b) it is clear that the strain gauges showed much greater strain in thinner samples compared to the thicker samples.

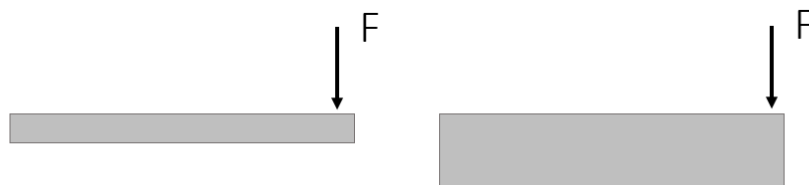


**Figure 4.4** Schematic to imagine how two equal forces applied to two beams of different thicknesses in cantilever bending formation would lead to the thinner sample bending more and thus producing more strain.

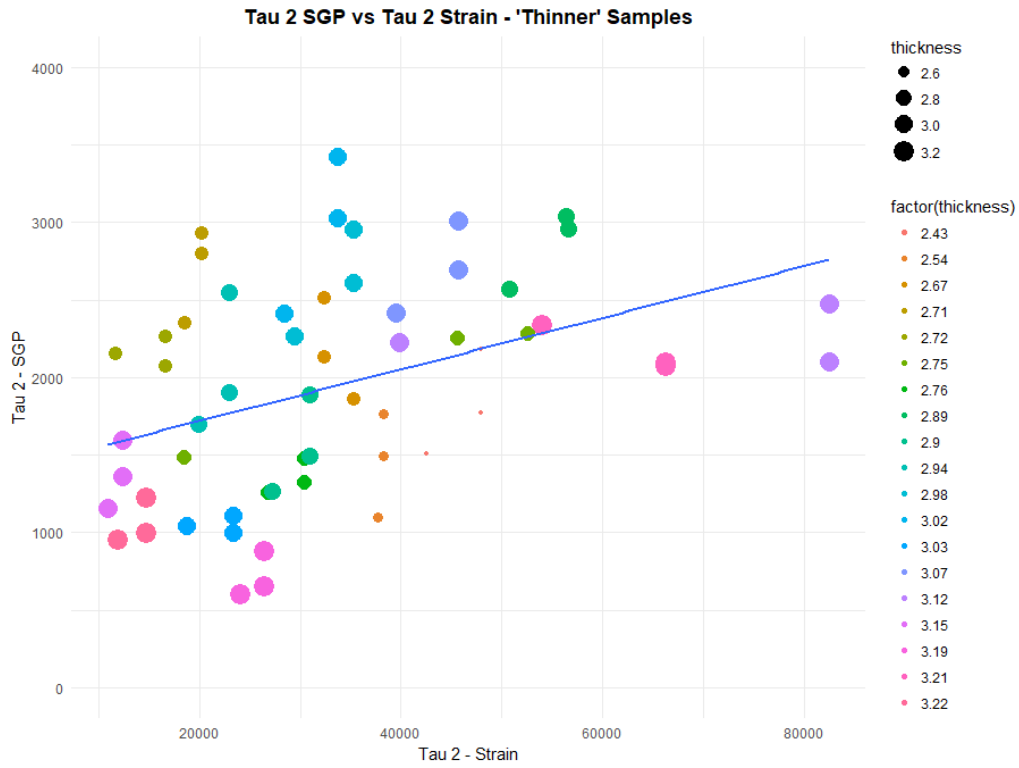
If we now look at figure 3.5b, we can see that the maximum SGP collected from the samples follows a trend similar to that found for strain. Thinner samples, which experienced more strain, produced larger SGPs. Since all the samples underwent the exact same test (Table 2.6), the only obvious factor that was different between the samples was thickness. To explore other factors that influence strain and SGP, the force and rate tests were performed (section 4.2.1).

These tests also gave valuable insight to how sample thickness affects the  $\tau_1$  and  $\tau_2$  values.  $\tau_1$  seemed to follow a trend where higher strain  $\tau_1$  values caused slightly smaller SGP  $\tau_1$  values. The opposite effect was seen in  $\tau_2$ . Higher  $\tau_2$  values for strain led to higher  $\tau_2$  values for SGP meaning



it took longer for the SGP to reach a steady-state value when the sample experienced more strain (or more displacement). This makes sense intuitively since the fluid within the sample would be more displaced under higher strains and thus take more time to settle back into place. The scatter plots in figure 4.5a-b do a better job at showing how the thicker samples have lower  $\tau_2$  values for both SGP and strain.

a)



B)

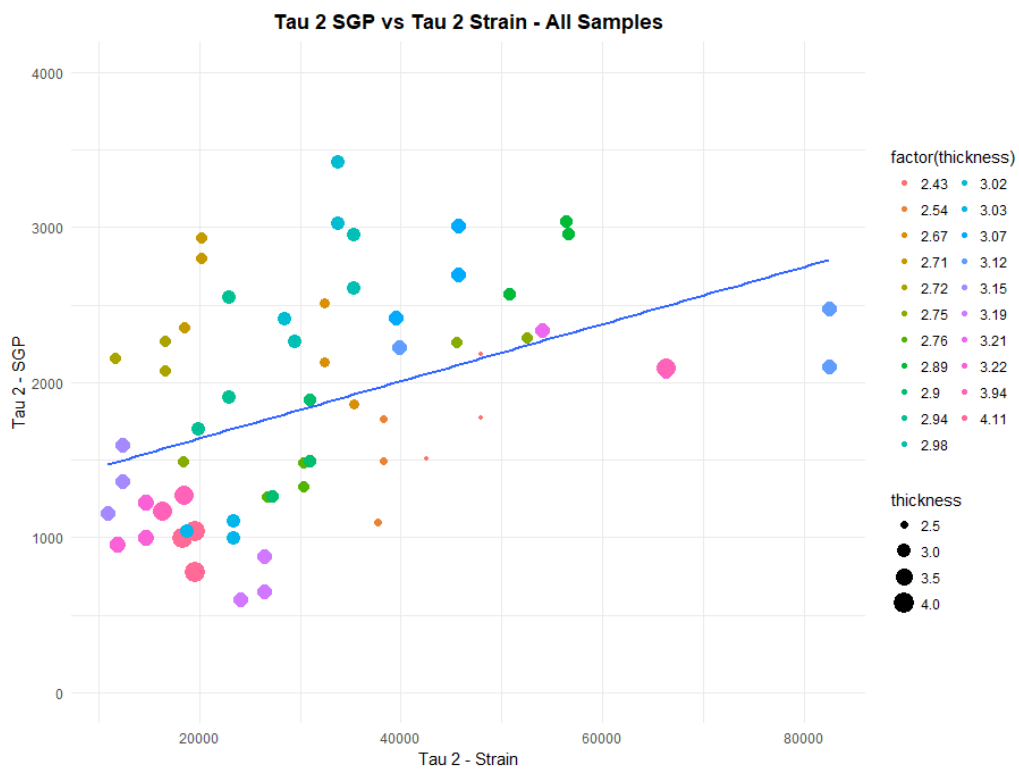


Figure 4.5a:  $\tau_2$  values for samples thinner than 3.15mm.

Figure 4.5b:  $\tau_2$  values for all samples.

## 4.2 Effect of Varying Load and Displacement Rate

### 4.2.1 Force and Rate Tests

Overall, mean max SGP and delta SGP both increased with increasing force and increasing deformation rate, similar to what Steinberg found (Steinberg et al., 1973). It is difficult to tell if increased deformation rate was the cause of the difference in max SGP in rate tests due to the possible effect of overshoot. Although this overshoot is not ideal, it is not so drastic that it prevented us from collecting the information we need. We were still able to see the effect of increasing displacement rates on the other variables even though the target load of 30N was slightly overshoot. The only two variables that were possibly affected were the max mean SGP and the delta SGP, but since the A and C-coefficients directly contribute to these values they provide supplementary insight on the effect.

Interestingly, there were opposite effects on the various SGP values for the force magnitude and rate tests. The mean max SGP increased more for the force magnitude tests (Fig. 4.6a) whereas the mean delta SGP increased more for the rate tests (Fig. 4.6d). It seems as though, for both rate tests, a possible asymptotic value was reached around  $150 \frac{mm}{min}$  and  $200 \frac{mm}{min}$ . Steinberg also found an asymptotic value at their 'higher' deformation rates, but their rates were much lower than the ones we used (Steinberg et al., 1973).

The results from curve fitting suggest that the A-coefficient increased significantly with increasing deformation rate and the C-coefficient increased significantly with increasing force. The A-coefficient remained relatively unchanged for increasing force and the C-coefficient for increasing deformation rate. In a similar fashion,  $\tau_1$  was dependent on deformation rate (significant decrease

with increasing deformation rate) whereas  $\tau_2$  was dependent on force (significant increase with larger forces).

Overall, there seemed to be a clear distinction as to what each value from curve fitting signifies (Table 4.1). The initial part of the curve, described by the A-coefficient and  $\tau_1$  (Fig. 4.7a-b), were dependent on strain/deformation rate, whereas the steady-state part of the curve, described by the C-coefficient and  $\tau_2$  (Fig. 4.7c-d), were dependent on force magnitude. Additionally, the mean max SGP value seemed to be related to the C-coefficient whereas the mean delta SGP value seemed to be related to the A-coefficient.

Steinberg also reported larger steady-state voltages for larger loads and higher deformation rates (Steinberg et al., 1973). Looking at the results from the C-coefficients for our curves it appears that the steady-state voltage clearly increased with larger loads but was less clear as to if the increasing loading rate affected the steady-state voltage. Note that Steinberg used much smaller loading rates ( $< 50 \frac{mm}{min}$ ) for their experiments (Steinberg et al., 1973) and this may be the reason for the discrepancy between our results.

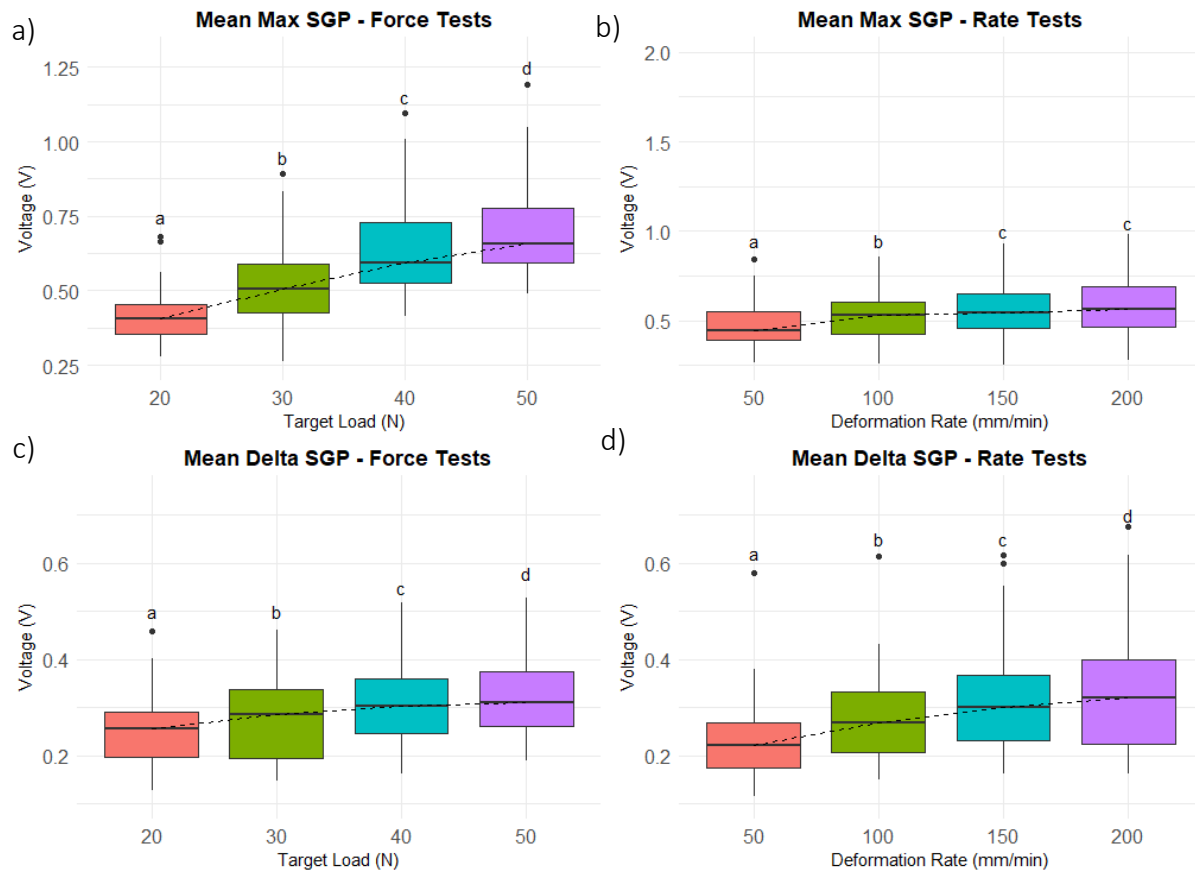
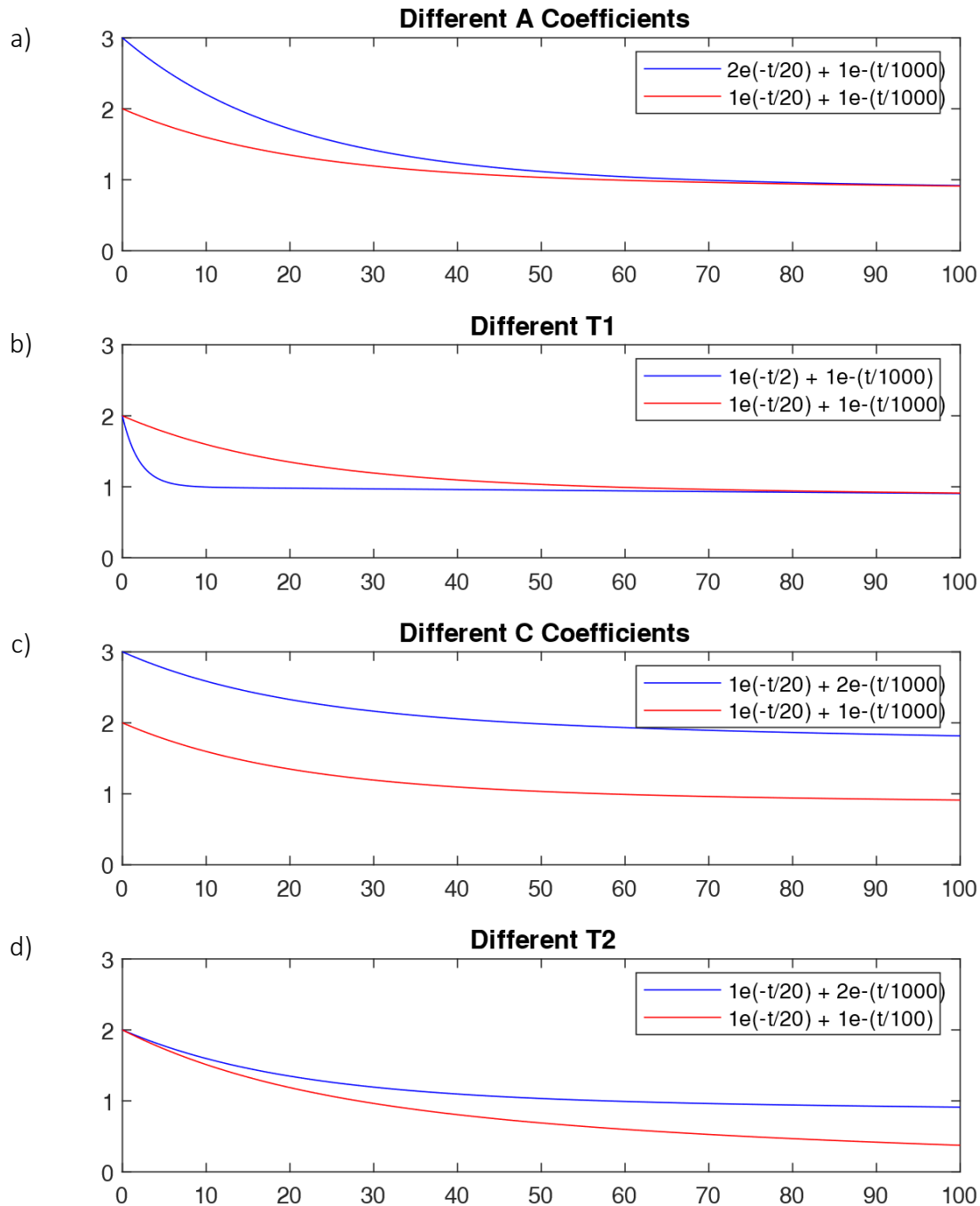


Figure 4.6a-d: Mean max SGP and max delta SGP values for the force and rate tests.

Table 4.1: Summary of Results of Curve Values from Force Magnitude and Rate Tests

|                      | <i>Increasing Force Magnitude</i> | <i>Increasing Deformation Rate</i> |
|----------------------|-----------------------------------|------------------------------------|
| <i>A-coefficient</i> | -                                 | ↑                                  |
| $\tau_1$             | -                                 | ↓                                  |
| <i>C-coefficient</i> | ↑                                 | -                                  |
| $\tau_2$             | ↑                                 | -                                  |



**Figure 4.7a:** The blue line has an A-coefficient that is twice the size of the A-coefficient of the red line. This simply causes the max value to increase.

**Figure 4.7b:** The blue line has a  $\tau_1$  value that is ten times larger than the  $\tau_1$  value of the red line. This causes a more rapid decrease from the A to the C-coefficient.

**Figure 4.7c:** The blue line has a C-coefficient that is twice the size of the C-coefficient of the red line. This just causes an offset.

**Figure 4.7d:** The blue line has a  $\tau_2$  value that is ten times larger than the  $\tau_2$  value of the red line. This causes the blue line to take less time to reach steady state.

#### 4.2.2 Related Work

In a similar set of tests, Cochran, Pawluk, and Bassett (Cochran et al., 1968) explored how SGPs changed with increasing load and deformation rates. Unlike Steinberg who used whole bones (Steinberg et al., 1973), Cochran used beams of cortical bone of various thicknesses (0.6, 1.2 and 2.4 mm). Their loading rates were much higher ( $20-40 \frac{cm}{sec}$  or  $> 12,000 \frac{mm}{min}$ ) and they loaded the beams until fracture occurred.

What was interesting in the results of the tests by Cochran et al. was that, granted a high enough deformation rate<sup>13</sup>, a linear relationship was found between load<sup>14</sup> and SGP until fracture (Fig. 4.8a). All sample thicknesses followed this relationship and were not significantly different from each other. They also found that the thickest samples (at 2.4 mm thickness) produced larger loads and larger SGPs than the thinner samples. Since they were deforming until a target displacement was reached, rather than a target load like we did, this makes sense since it would require significantly more force to deform a 2.4 mm sample by 4 mm than it would a 0.6 mm sample.

For increasing deformation<sup>15</sup>, Cochran et al. found a linear relationship between SGPs and rate within the elastic region (no significant difference for  $< 0.5$  mm of deformation) and a non-linear relationship in the plastic region (significant difference for  $> 3$ mm of deformation) (Fig. 4.8b). They also reported that past a certain rate the SGP appeared to be independent of rate (no data shown) and at slow enough rates there was no SGP collected at all (Fig. 4.9).

---

<sup>13</sup> They did not state what constitutes a 'high enough' deformation rate but did show an example of a deformation rate that was too slow in (Fig. 4.8).

<sup>14</sup> They did not explicitly report the loads used in this paper as they based their loads from the amount of deformation. They reported their loads as a percent increase in SGP past their 'baseline' deformation of 1 mm.

<sup>15</sup> Although they varied deformation rates, they did not plot SGP vs. deformation rate. They plotted SGP vs. deformation and it is not clear what deformation rate was used for this collected data.

Another paper reported similar results for variations in load and deformation rate. Gross and Williams (Gross & Williams, 1982) examined the effect of load and deformation in two beams of wet bovine bones with thicknesses of  $\sim 2$  and 6.6 mm. For their load variations they deformed the samples at a constant deformation rate of  $100 \frac{cm}{min}$  ( $1000 \frac{mm}{min}$ ) and increased the load from 0.1 to 1 N. Like the others, they also found a linear relationship between load and voltage at this deformation rate (Fig. 4.10a). They also found a non-linear relationship between deformation rate and SGP, although they reported using a strain rate from 0-10  $S/S_0$  but do not state any explicit rate (Fig. 4.10b).

Based off our results and the results from Steinberg (1973), Cochran (1968) and Gross (1982) it appears that there is a linear relationship between SGP and load magnitude at sufficiently large deformation rates ( $> 10 \frac{mm}{min}$ ) and a nonlinear relationship between SGP and deformation rate.



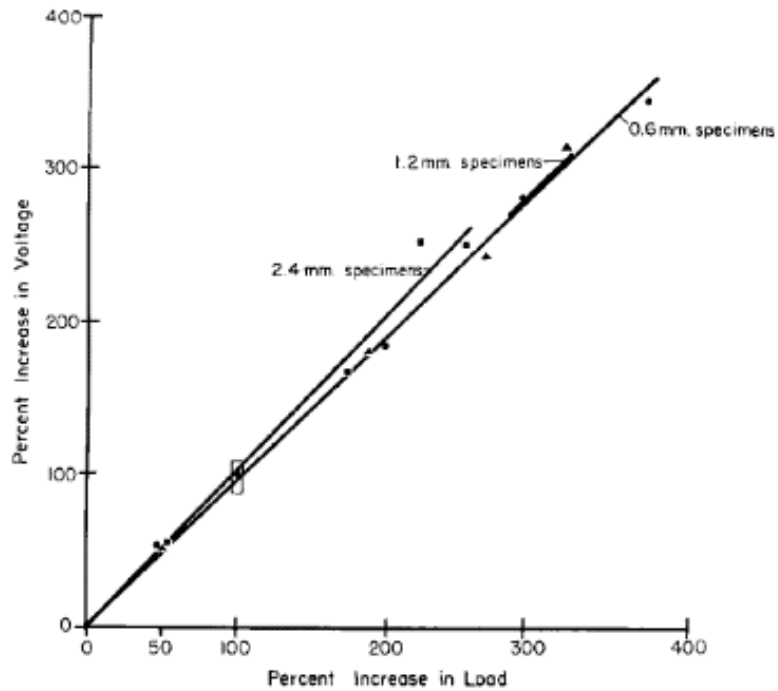


**Figure 4.8a:** Plot of SGP magnitude vs. 'load' for varying sample thicknesses. The percent change in voltage is in reference to the baseline deformation of 1 mm (the vertical rectangle) (Cochran et al., 1968).

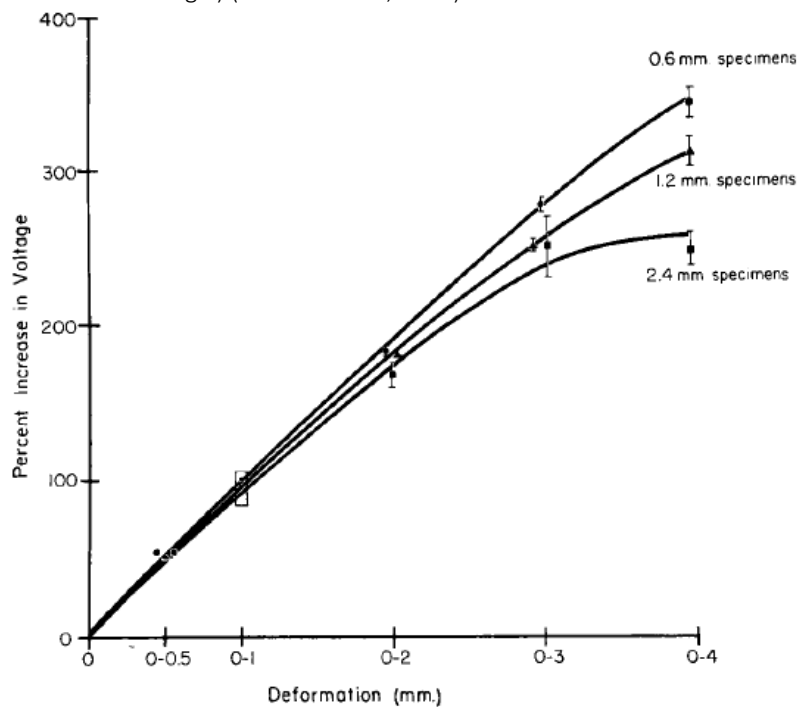


**Figure 4.8b:** Plot of SGP vs deformation for varying sample thicknesses (Cochran et al., 1968).

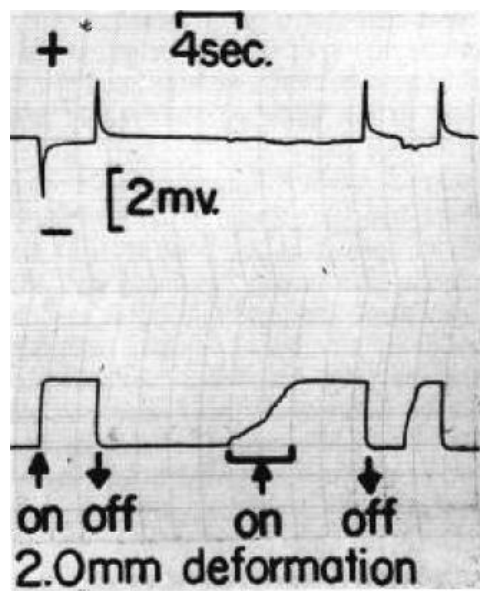


**Figure 4.9:** Result from Cochran's tests showing how lower deformation rates resulted in no measured SGPs (Cochran et al., 1968).

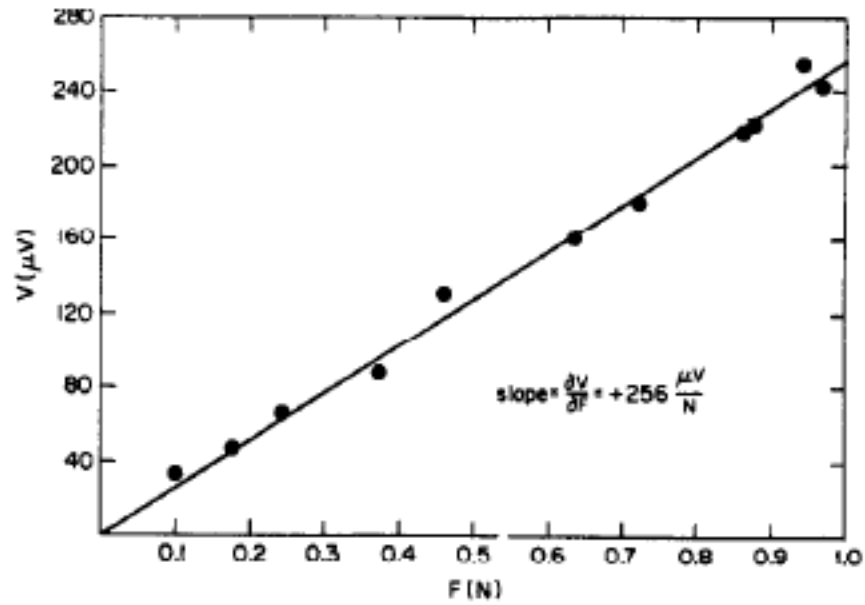


Figure 4.10a: Plot of load vs. SGP for an increasing load from 0.1 to 1 N at a constant deformation rate of  $100 \frac{cm}{min}$  (Gross & Williams, 1982).

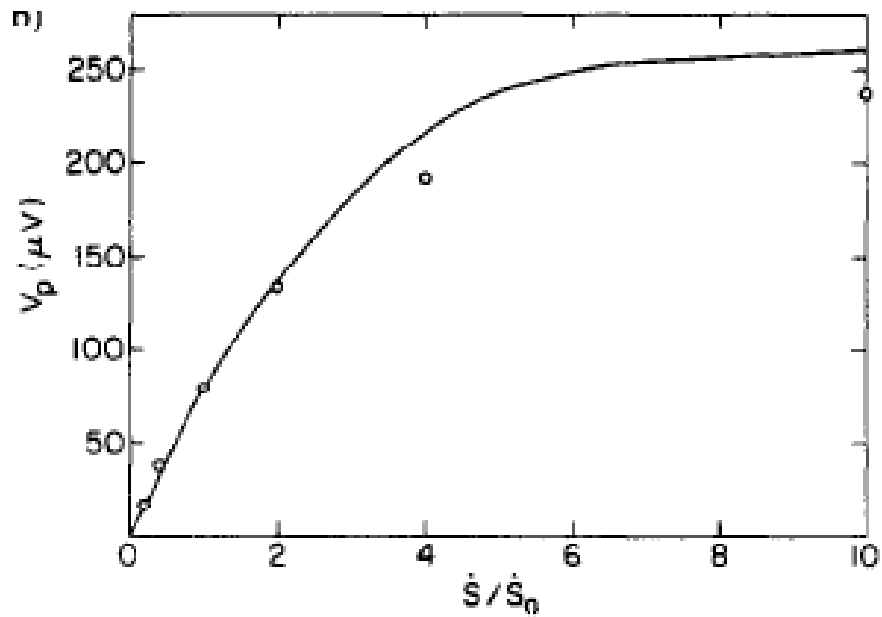


Figure 4.10b: Plot of strain rate vs. SGP (Gross & Williams, 1982).

In conclusion, the results from these tests give us more insight as to what the two-term exponential equation is modeling and how the terms in the equation relate to the viscoelastic properties of bone and the properties of streaming potentials.

If we consider the streaming potential equation (Equation 1.3), note that there is proportionality between the electrical potential and pressure gradient. This is the only variable in the equation that we modified through testing. By dehydrating the samples, and thus decreasing the amount of fluid within them, we decreased the amount of pressure the fluid produced within the sample. By deforming the samples to larger loads and at different rates, we changed the amount of pressure associated with the speed at which the sample must relax in response to an applied load or deformation rate.

Eriksson (Eriksson, 1974) and Walsh (Walsh & Guzelsu, 1993) proved, through experimentation, that higher pressure caused larger streaming potentials and SGPs by forcing fluid through bone samples at different rates.

Although the effects of strain on the bone remodeling were not explored in this study, there has been other work suggesting that the adaptive response of bone is directly proportional to the strain rate *in vivo* (Duncan & Turner, 1995). Since larger strain rate leads to larger SGPs in bone (within reason), it is likely that the combination of mechanical (Currey, 1968; Frost, 1992) and electrical effects (Isaacson & Bloebaum, 2010; Noris-Suárez et al., 2007) lead to higher bone densities and deposition of new bone.

## 5 Conclusion

There are clear effects of drying, increasing load, and increasing deformation rate on the SGPs produced by the displacement of fluid in beams of wet cortical bone.

There was a clear difference between wet and dry samples. The wet bones produced signals that decayed over time whereas the signals from the dry bone samples were consistently noisy (consisting of both ambient noise and motion artifact) and did not contain any signal worth analyzing.

- SGP signal quality diminished as the unbound water within the samples evaporated. This was shown through both the evaporation tests and the drying experiments.
  - While the evaporation tests showed a clear loss of SGP signal post-dehydration, the drying tests displayed a gradual loss of signal over time (approximately 1 hour of testing) associated with evaporation of unbound water within the sample.
  - We were able to mitigate some of the signal deterioration due to evaporation by wrapping the samples in plastic wrap.

By fitting two-term exponential equations to the SGPs we were able to determine how the time constants and the magnitude of maximum and steady-state voltages were affected by hydration levels, strain, and pressure gradients associated with changing load and deformation rate.

- The first term of the exponential equation, which is made up of the A-coefficient and  $\tau_1$ , describes the initial rapid decay after a step load and is dependent on deformation rate
- The second term of the exponential equation, which contains the C-coefficient and  $\tau_2$ , describes the steady-state portion of the SGP and is dependent on load.

- The A and C-coefficient together determine the maximum voltage the SGP can reach.
- The first time constant ( $\tau_1$ ) decreases with increasing deformation rate resulting in a more rapidly decaying maximum SGP and is relatively unchanged by dehydration over a reasonable time period (i.e. within 10-20 minutes after removal from wrapping).
- $\tau_2$  decreases with increasing strain as well as with decreasing hydration levels.

## **5.1 Future Work**

It would be interesting to explore how SGPs would be affected by a various deformation rates over a longer testing period to allow for some dehydration to occur. Since all the tests performed in this research explored the SGP response associated with stress-relaxation of bone, it would be of interest to see how the SGP signal changed for creep and if a two-term exponential would also be the optimal fit for such a curve.

## References

- Ahn, A. C., & Grodzinsky, A. J. (2009). Relevance of collagen piezoelectricity to “Wolff’s Law”: A critical review. *Medical Engineering and Physics*, 31(7), 733–741. <https://doi.org/10.1016/j.medengphy.2009.02.006>
- Anderson, J. C., & Eriksson, C. (1968). Electrical properties of wet collagen. *Nature*, 218(5137), 166–168. <https://doi.org/10.1038/218166a0>
- Anderson, J. C., & Eriksson, C. (1970). Piezoelectric properties of dry and wet bone. *Nature*, 227, 491–492. <https://doi.org/10.1038/227491a0>
- Bassett, C. A., & Becker, R. O. (1962). Generation of electric potentials by bone in response to mechanical stress. *Science (New York, N.Y.)*, 137(3535), 1063–1064. <https://doi.org/10.1126/science.137.3535.1063>
- Bassett, C. A., Pawluk, R. J., & Pilla, A. A. (1974). Augmentation of Bone Repair by Inductively Coupled Electromagnetic Fields. *Science (New York, N.Y.)*, 184(4136), 575–577.
- Buckwalter, J. A., Glimcher, M. J., Cooper, R. R., & Recker, R. (1995). Bone Biology. *Journal of Bone and Joint Surgery*, 77, 1256–1275. Retrieved from [www.jbjs.org](http://www.jbjs.org)
- Bur, A. J. (1976). Measurements of dynamic piezoelectric properties of bone as a function of temperature and humidity. *Journal of Biomechanics*, 9, 495–507.
- Burger, E. H., & Klein-Nulend, J. (1999). Mechanotransduction in bone - role of the lacuno-canalicular network. *The FASEB Journal*, 13(9001), S101–S112.
- Chen, J. H., Liu, C., You, L., & Simmons, C. A. (2010). Boning up on Wolff’s Law: Mechanical regulation of the cells that make and maintain bone. *Journal of Biomechanics*, 43(1), 108–118. <https://doi.org/10.1016/j.jbiomech.2009.09.016>
- Cochran, G. V. B., Pawluk, R. J., & Bassett, C. A. L. (1967). Stress Generated Electric Potentials in the Mandible and Teeth. *Archives of Oral Biology*, 12, 917–920. [https://doi.org/10.1016/0003-9969\(67\)90117-3](https://doi.org/10.1016/0003-9969(67)90117-3)
- Cochran, G. V. B., Pawluk, R. J., & Bassett, C. A. L. (1968). Electromechanical Characteristics of Bone Under Physiologic Moisture Conditions. *Clinical Orthopaedics and Related Research*, 58, 249–270.
- Cowin, S. C., & Hegedus, D. H. (1976). Bone remodeling I: theory of adaptive elasticity. *Journal of Elasticity*, 6(3), 313–326. <https://doi.org/10.1007/BF00041724>
- Currey, J. D. (1968). The adaptation of bones to stress. *Journal of Theoretical Biology*, 20, 91–106.
- Duncan, R. L., & Turner, C. H. (1995). Mechanotransduction and the functional response of bone to mechanical strain. *Calcified Tissue International*, 57(5), 344–358. <https://doi.org/10.1007/BF00302070>

- Ehrlich, P. J., & Lanyon, L. E. (2002). Mechanical strain and bone cell function: A review. *Osteoporosis International*, 13(9), 688–700. <https://doi.org/10.1007/s001980200095>
- Eriksson, C. (1974). Streaming potentials and other water- dependent effects in mineralized tissue. *New York Academy of Sciences*, 238, 321–333.
- Fernández, J. R., García-Aznar, J. M., & Martínez, R. (2012). Piezoelectricity could predict sites of formation/resorption in bone remodelling and modelling. *Journal of Theoretical Biology*, 292, 86–92. <https://doi.org/10.1016/j.jtbi.2011.09.032>
- Ferrier, J., Ross, S. M., Kanehisa, J., & Aubin, J. E. (1986). Osteoclasts and Osteoblasts Migrate in Opposite Directions in Response to a Constant Electrical Field. *Journal of Cellular Physiology*, 288, 283–288.
- Frost, H. M. (1992). Perspectives: bone's mechanical usage windows. *Bone and Mineral*, 19(3), 257–271. [https://doi.org/10.1016/0169-6009\(92\)90875-E](https://doi.org/10.1016/0169-6009(92)90875-E)
- Fukada, E. (1968). Piezoelectricity in polymers and biological materials. *Ultrasonics*, 6(4), 229–234. [https://doi.org/10.1016/0041-624X\(68\)90132-7](https://doi.org/10.1016/0041-624X(68)90132-7)
- Fukada, E., Ueda, H., & Rinaldi, R. (1976). Piezoelectric and related properties of hydrated collagen. *Biophysical Journal*, 16(8), 911–918. [https://doi.org/10.1016/S0006-3495\(76\)85741-4](https://doi.org/10.1016/S0006-3495(76)85741-4)
- Fukada, E., & Yasuda, I. (1957). On the Piezoelectric Effect of Bone. *Journal of the Physical Society of Japan*, 12, 1158–1162. <https://doi.org/10.1143/JPSJ.12.1158>
- Fukada, E., & Yasuda, I. (1964). Piezoelectric Effects in Collagen. *Japanese Journal of Applied Physics*, 3(8), 502B–502B. <https://doi.org/10.1143/JJAP.3.502B>
- Gjelsvik, A. (1973). Bone remodeling and piezoelectricity. *Journal of Biomechanics*, 6(February 1972), 69–77. Retrieved from <http://www.sciencedirect.com/science/article/pii/0021929073900390>
- Gross, D., & Williams, W. S. (1982). Streaming potential and the electromechanical response of physiologically-moist bone. *Journal of Biomechanics*, 15(4), 277–295. [https://doi.org/10.1016/0021-9290\(82\)90174-9](https://doi.org/10.1016/0021-9290(82)90174-9)
- Guzelsu, N., & Walsh, W. R. (1990). Streaming potential of intact wet bone. *Journal of Biomechanics*, 23(7), 673–685.
- Hiratai, R., Nakamura, M., & Yamashita, K. (2014). Role of collagen and inorganic components in electrical polarizability of bone. *The Journal of Veterinary Medical Science / the Japanese Society of Veterinary Science*, 76(2), 205–210. <https://doi.org/10.1292/jvms.13-0229>
- Hou, Z., Fu, D., & Qin, Q. H. (2011). An exponential law for stretching-relaxation properties of bone piezovoltages. *International Journal of Solids and Structures*, 48(3–4), 603–610. <https://doi.org/10.1016/j.ijsolstr.2010.10.024>
- Iller, P. D., & Papapoulos, S. E. (2013). Osteoporosis. In *Primer on the Metabolic Bone Diseases and Disorders of Mineral Metabolism* (8th ed., pp. 343–533). John Wiley & Sons, Inc.



- Isaacson, B. M., & Bloebaum, R. D. (2010). Bone bioelectricity: What have we learned in the past 160 years? *Journal of Biomedical Materials Research - Part A*, *95*(4), 1270–1279. <https://doi.org/10.1002/jbm.a.32905>
- Jacob, J., More, N., Kalia, K., & Kapusetti, G. (2018). Piezoelectric smart biomaterials for bone and cartilage tissue engineering. *Inflammation and Regeneration*, *38*(1), 2. <https://doi.org/10.1186/s41232-018-0059-8>
- Johnson, M. W., Chakkalakal, D. A., Harper, R. A., & Katz, J. L. (1980). Comparison of the Electromechanical Effects in Wet and Dry Bone. *Journal of Biomechanics*, *13*(1976), 437–442.
- Jones, H. H., Preist, J. D., Hayes, W. C., Tichenor, C. C., & Nagel, D. A. (1977). Humeral hypertrophy in response to exercise. *Journal of Bone and Joint Surgery*, *59*(2), 204–208.
- Karki, J. (2000). *Application Report Signal Conditioning Piezoelectric Sensors*. Retrieved from <http://www.ti.com/lit/an/sloa033a/sloa033a.pdf>
- Marino, A. A., & Becker, R. O. (1974). Piezoelectricity in Bone as a Function of Age. *Calcified Tissue Research*, *331*, 327–331.
- Marino, A. A., & Becker, R. O. (1975). Piezoelectricity in hydrated frozen bone and tendon. *Nature*, *253*(5493), 627–628. <https://doi.org/10.1038/253627a0>
- Marino, A. A., Becker, R. O., & Bachman, C. H. (1967). Dielectric determination of bound water of bone. *Physics in Medicine and Biology*, *12*(3), 367–378. <https://doi.org/10.1088/0031-9155/12/3/309>
- Marino, A. A., Becker, R. O., & Soderholm, S. C. (1971). Origin of the piezoelectric effect in bone. *Calcified Tissue Research*, *180*, 177–180. <https://doi.org/10.1007/BF02010135>
- Marks Jr, S. C., & Popoff, S. N. (1988). Bone cell biology: the regulation of development, structure and function in the skeleton. *American Journal of Anatomy*, *183*(1), 1–44.
- Marzec, E., Kubisz, L., & Jaroszyk, F. (1996). Dielectric studies of proton transport in air-dried fully calcified and decalcified bone. *International Journal of Biological Macromolecules*, *18*, 27–31.
- McElhaney, J. H. (1967). The Charge Distribution on the Human Femur Due to Load. *The Journal of Bone & Joint Surgery*, *49*(8), 1561–1571.
- Mcleod, K. J., & Clinton, T. R. (1992). The Effect of Low-Frequency Electrical Fields on Osteogenesis. *Journal of Bone and Joint Surgery*, *74*–A(6), 920–929.
- Nakamura, M., Hiratai, R., & Yamashita, K. (2012). Bone mineral as an electrical energy reservoir. *Journal of Biomedical Materials Research - Part A*, *100* A(5), 1368–1374. <https://doi.org/10.1002/jbm.a.34076>
- Netto, T. G., & Zimmerman, R. L. (1975). Effect of water on piezoelectricity in bone and collagen. *Biophysical Journal*, *15*(6), 573–576. [https://doi.org/10.1016/S0006-3495\(75\)85839-5](https://doi.org/10.1016/S0006-3495(75)85839-5)
- Noris-Suárez, K., Lira-Olivares, J., Ferreira, A. M., Feijoo, J. L., Suárez, N., Hernández, M. C., & Barrios, E. (2007). In vitro deposition of hydroxyapatite on cortical bone collagen stimulated

- by deformation-induced piezoelectricity. *Biomacromolecules*, 8(3), 941–948. <https://doi.org/10.1021/bm060828z>
- Otter, M., Goheen, S., & Williams, W. S. (1988). Streaming potentials in chemically modified bone. *Journal of Orthopaedic Research*, 6(3), 346–359. <https://doi.org/10.1002/jor.1100060306>
- Pienkowski, D., & Pollack, S. R. (1983). The Origin of Stress-Generated Potentials in Fluid-Saturated Bone. *Journal of Orthopaedic Research*, 30–41. <https://doi.org/10.1002/jor.1100010105>
- Pollack, S. R., Salzstein, R., & Pienkowski, D. (1984). The Electric Double Layer in Bone and its Influence on Stress-Generated Potentials. *Calcified Tissue International*, 36(1 Supplement). <https://doi.org/10.1007/BF02406138>
- Reinish, G. B., & Nowick, A. S. (1975). Piezoelectric properties of bone as functions of moisture content. *Nature*, 253, 626.
- Robling, A. G., Castillo, A. B., & Turner, C. H. (2006). Biomechanical and Molecular Regulation of Bone Remodeling. *Annual Review of Biomedical Engineering*, 8(1), 455–498. <https://doi.org/10.1146/annurev.bioeng.8.061505.095721>
- Saha, S., & Williams, P. A. (1992). Electric and Dielectric Properties of Wet Human Cortical Bone as a Function of Frequency. *IEEE Transactions on Biomedical Engineering*, 39(12), 1298–1304. <https://doi.org/10.1109/10.184706>
- Shamos, M. H., & Lavine, L. S. (1964). Physical bases for bioelectric effects in mineralized tissues. *Clinical Orthopaedics and Related Research*, 35, 177–188.
- Steinberg, M. E., Wert, R. E., Korostoff, E., & Black, J. (1973). Deformation Potentials in Whole Bone. *Journal of Surgical Research*, 259, 254–259.
- Walsh, W. R., & Guzelsu, N. (1993). Ion concentration effects on bone streaming potentials and zeta potentials. *Biomaterials*, 14(5), 331–336. <https://doi.org/10.1002/jor.1100040310>
- Whitney, S. (1999). Vibrations of Cantilever Beams: Deflection, Frequency, and Research Uses. Retrieved August 5, 2018, from <http://emweb.unl.edu/Mechanics-Pages/Scott-Whitney/325hweb/Beams.htm>
- Williams, W. S., & Breger, L. (1975). Piezoelectricity in tendon and bone. *Journal of Biomechanics*, 8, 407–413.

## APPENDICES

### Appendix 1

#### 1.1 Sample Info

| Sample #                 | Length (mm)  | Width (mm)   | Thickness (mm) |        |        |             | History           |
|--------------------------|--------------|--------------|----------------|--------|--------|-------------|-------------------|
|                          |              |              | Top            | Middle | Bottom | Average     |                   |
| 1                        | 51.91        | 18.77        | 2.87           | 3.21   | 3.37   | 3.15        | wet (S16)         |
| 3                        | 54.33        | 19.28        | 3.2            | 3.27   | 3.18   | 3.22        | wet (S16)         |
| 4                        | 53.12        | 18.48        | 2.51           | 3.04   | 3.52   | 3.02        | wet (S16)         |
| 6                        | 53.09        | 20.93        | 2.96           | 2.96   | 3.02   | 2.98        | wet (S16)         |
| 7                        | 52.99        | 19.44        | 3.95           | 4.08   | 4.31   | 4.11        | wet (S16)         |
| 8                        | 53.53        | 20.41        | 2.79           | 2.9    | 2.97   | 2.89        | dry (S16)         |
| 9                        | 52.82        | 18.79        | 2.57           | 2.83   | 2.89   | 2.76        | wet (S16)         |
| 10                       | 54.1         | 19.34        | 3.24           | 3.07   | 3.32   | 3.21        | dry (S16)         |
| 11                       | 53.22        | 20.93        | 3.81           | 4      | 4      | 3.94        | dry (S16)         |
| 12                       | 54           | 18           | 1.66           | 2.16   | 2.46   | 2.09        | test (charge amp) |
| 15                       | 52.93        | 19.94        | 2.69           | 2.7    | 2.85   | 2.75        | wet (S16)         |
| 16                       | 53.03        | 19.67        | 2.62           | 2.7    | 2.82   | 2.71        | dry (S16)         |
| 17                       | 52.94        | 19.88        | 2.86           | 2.95   | 3.01   | 2.94        | dry (S16)         |
| 18                       | 49.6         | 17.79        | 3.03           | 3.04   | 3.03   | 3.03        | wet (S17)         |
| 19                       | 50.17        | 20.41        | 2.48           | 2.36   | 2.45   | 2.43        | wet (S17)         |
| 20                       | 50.21        | 20.06        | 2.8            | 2.7    | 2.65   | 2.72        | wet (S17)         |
| 21                       | 51.73        | 20.84        | 2.71           | 2.89   | 3.1    | 2.90        | wet (S17)         |
| 22                       | 51.67        | 20.97        | 2.94           | 3.09   | 3.17   | 3.07        | wet (S17)         |
| 23                       | 51.67        | 20.01        | 2.55           | 2.54   | 2.52   | 2.54        | wet (S17)         |
| 24                       | 51.58        | 21.51        | 2.63           | 2.76   | 2.62   | 2.67        | wet (S17)         |
| 25                       | 51.55        | 21.46        | 2.93           | 3.11   | 3.32   | 3.12        | wet (S17)         |
| 26                       | 50.94        | 20.17        | 2.89           | 3.15   | 3.54   | 3.19        | wet (S17)         |
| <b>Average<br/>± StD</b> | 52.32 ± 0.64 | 19.87 ± 0.90 |                |        |        | 2.97 ± 0.52 |                   |

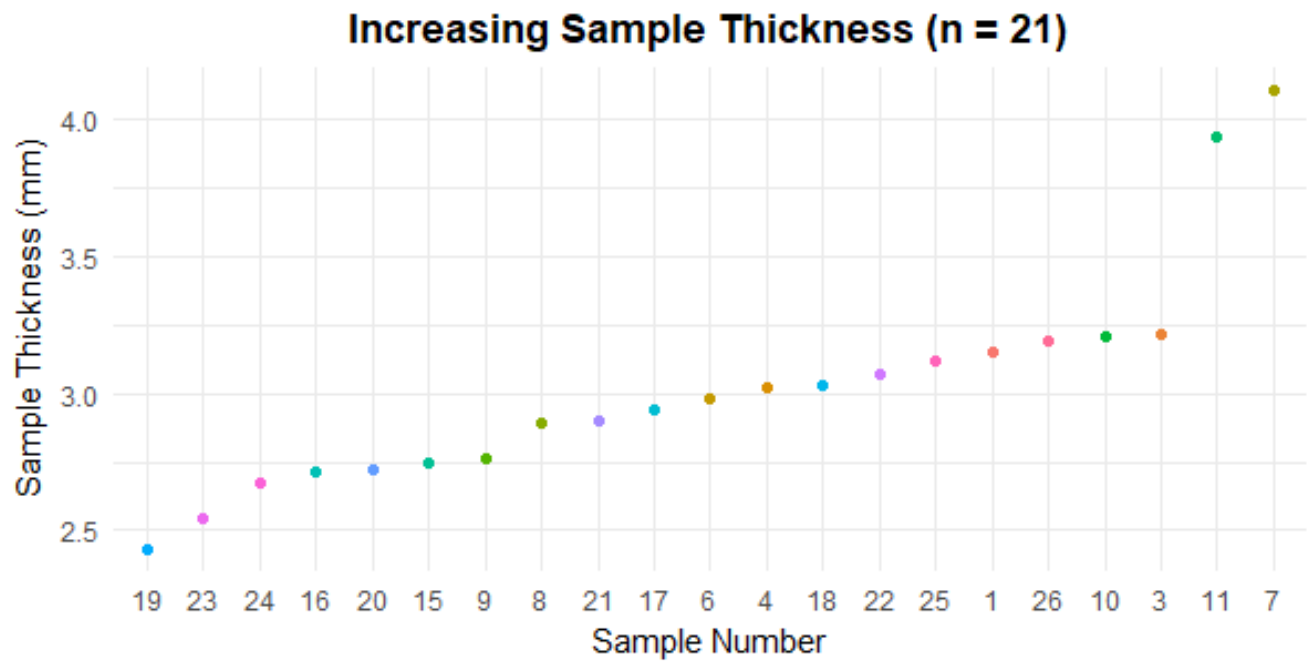
| Group S16 - d (n = 5) |              |              |                     |
|-----------------------|--------------|--------------|---------------------|
| Sample #              | Length (mm)  | Width (mm)   | Avg. Thickness (mm) |
| 16                    | 53.03        | 19.67        | 2.71                |
| 8                     | 53.53        | 20.41        | 2.89                |
| 17                    | 52.94        | 19.88        | 2.94                |
| 10                    | 54.1         | 19.34        | 3.21                |
| 11                    | 53.22        | 20.93        | 3.94                |
| <b>Avg ± StD</b>      | 53.36 ± 0.47 | 20.05 ± 0.63 | 3.14 ± 0.48         |

| <b>Group S16 - w (n = 7)</b> |                     |                     |                            |
|------------------------------|---------------------|---------------------|----------------------------|
| <i>Sample #</i>              | <i>Length (mm)</i>  | <i>Width (mm)</i>   | <i>Avg. Thickness (mm)</i> |
| 15                           | 52.93               | 19.94               | 2.75                       |
| 9                            | 52.82               | 18.79               | 2.76                       |
| 6                            | 53.09               | 20.93               | 2.98                       |
| 4                            | 53.12               | 18.48               | 3.02                       |
| 1                            | 51.91               | 18.77               | 3.15                       |
| 3                            | 54.33               | 19.28               | 3.22                       |
| 7                            | 52.99               | 19.44               | 4.11                       |
| <b>Avg ± StD</b>             | <b>53.03 ± 0.71</b> | <b>19.38 ± 0.84</b> | <b>3.14 ± 0.46</b>         |

| <b>Group S17 (n = 9)</b> |                     |                     |                            |
|--------------------------|---------------------|---------------------|----------------------------|
| <i>Sample #</i>          | <i>Length (mm)</i>  | <i>Width (mm)</i>   | <i>Avg. Thickness (mm)</i> |
| 19                       | 50.17               | 20.41               | 2.43                       |
| 23                       | 51.67               | 20.01               | 2.54                       |
| 24                       | 51.58               | 21.51               | 2.67                       |
| 20                       | 50.21               | 20.06               | 2.72                       |
| 21                       | 51.73               | 20.84               | 2.90                       |
| 18                       | 49.6                | 17.79               | 3.03                       |
| 22                       | 51.67               | 20.97               | 3.07                       |
| 25                       | 51.55               | 21.46               | 3.12                       |
| 26                       | 50.94               | 20.17               | 3.19                       |
| <b>Avg ± StD</b>         | <b>51.01 ± 0.82</b> | <b>20.36 ± 1.12</b> | <b>2.85 ± 0.27</b>         |

| <b>Total (n = 21)</b> |                     |                     |                       |
|-----------------------|---------------------|---------------------|-----------------------|
|                       | <i>Length (mm)</i>  | <i>Width (mm)</i>   | <i>Thickness (mm)</i> |
| <b>Average ± StD</b>  | <b>52.47 ± 0.67</b> | <b>19.93 ± 0.86</b> | <b>3.04 ± 0.41</b>    |

This is a plot of the thicknesses of all samples used in the unified sample preparation tests.



## Appendix 2

### 2.1 SGP Circuit Info

#### 2.1.1 Calculations

Stage 1: Instrumentation Amplifier (LT1920):

$$G = 100$$

$$G = \frac{49.4 \text{ k}\Omega}{R_G} + 1$$

$$R_G = 500 \Omega$$

Stage 2: Non-Inverting Gain (TLC2274):

$$G = 2$$

$$G = \frac{R_2}{R_1} + 1$$

$$R_1 = 1 \text{ k}\Omega$$

$$R_2 = 1 \text{ k}\Omega$$

Stage 3: Sallen-Key Fourth Order Chebyshev LPF + Unity Gain (TLC2274):

$$f_c = 6 \text{ Hz}$$

$$R_{3,4}, R_{5,6} = \frac{a_{1,2} C_{2,4} \pm \sqrt{(a_{1,2} C_{2,4})^2 - 4b_{1,2} C_{1,3} C_{2,4}}}{4\pi f_c C_{1,3} C_{2,4}}$$

$$a_1 = 2.5904$$

$$b_1 = 4.1301$$

$$a_2 = 0.3039$$

$$b_2 = 1.1697$$

$$C_1 = 33 \text{ nF}$$

$$C_2 = C_4 = 330 \text{ nF}$$

$$C_3 = 4.7 \text{ nF}$$

$$R_3 = 137 \text{ k}\Omega \text{ (use 100k + 36.5k)}$$

$$R_4 = 1.94 \text{ M}\Omega \text{ (used 2M)}$$

$$R_5 = 405 \text{ k}\Omega \text{ (used 402k)}$$

$$R_6 = 1.31 \text{ M}\Omega \text{ (used 1M + 30.1k)}$$

$$C_2 \geq C_1 \frac{4b_1}{a_1^2}$$

$$C_2 = 330 \text{ nF} \geq 81 \text{ nF}$$

$$C_4 \geq C_3 \frac{4b_2}{a_2^2}$$

$$C_4 = 330 \text{ nF} \geq 238 \text{ nF}$$

Stage 4: Inverting Voltage Offset:

$$G = 1$$

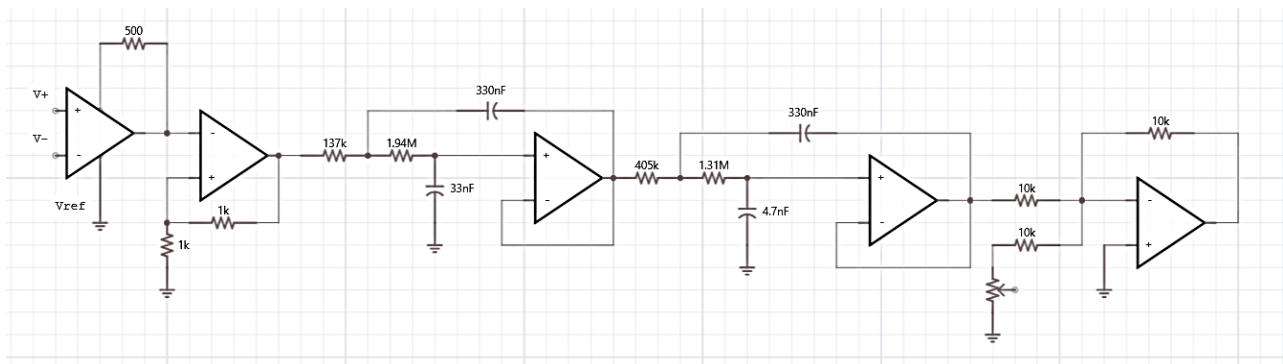
$$R_7 = R_8 = R_9 = 10 \text{ k}\Omega$$

$$R_2 = 1 \text{ k}\Omega$$

### 2.1.2 Circuit Summary:

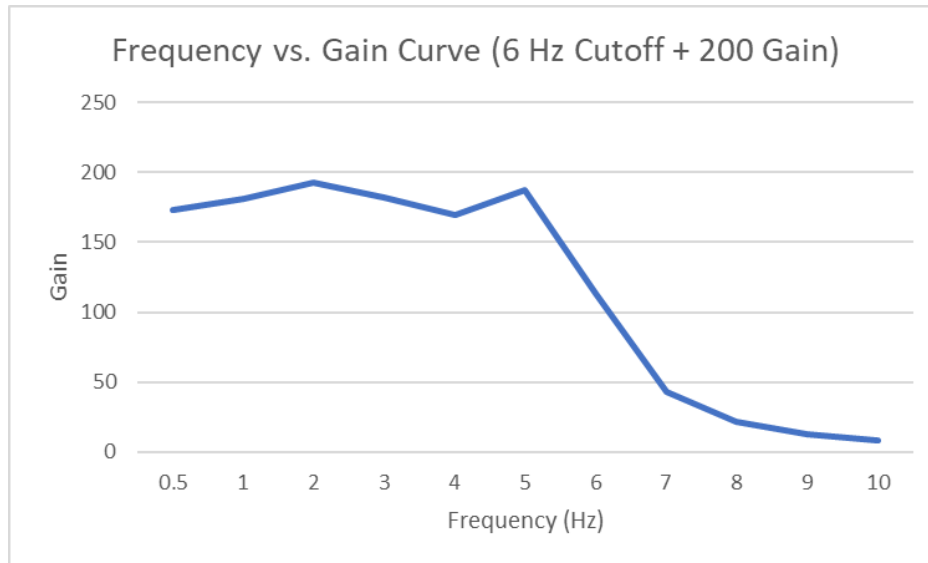
- Stage 1: This stage amplifies the incoming signal by 100 and removes common mode signals.
- Stage 2: This stage amplifies the incoming, already amplified, signal by 2 for a total gain of 200. We need to amplify the signal so that it is large enough to be read by the electronics. The signal is in the  $\mu\text{V}$ - $\text{mV}$  range and needs to be in the  $\text{V}$  range, but not so large that it saturates the amplifier.
- Stage 3: This stage filters out 'high' frequency signals, most importantly 60 Hz, so that they do not pollute the signal.
- Stage 4: This stage adds a DC offset to our signal. It also inverts the signal.

### 2.1.3 Circuit Schematic



### 2.1.4 Gain Characteristics

This is the frequency-gain curve for the SGP circuit. Below the cut-off frequency of 6 Hz, the gain is approximately 175 – 190.





## 2.2 Charge Amplifier Circuit Info

### 2.2.1 Calculations

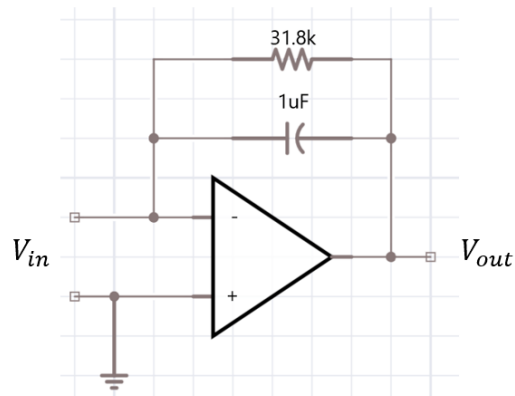
$$f_c = 0.5 \text{ Hz}$$

$$f_c = \frac{1}{2\pi RC}$$

$$R = 31.8 \text{ k}\Omega$$

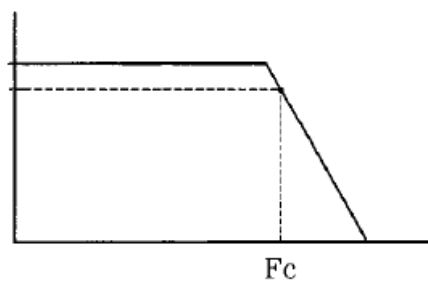
$$C = 1 \mu\text{F}$$

### 2.2.2 Circuit Schematic



### 2.2.3 Gain Characteristics

The theoretical gain characteristics for the charge amplifier circuit.



## Appendix 3

### 3.1 Strain and Force Amplifier

The Vishay signal conditioning amplifier settings can be seen below. The model was the 2130.

|               | Gain | Excitation | Filter |
|---------------|------|------------|--------|
| <b>Strain</b> | 1000 | 2          | 100    |
| <b>Force</b>  | 100  | 10         | None   |

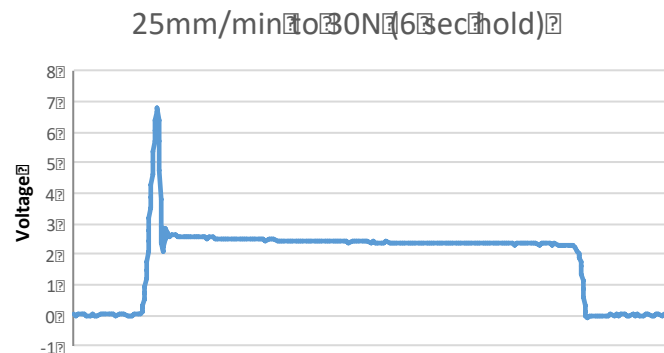
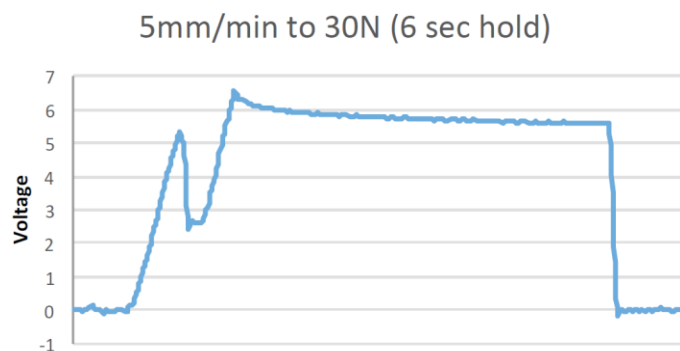


The amplifier with the red tape was the strain amplifier and the green tape was the force amplifier.

## Appendix 4

### 4.1 Admet Evaluation

Before performing force calibration, the performance of the Admet was assessed. It was discovered that if the loading rate was too low the Admet would not work as expected. This can be seen in the 5mm/min displacement rate where there is a malfunction that takes place during loading. At 25 mm/min this malfunction no longer occurs.

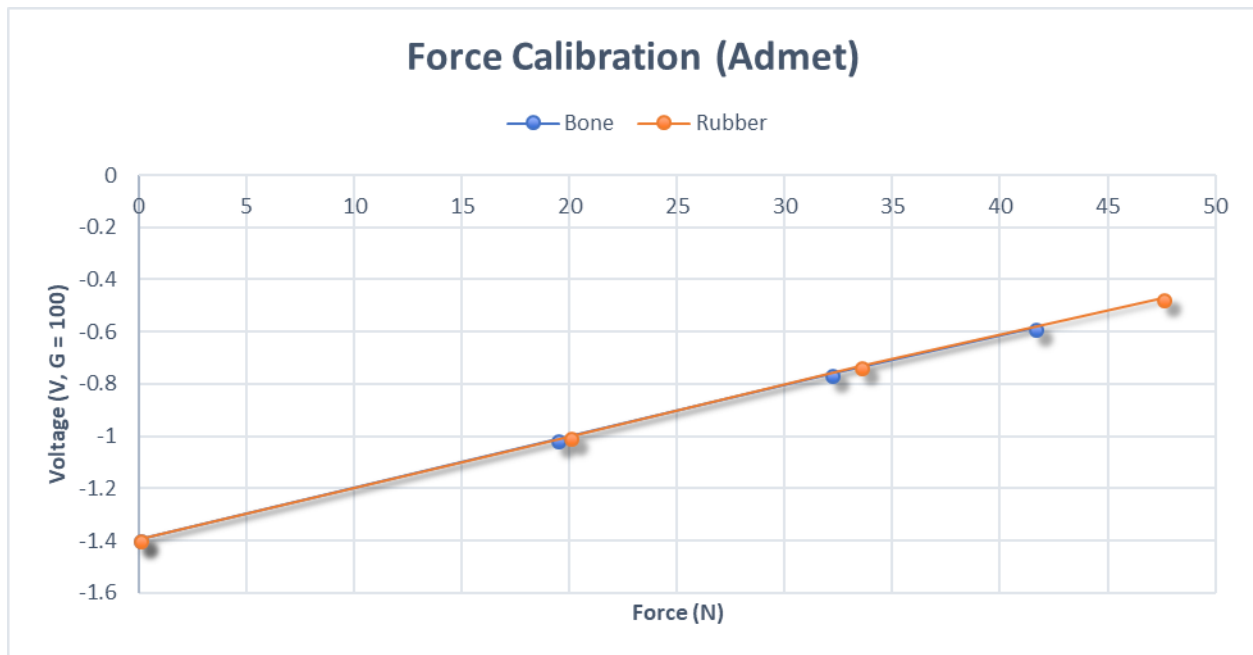


## 4.2 Force Calibration Results

Force calibration was performed to find out what force corresponded with the voltage being collected. Overall, it appears that 0.2 V results from 10N of force.

| Force | Voltage |
|-------|---------|
| 0     | -1.396  |
| 20    | -1      |
| 33.5  | -0.733  |
| 47.5  | -0.47   |

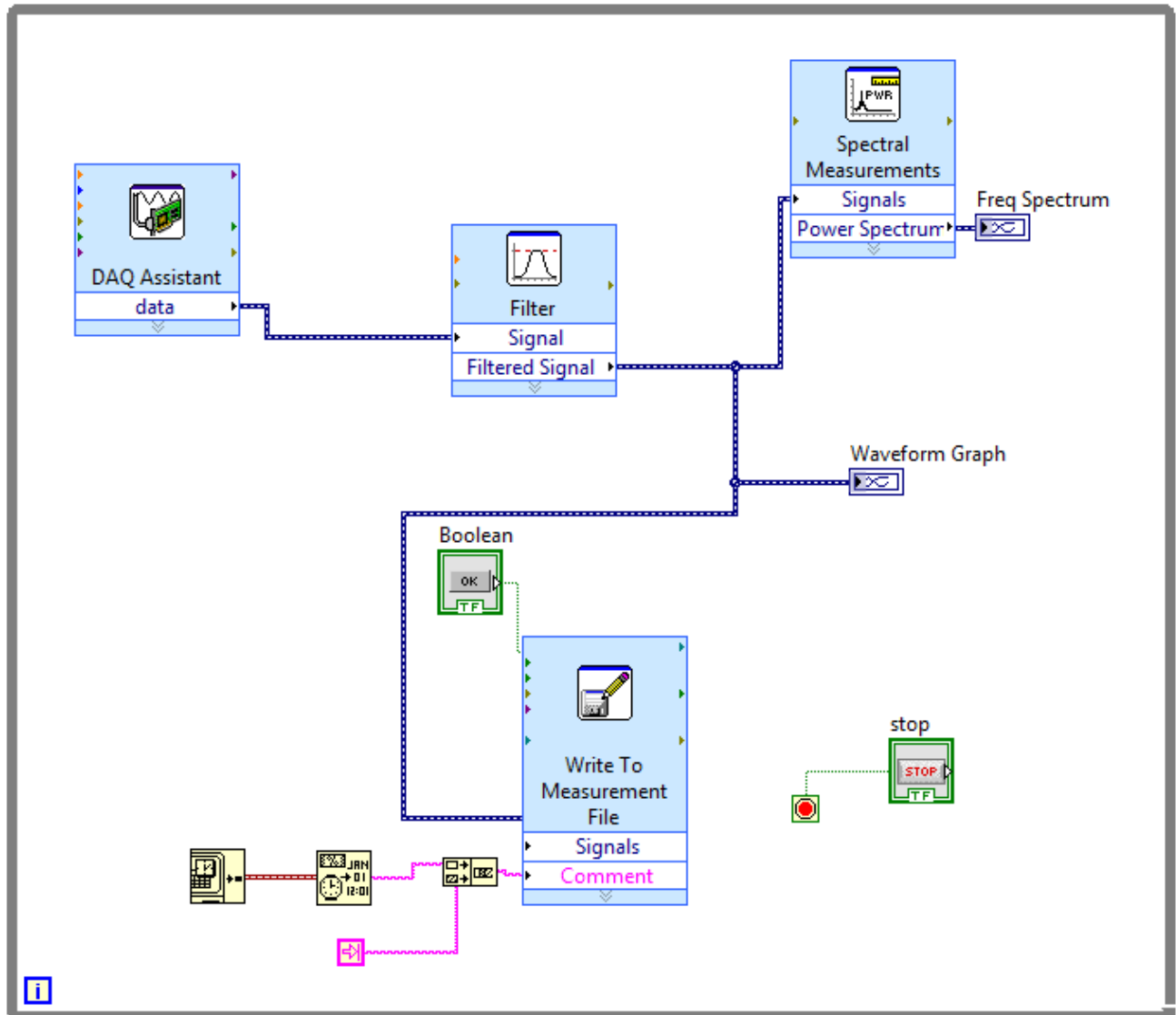
| Force | Voltage |
|-------|---------|
| 0     | -1.395  |
| 19.4  | -1.01   |
| 32.1  | -0.762  |
| 41.6  | -0.582  |

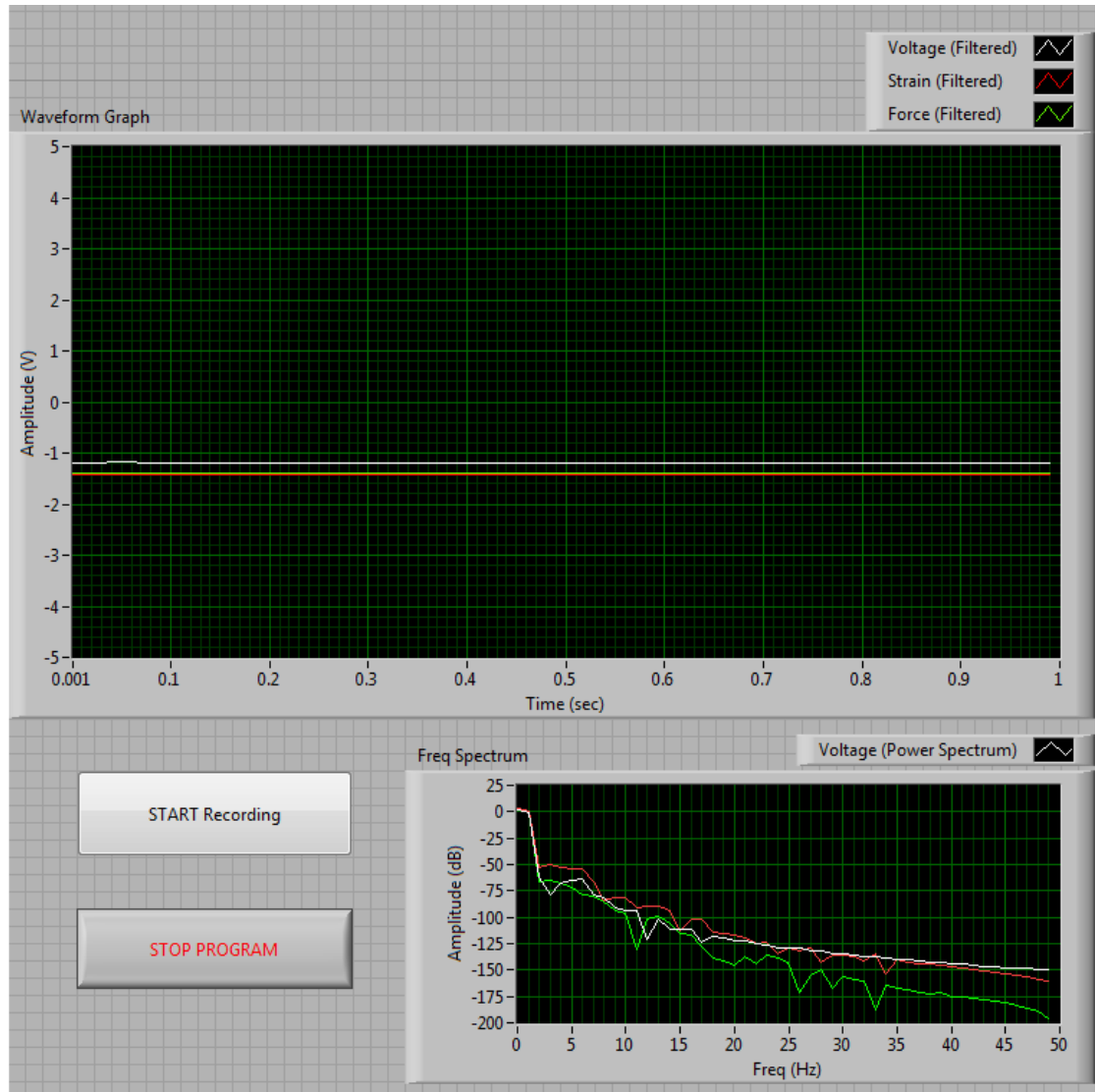


| Force (N) | Voltage Magnitude (V) |
|-----------|-----------------------|
| 10        | 0.2                   |
| 20        | 0.4                   |
| 30        | 0.6                   |
| 40        | 0.8                   |
| 50        | 1.0                   |

## Appendix 5

### 5.1 LabVIEW Program for Data Acquisition





**Filtering Type**

Lowpass

**Filter Specifications**

Cutoff Frequency (Hz)  
5

High cutoff frequency (Hz)  
400

Finite impulse response (FIR) filter

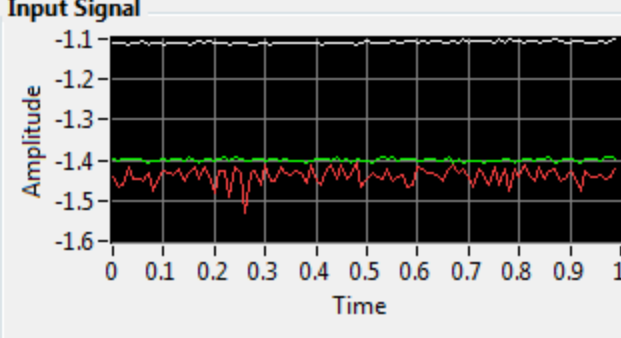
Taps  
29

Infinite impulse response (IIR) filter

Topology  
Butterworth

Order  
5

**Input Signal**



Amplitude

Time

Result Preview and Transfer Function cannot be displayed.

The current Filter Specifications do not meet the Nyquist criterion for the given Input Signal.

**View Mode**

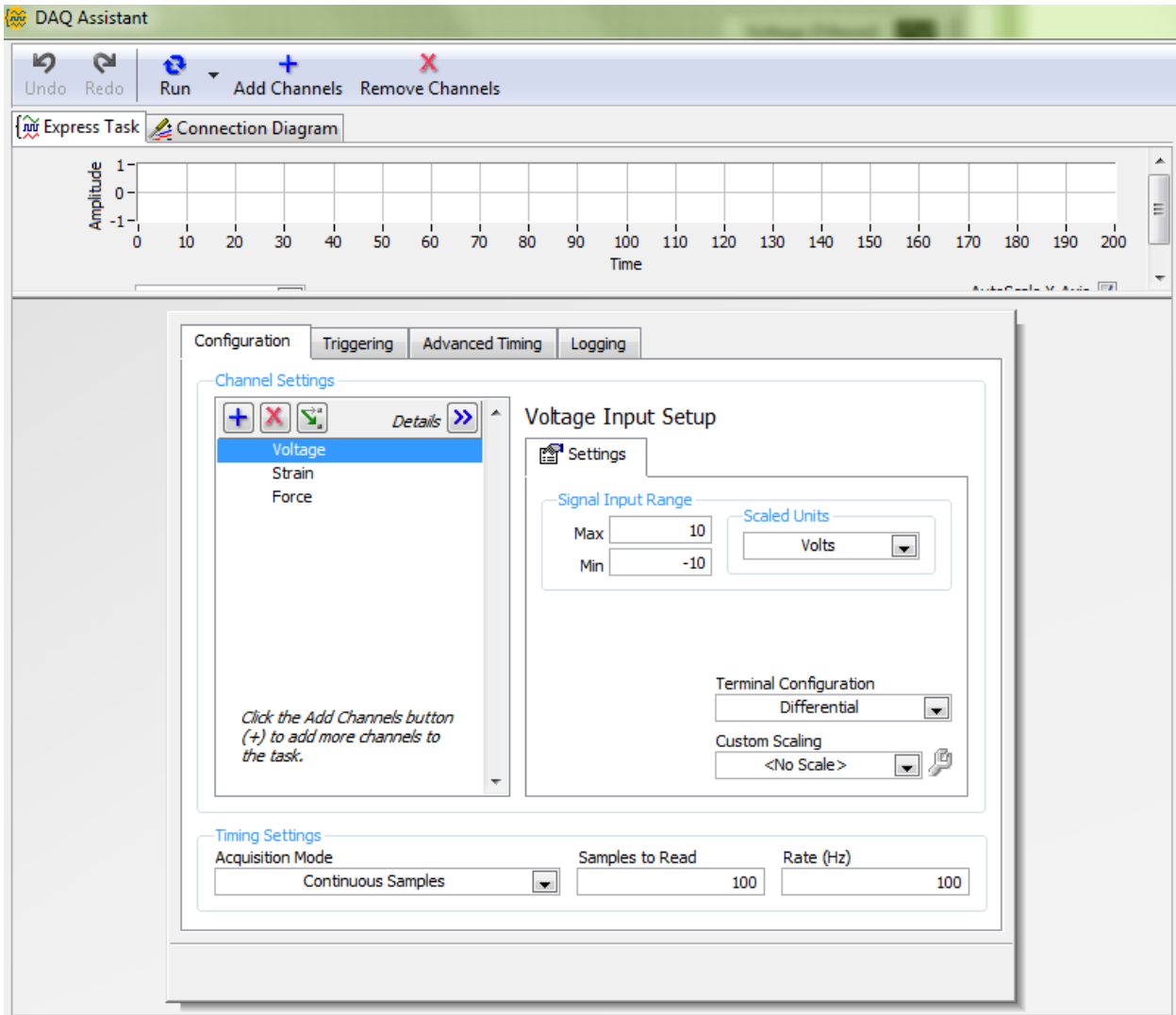
Signals  Show as spectrum

Transfer function

**Scale Mode**

Magnitude in dB

Frequency in log

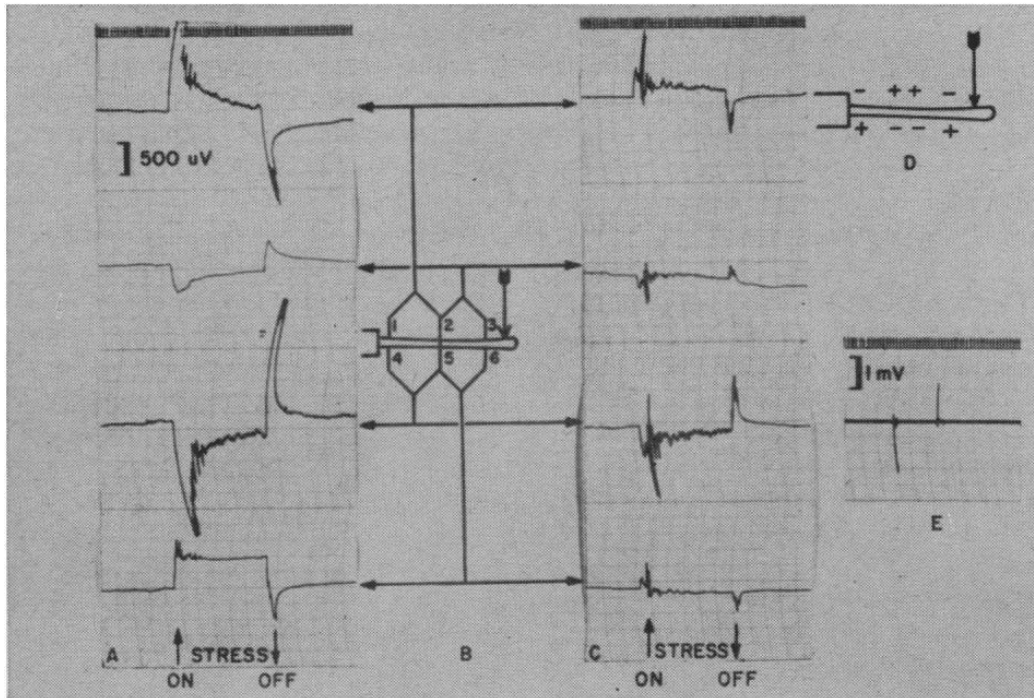




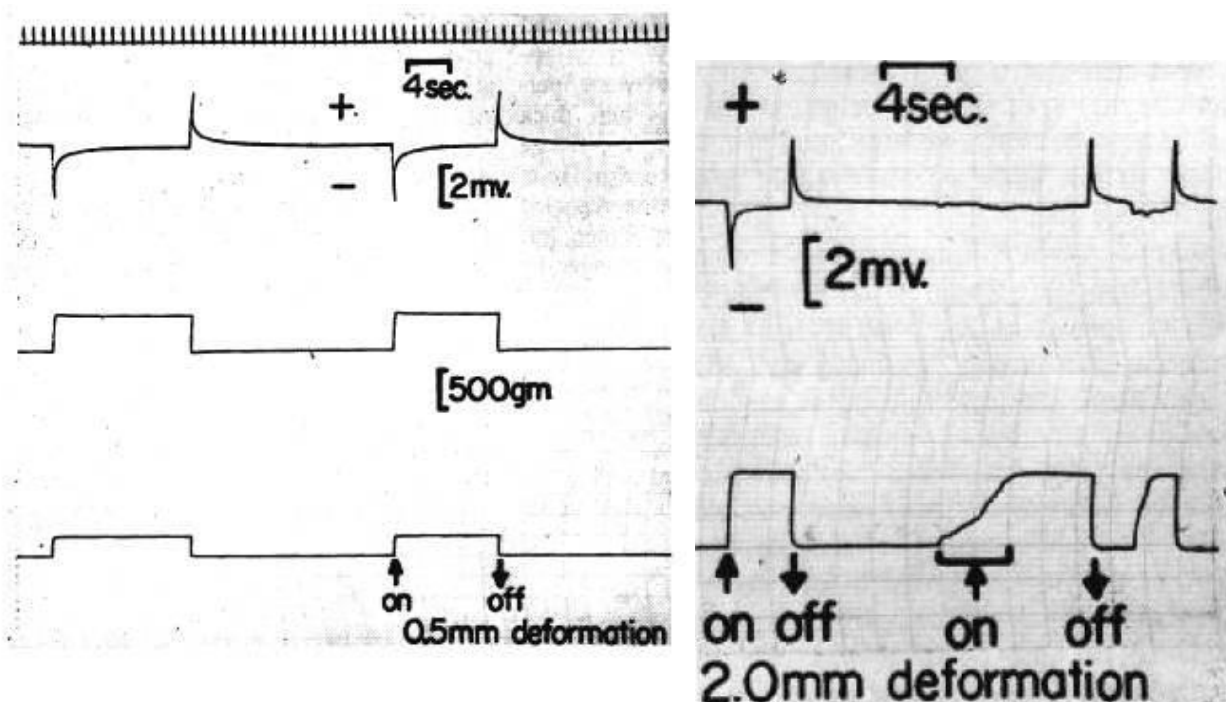
## Appendix 6

### 6.1 Images of Similar SGPs from Other Papers

Bassett (1962)



Cochran (1968)



Steinberg (1973)

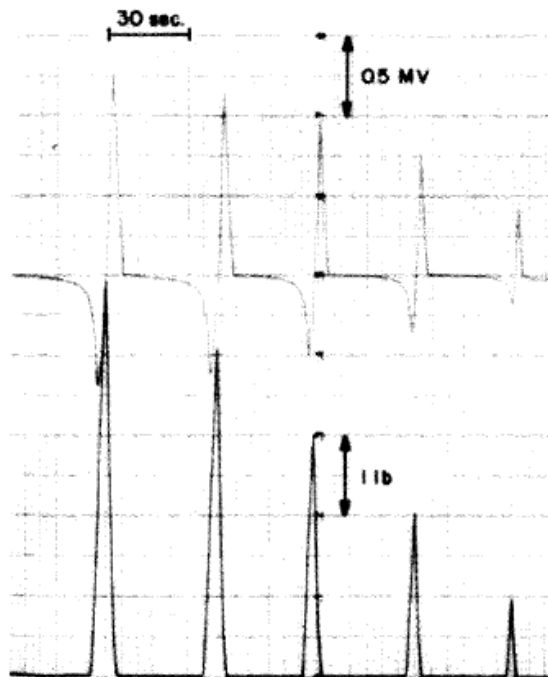


*Fig. 2.* Recording of electrical potential (top) and load/deformation curve (bottom) from normal femur subjected to sequential loading of 1, 2, 3, 4, and 5 pounds at a deformation rate of 0.5 in./min, with immediate release. (Read right to left.)

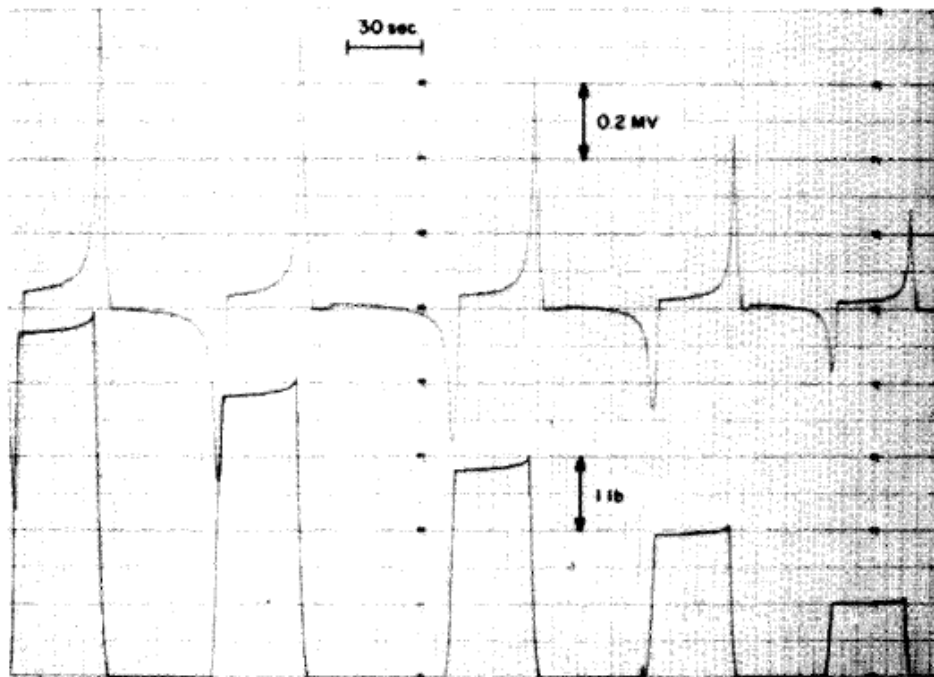


*Fig. 3.* Recording of electrical potential (top) and load/deformation curve (bottom) from normal femur subjected to sequential loading at 0.5 in./min, with each deformation maintained for 30 sec prior to release. (Read right to left.)

Williams (1975)

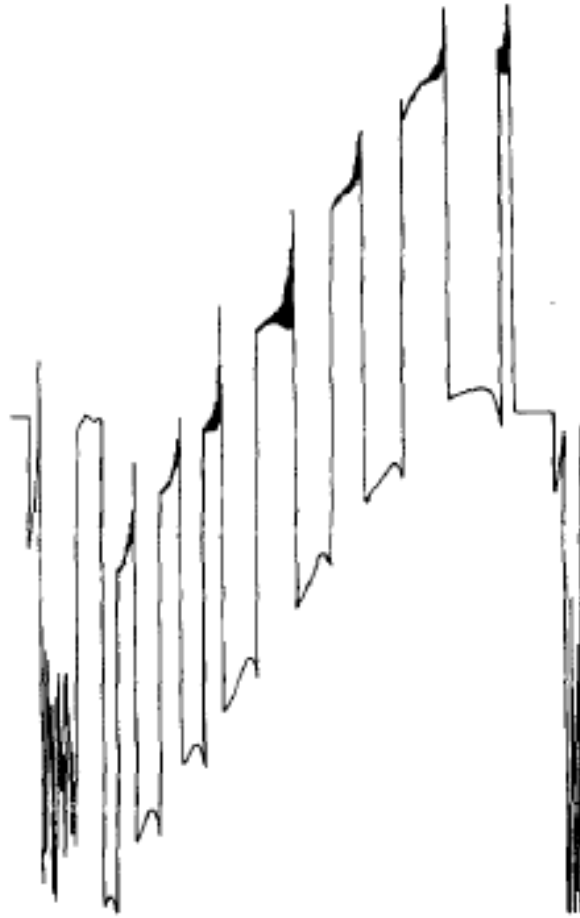
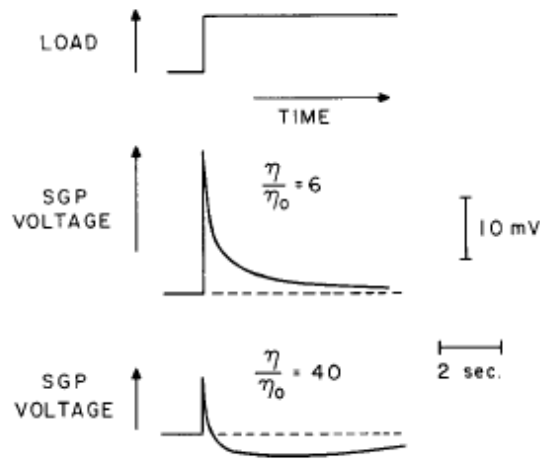


Fig. 6. Voltage signal from tendon deflected in cantilever bending with input impedance  $10^{16} \Omega$  used. One direction only tested. Signal is approximately a square wave, with evidence of slight relaxation. Zero drift due to thermal effects visible but unimportant.

Pienkowski (1983)



SOLUTION CONDUCTIVITY  $<.01 \frac{S}{M}$

**FIG. 7.** The effect of solution viscosity on the stress-generated potential waveform.

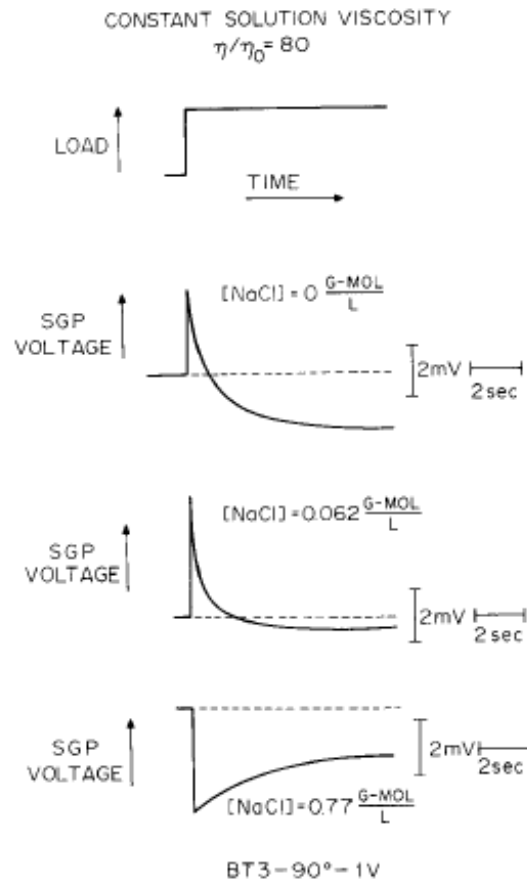


**FIG. 8.** The combined effect of NaCl concentration and solution viscosity on the stress-generated potential waveform.

Gross (1984)

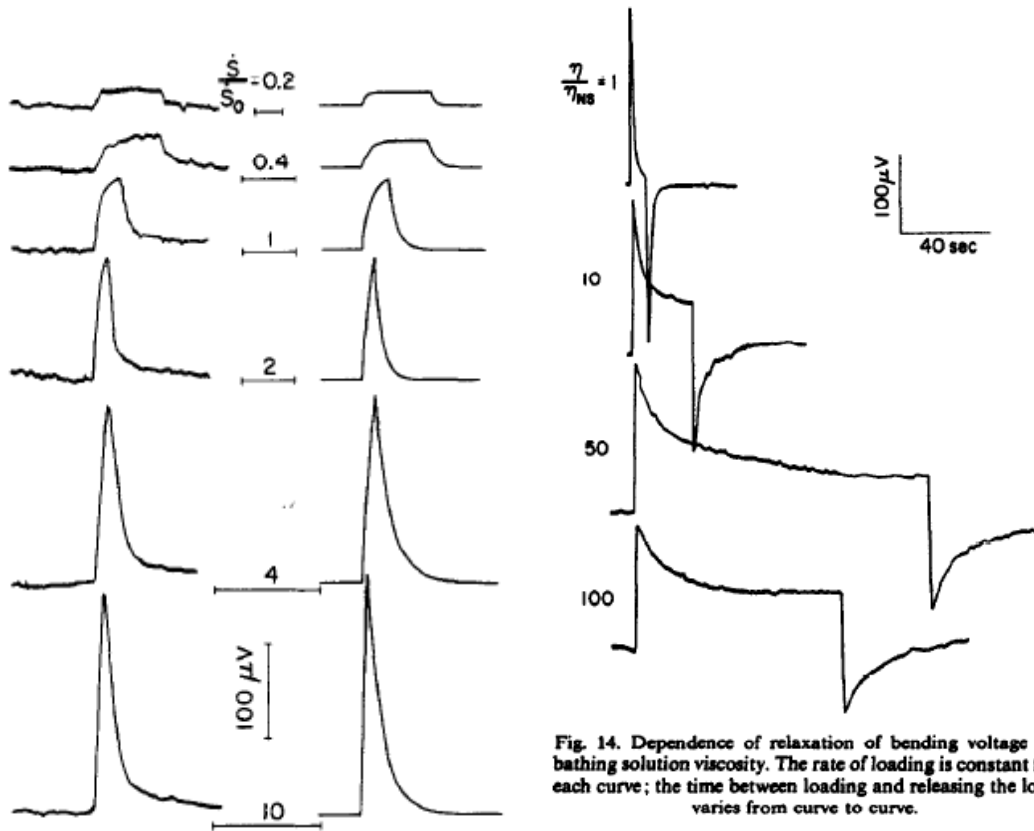


Fig. 14. Dependence of relaxation of bending voltage on bathing solution viscosity. The rate of loading is constant for each curve; the time between loading and releasing the load varies from curve to curve.

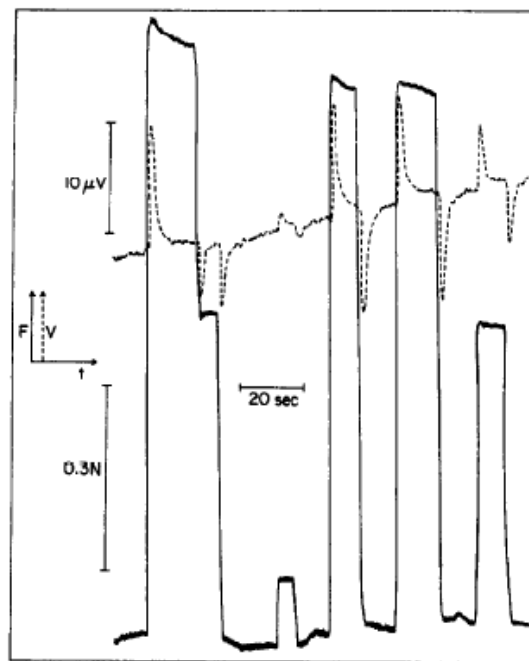
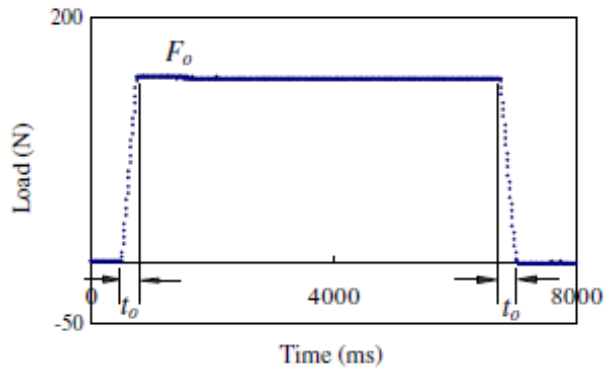
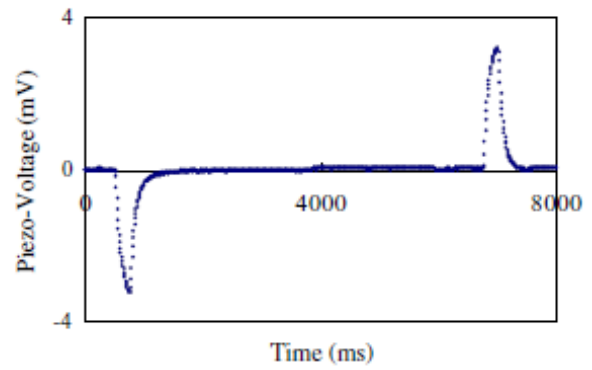


Fig. 10. Chart recorder tracing of the electrical response (dashed line) of a cantilever bent bone saturated with 0.155 M NaCl, pH 7.2, to the applied force (solid line).

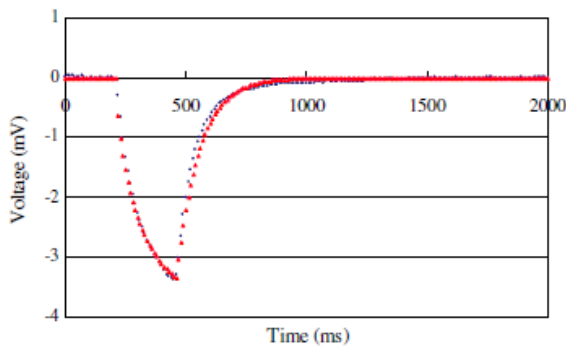
Hou (2011)



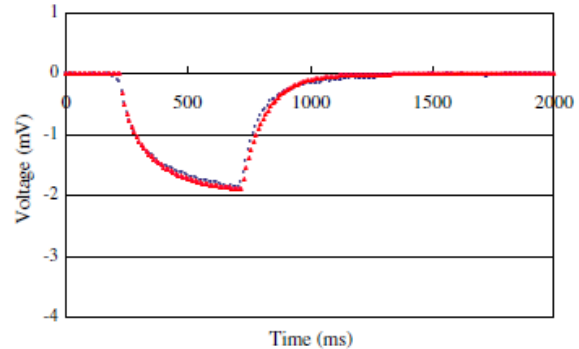
(a) Loading waveform



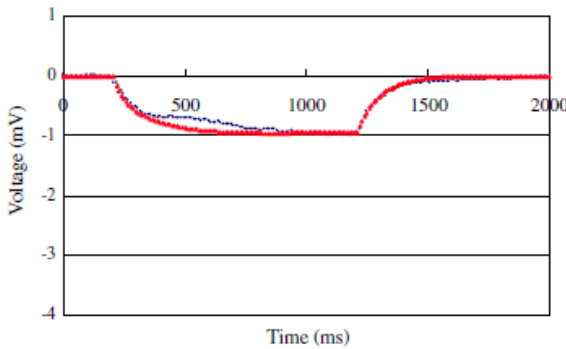
(b) Piezovoltage waveform



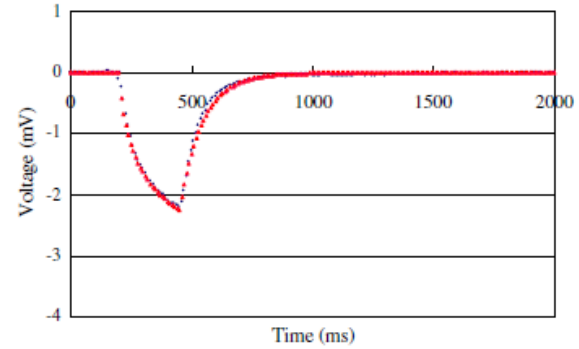
(a) Measured voltage and fitted curve at  $F_0=150$  N and  $T_0=250$  ms



(b) Measured voltage and fitted curve at  $F_0=150$  N and  $T_0=500$  ms



(c) Measured voltage and fitted curve at  $F_0=150$  N and  $T_0=1000$  ms



(d) Measured voltage and fitted curve at  $F_0=100$  N and  $T_0=250$  ms

## 6.2 Summary of Signals Collected from Other Papers

| <i>Author (Year)</i>     | <i>Wet/Dry</i> | <i>Sample Type</i> | <i>Bending Type</i> | <i>Signal Type</i> | <i>Steady State Voltage?</i> | <i>Varied load?</i> | <i>Varied rate?</i> | <i>Magnitude (mV)</i> | <i>Input Impedance (Ohms)</i> |
|--------------------------|----------------|--------------------|---------------------|--------------------|------------------------------|---------------------|---------------------|-----------------------|-------------------------------|
| <b>Bassett (1962)</b>    | Both           | Cortical beams     | Cantilever?         | Equal, bipolar     | Yes                          | Yes                 |                     | ~1.5-3                | $10^6 - 10^{14}$              |
| <b>Cochran (1968)</b>    | Wet            | Cortical beams     | Cantilever          | Equal, bipolar     | Yes and No                   | Yes                 | Yes                 | 0.5-5                 | $10^9$                        |
| <b>Steinberg (1973)</b>  | Wet            | Whole bone         | Four-point          | Unequal bipolar*   | Yes                          | Yes                 | Yes                 | Up to 2.7             | $10^{16}$                     |
| <b>Williams (1975)</b>   | Dry            | Beams?             | Cantilever          | unclear            | Yes                          | No                  | No                  | N/A                   | $10^{11} - 10^{16}$           |
| <b>Gross (1982)</b>      | Wet            | Cortical beams     | Cantilever          | Unequal, bipolar   | Yes and No                   | Yes                 | Yes                 | < 1                   | $>10^{16}$                    |
| <b>Plenkowski (1983)</b> | Wet            | Cortical beams     | Four-point          | Equal, bipolar     | No                           | No                  | No                  | 2-4                   | $10^{14}$                     |
| <b>Hou (2011)</b>        | Dry            | Cortical beams     | Three-point         | Equal, bipolar     | No                           | Yes                 | Yes                 | <1                    | $10^{12}$                     |
| <b>Me</b>                | Wet            | Cortical beams     | Cantilever          | Unequal, bipolar*  | Yes                          | Yes                 | Yes                 | 1-5                   | $10^{11}$                     |

## Appendix 7

### 7.1 MATLAB Code

```

clear;
%% Load zeroed tests
sample_num = '1';
two = '(2)';
date = ' June 11';

curve_len = 580; % isolate curve for slightly less than 6 seconds

% file name, edit for the sample and date
dest = 'C:\Users\laura\Dropbox\Masters\MATLAB\Steinberg Tests\';
s_date = strcat('S',sample_num,two,' - ',date,'\');
folder = 'Zeroed Tests\';
st_num = strcat('s',sample_num,'_0');
id = ['1' '2' '3' '4' '5' '6' '7' '8']; % id of test for opening files
ftype = '.mat';

len = 1:8; % array to store lengths of the test files
A = cell(8,4); % cell array to store test vals
    % col 1 for t col 2 for v, col 2 for s, col 3 for f
for d = 1:8
    test_id = id(d);
    % concatenate the file strings to load the proper file
    load_f = strcat(dest,s_date,folder,st_num,test_id,ftype);
    load(load_f);

    % rename variables and store them in the cell array where n is test #
    len(d) = length(v_new);
    A{d,1} = 1:len(d); % time
    A{d,2} = v_new; % SGP
    A{d,3} = s_new; % strain
    A{d,4} = f_new; % force
end
%% isolate cycles
B = cell(8,4); % the cycles will be separated and stored in a new cell array

for e = 1:8
    inc = len(e)/5; % divide length of each test by 5 to find cycle length
    for f = 1:4
        B{e,f} = reshape(A{e,f},[inc,5]); % separate the 5 cycles
    end
end

for g = 1:8
    % check plot to see if they are well isolated
    subplot(8,1,g); plot(B{g,1},B{g,2},B{g,1},B{g,3},B{g,1},B{g,4});
    tl = 'Test '; tn = id(g); ttl = strcat(tl, tn);
    title(ttl); ylabel('Voltage'); xlabel('Time');
end

%% save isolated cycles to test files
test1 = cell(5,4); test2 = test1; test3 = test1; test4 = test1;
test5 = test1; test6 = test1; test7 = test1; test8 = test1;

```



```

for g = 1:4
    for h = 1:5
        test1{h,g} = B{1,g}(:,h);
        test2{h,g} = B{2,g}(:,h);
        test3{h,g} = B{3,g}(:,h);
        test4{h,g} = B{4,g}(:,h);
        test5{h,g} = B{5,g}(:,h);
        test6{h,g} = B{6,g}(:,h);
        test7{h,g} = B{7,g}(:,h);
        test8{h,g} = B{8,g}(:,h);
    end
end

folder = 'Isolated Tests\';
save_f = strcat(dest,s_date,folder,'alltests',ftype);
save(save_f, 'test1', 'test2', 'test3', 'test4', 'test5', 'test6', 'test7', 'test8');

% calculate max and min values from isolated tests
max_v = zeros(8,5); max_s = max_v; max_f = max_v; % store max vals
i_max = cell(8,3); % store max vals 2.0
ind_v = zeros(1,5); ind_s = ind_v; ind_f = ind_s; % store index of max val

for i = 1:8
    for j = 1:5
        max_v(i,j) = max(B{i,2}(:,j)); % find max SGP value
        ind_v(1,j) = find(B{i,2}(:,j) == max_v(i,j)); % function to find
index
        max_s(i,j) = max(B{i,3}(:,j)); % find max strain value
        ind_s(1,j) = find(B{i,3}(:,j) == max_s(i,j));
        max_f(i,j) = max(B{i,4}(:,j)); % find max force value
        ind_f(1,j) = find(B{i,4}(:,j) == max_f(i,j));
    end
    i_max{i,1} = ind_v; % store index of max SGP value
    i_max{i,2} = ind_s;
    i_max{i,3} = ind_f;
end

mean_max_vals = zeros(8,3); % store mean of 5 cycles max values
mv = zeros(1,8); ms = mv; mf = mv;
for k = 1:8
    mean_max_vals(k,1) = mean(max_v(k,:)); % store mean of 5 max SGP
    mean_max_vals(k,2) = mean(max_s(k,:));
    mean_max_vals(k,3) = mean(max_f(k,:));
end

% save mean max values to a text file
ftype = '.txt';
write_f = strcat(dest,s_date,'mean_max_vals',ftype);
file = fopen(write_f,'w');

fprintf(file, '%6s\t %6s\t %6s\t %6s\t %6s\t
%6s\r\n', 'v_max', 's_max', 'f_max', 'sample_num', 'date', 'test_num');
for v = 1:8
    fprintf(file, '%6.4f\t %6.4f\t %6.4f\t %6s\t %6s\t %i\r\n',
mean_max_vals(v,:), sample_num, date, v);
end

```

```

fclose(file);

%% isolate positive curves from cycles
C = cell(8,4); % cell array to store isolated cycles
v_curves = cell(1,5); s_curves = v_curves; f_curves = v_curves;

% isolate curve from the max value index to the end of the curve
for L = 1:8
    for m = 1:5
        C{L,1} = 1:curve_len+1;
        v_curves{1,m} = B{L,2}(i_max{L,1}(m):(i_max{L,1}(m)+curve_len),m);
        C{L,2}(:,m) = v_curves{1,m};
        s_curves{1,m} = B{L,3}(i_max{L,2}(m):(i_max{L,2}(m)+curve_len),m);
        C{L,3}(:,m) = s_curves{1,m};
        f_curves{1,m} = B{L,4}(i_max{L,3}(m):(i_max{L,3}(m)+curve_len),m);
        C{L,4}(:,m) = f_curves{1,m};
    end
end

figure;
for n = 1:8
    % check plot to see if the curves are well isolated
    subplot(8,1,n); plot(C{n,1},C{n,2},C{n,1},C{n,3},C{n,1},C{n,4});
    t1 = 'Test '; tn = id(n); ttl = strcat(t1,tn);
    title(ttl); ylabel('Voltage'); xlabel('Time');
end

%% save isolated curves to files
for p = 1:4
    for q = 1:5
        test1{q,p} = C{1,p}(:,q);
        test2{q,p} = C{2,p}(:,q);
        test3{q,p} = C{3,p}(:,q);
        test4{q,p} = C{4,p}(:,q);
        test5{q,p} = C{5,p}(:,q);
        test6{q,p} = C{6,p}(:,q);
        test7{q,p} = C{7,p}(:,q);
        test8{q,p} = C{8,p}(:,q);
    end
end

ftype = '.mat';
folder = 'Isolated Curves\';
save_f = strcat(dest,s_date,folder,'allcurves',ftype);
save(save_f,'test1','test2','test3','test4','test5','test6','test7','test8','
sample_num','date');

%% calculate delta v_max
dv_max = zeros(8,5); % store max values
mean_dv_max = zeros(1,8); % store mean of max values
for r = 1:8
    for s = 1:5
        % delta SGP is the difference between first/last value of curve
        dv_max(r,s) = C{r,2}(1,s) - C{r,2}(curve_len,s);
    end
    mean_dv_max(1,r) = mean(dv_max(r,:));
end
end

```

```
% plot to see how dv_max changes over time
figure; ylims = [0, 1]; xlims = [1, 8];
plot(mean_dv_max); title('Delta V Max'); ylabel('Voltage'); xlabel('Test
Number');
xlim(xlims); ylim(ylims);

% save mean dv_max values to text file
ftype = '.txt';
write_f = strcat(dest,s_date,'mean_dv_max_vals',ftype);
file = fopen(write_f,'w');

fprintf(file,'%6s\t %6s\t %6s\t
%6s\r\n','dv_max','sample_num','date','test_num');
for u = 1:8
    fprintf(file,'%6.4f\t %6s\t %6s\t %i\r\n',
mean_dv_max(u),sample_num,date,u);
end
fclose(file);
```